2021

FXS-Causing Point Mutations in FMRP Disrupt Neuronal Granule Formation and Function

Emily L. Starke

FXS-causing point mutations in FMRP disrupt neuronal granule formation and function

_____

A Dissertation

Presented to

the Faculty of the College of Natural Sciences and Mathematics

University of Denver

_____

In Partial Fulfillment

of the Requirements for the Degree

Doctor of Philosophy

_____

by

Emily L. Starke

June 2021

Advisor: Scott A. Barbee

Author: Emily L. Starke
Title: FXS-causing point mutations in FMRP disrupt neuronal granule formation and function
Advisor: Scott A. Barbee
Degree Date: June 2021

ABSTRACT

Fragile X Syndrome (FXS) is a neurodevelopmental disorder caused by the disruption of Fragile X Mental Retardation Protein (FMRP) function in neurons, affecting nearly 1 in 7,500 individuals. Although FXS typically occurs from a complete loss of FMRP expression due to a CGG trinucleotide expansion within the 5'UTR of the *FMR1* gene, single nucleotide polymorphisms (SNPs) within the KH domains of FMRP have been shown to severely disrupt FMRP function. FMRP is an RNA-binding translation repressor that interacts with ~4% of the neuronal transcriptome. Many target mRNAs encode for proteins important for regulating synaptic processes and modulate synaptic plasticity. It is likely that FMRP differentially regulates this large subset of mRNAs via its association with specific membraneless organelles (MLOs), or granules, that are each involved in regulating different processes of the transcript lifecycle. How FMRP forms and interacts with different MLOs however, is largely unknown. Here we show that multivalent interactions via the two canonical KH domains, KH1 and KH2, and the C-terminal intrinsically disordered region (IDR) function cooperatively to promote FMRP granule formation in *Drosophila* S2 cells.

Two mutations within the KH domains of FMRP have been linked to severe forms of FXS. We were interested in determining whether these mutations disrupted the

formation or function of FMRP-containing MLOs. Here we studied these missense point mutations, by making the orthologous mutations in the fly KH1 (Gly269Glu) and KH2 (Ile307Asn) domains. Within FRAP experiments of fly S2 cells we found that each of the KH point mutants destabilized the dynamic mobile fraction of FMRP granules, while having no impact on immobile fractions. The KH1 mutant in particular has an important function in granule formation and FMRP association with other MLOs involved in post-transcriptional regulation including stress granules and RNA Processing-bodies. Additionally, we found that the KH1 mutation is defective in FMRP-mediated translation, while the KH2 mutant has no effect.

We also studied the impact of these mutations in *Drosophila* primary motor neurons (MNs) where FMRP associates with neuronal RNA transport granules (NGs). Within NGs FMRP is thought to translationally repress transcripts during their active transport from the soma out to the synapse. Interestingly, we found that the KH1 mutant severely disrupted the nucleation of FMRP-positive NGs. The KH2 mutant on the other hand destabilized NGs, impacting NG transport out in neurites. Interestingly, we found that these mutations had no impact on *camkii* transport, a well characterized FMRP target, suggesting that FMRP-NG association and RNA transport may not be functionally linked processes.

ACKNOWLEDGEMENTS

I would like to thank my advisor Dr. Scott Barbee for all his guidance and support, academically and personally. I would also like to thank my thesis committee members Dr. Nancy Lorenzon, Dr. Joseph Angelson, Dr. Erich Chapman, and Dr. Schuyler Van Engelenburg for their help shaping these projects and my external chair Dr. Michelle Knowles for her support. For assistance in learning new lab techniques and sharing in critical conversations about these projects I would like to thank Dr. Navneeta Kaul, Conner Langeberg, Jenna Triplett, Taylor Minckley, Nick Groves, Alan Weisgerber and Emily Wilkinson. For assistance with experiments that contributed to this work I would like to thank Samantha Patterson, Keelan Zius, William Moody, and Raul Orozco. And finally, I would like to give my profound gratitude to my family, friends and partner for their incredible love, guidance and support throughout this process.

TABLE OF CONTENTS

TABLE OF FIGURES

CHAPTER ONE

CHAPTER TWO

CHAPTER THREE

CHAPTER FOUR

CHAPTER ONE: BACKGROUND AND SIGNIFICANCE

1.1 Fragile X Syndrome

1.1.1 Disease occurrence and phenotypes

Fragile X Syndrome (FXS) is the most common monogenic cause of inherited mental and intellectual disability, affecting roughly 1 in 5,000 males and 1 in 10,000 females (Coffee et al., 2009). This developmental disorder can present various symptoms in those affected ranging from mild to severe. This includes developmental delays in walking and talking, as well as difficulty learning new tasks (Garber et al., 2008). Social and behavioral problems such as difficulty making eye contact, attention deficits, hand flapping, hyperactivity, and anxiety are also common in affected individuals. Additionally, seizures occur in roughly 15% of affected males and 5% of affected females (Garber et al., 2008). Physical symptoms typically manifest in individuals with FXS following puberty which include distinct facial features such as an enlarged head and ears with a long narrow face, prominent jaw and forehead, unusually flexible joints, flat feet, and in males, macroorchidism (Neri, 2017). FXS also has a high comorbidity with autism spectrum

disorders (ASD), which occurs in roughly 1 out of 3 individuals with FXS (Abbeduto et al., 2014).

1.1.2 Neuronal defects of FXS

FXS is caused by the disruption of the *fragile X mental retardation 1* (*FMR1*) gene which encodes the Fragile X Mental Retardation Protein (FMRP). FMRP is expressed throughout the body, but is enriched in the testes, ovaries and throughout the brain (Christie et al., 2009). FMRP is an RNA-binding protein (RBP) that interacts with roughly 4% of neuronal transcripts, many of which encode for proteins required for synaptic plasticity (Ashley et al., 1993; Brown et al., 2001; Sidorov et al., 2013).

Synaptic plasticity is the dynamic ability of neurons to strengthen or weaken connections with other neurons in an activity-dependent manner over time. Activity-dependent alterations in synaptic strength include: 1) retaining and strengthening synapses commonly referred to as long-term potentiation (LTP) and 2) synapse weakening and elimination referred to as long-term depression (LTD) (Magee and Grienberger, 2020). This orchestration of strengthening and pruning synapses in response to activity is thought to be the mechanism underlying learning and memory formation (Nabavi et al., 2014). Neurons are capable of regulating synaptic strength cell-wide in response to drastic changes in network activity in a process called synaptic scaling (Turrigiano, 2008). On the molecular level, this process is carried out via the regulation of receptor trafficking out to the synapse (e.g. increased network activity will stimulate the neuron to scale down synaptic strength by reducing receptor trafficking out to synaptic sites). FMRP particularly

affects new protein synthesis-dependent mechanisms of synaptic plasticity and synaptic scaling. Loss of synaptic scaling up in *FMR1* KO neurons was able to be rescued with the reintroduction of FMRP in the postsynaptic neuron (Soden and Chen, 2010).

A major phenotype observed in FXS is an overelaboration of immature dendritic spines due to aberrant activity-independent translation at synapses (Scotto-Lomassese et al., 2011). Loss of FMRP causes an increased density, or overgrowth, of dendritic and axonal protrusions which is thought to result from a loss of regulation of some cytoskeletal targets of FMRP, such as the microtubule associated protein, futsch (Zhang et al., 2001).

The mGluR theory of FXS (Figure 1) posits that FMRP modulates synaptic plasticity by regulating protein synthesis of postsynaptic transcripts required to maintain LTD triggered by group 1 and 5 metabotropic glutamate receptor (mGluR1/5) activation (Bear et al., 2004; Stoppel et al., 2017). LTD initiated by mGluR activation is dependent on rapid, local translation of synaptic mRNAs. Within the postsynaptic density (PSD) phosphorylated FMRP is bound to translationally stalled transcripts. Upon mGluR activation FMRP is dephosphorylated, allowing repressed transcripts to re-enter the translating pool and for rapid synaptic protein synthesis to occur (Santoro et al., 2012). These nascent proteins are then involved in the internalization of α-amino-3-hydroxyl-4-isoxazole propionic acid (AMPA) receptors and subsequent LTD. AMPA receptors on the postsynaptic neuron allow Na^+ influx in response to the ligand glutamate binding to the receptor and are integral for LTP to occur. In FMRP-deficient neurons however, translational "brakes" on these PSD transcripts are removed causing their constitutive

overexpression regardless of mGluR activation. Excessive AMPA receptor internalization leads to a synaptic imbalance in favor of LTD, resulting in the hyperproduction of immature dendritic spines that have a severely reduced function (Dölen et al., 2007; Sidorov et al., 2013).

Naturally, studies looking at mGluR-pathway antagonists promptly followed this discovery, in a hope that inhibiting downstream effectors in this pathway may ameliorate some of the cognitive and behavioral deficits in FXS. Knockdown of mGluR5 expression is capable of rescuing many of these phenotypes in mice, further supporting the mGluR theory (Dölen et al., 2007). Additionally, multiple studies using the mGluR5 antagonist 2-methyl-6-phenylethyl-pyridine (MPEP) have been able to restore proper AMPA receptor internalization and dendritic spine morphologies in mice as well as various cognitive and behavioral deficits in mice, zebrafish and fly models of FXS (McBride et al., 2005; Nakamoto et al., 2007; Tucker et al., 2006; Yan et al., 2018). Recent clinical trials testing two mGluR5 antagonists seemed optimistic at first, but rather unexpectedly showed no significant efficacy or clinical improvement in FXS patients (Scharf et al., 2015). Devastatingly, there are no treatments for FXS and current pharmacotherapy available for FXS only treat specific behavioral symptoms, mood disorders or seizures. The search for new and effective FXS therapies has been a major push in the field driving the need to understand FMRP functions and molecular/cellular targets within the nervous system.

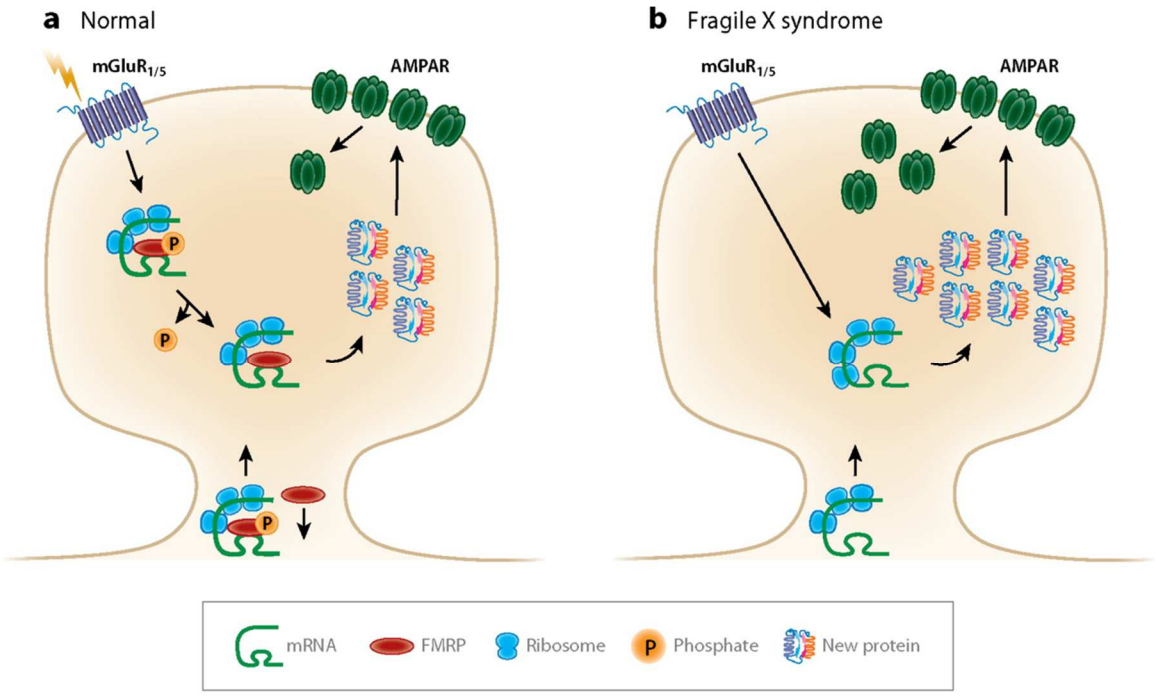

Figure 1. The mGLuR theory of FXS

Used with permission of Annual Reviews, Inc., from [Molecular Mechanisms of Fragile X Syndrome: A Twenty-Year Perspective, Michael R. Santoro, Steven M. Bray, and Stephen T. Warren, volume 7, and Copyright (2011)]; permission conveyed through Copyright Clearance Center, Inc.

(A) Within the postsynaptic density, phosphorylated FMRP is bound to translationally stalled mRNAs. Following mGLuR1/5 activation FMRP is dephosphorylated, allowing bound mRNA to reenter the translation pool. *De novo* protein synthesis following mGLuR1/5 activation increases AMPA receptor (AMPAR) internalization, a requirement for LTD. (B) Loss of FMRP function in FXS results in the loss of activity dependent translation regulation of synaptic mRNAs by FMRP. mRNAs are maintained in a translationally active state regardless of mGluR1/5 activation. Aberrant protein synthesis causes an excess of AMPAR internalization and amplified LTD.

1.1.3 FXS is caused by the disruption of the encoding FMRP protein

FXS is caused by the transcriptional silencing of the *FMR1* gene due to a CGG trinucleotide-repeat expansion in its 5'UTR (Figure 2). Normal repeat numbers range from 5-49, whereas premutation alleles contain 50-200 repeats and are referred to as such due to their proclivity to undergo further expansion and give rise to the full mutations allele (>200 repeats) in their offspring (Fu et al., 1991). Although the premutation does not cause FXS, it puts individuals at a higher risk of developing the neurodegenerative disorder Fragile X-associated tremor/ataxia syndrome (FXTAS). Females have an additional risk of developing Fragile X-Associated Primary Ovarian Insufficiency (FXPOI) which causes severely reduced ovary function (Fink et al., 2018). The full mutation triggers a hypermethylation event at the *FMR1* promoter, preventing *FMR1* gene expression (Pieretti et al., 1991). Although complete loss of FMRP expression is the primary cause of FXS, gene sequencing has led to the identification of over 130 single nucleotide polymorphisms (SNPs) within the *FMR1* coding region. This study sequenced the *FMR1* gene of 963 males presenting with FXS-like phenotypes, but had normal CGG repeat numbers (Collins et al., 2010). In addition to this, there have been upwards of 100 *FMR1* deletions that have been identified in individuals, which we did not focus on in this study (Coffee et al., 2008). Of the 130 SNPs identified, there are a handful of potentially pathogenic mutations that occur within the coding region of the *FMR1* including 3 mutations of interest that occurred within one of the FMRP RNA-binding domains (RBDs). Before describing these point mutations,

however, the FMRP domains and their predicted functions must be discussed in order to understand how these mutations could be disrupting essential FMRP functions.

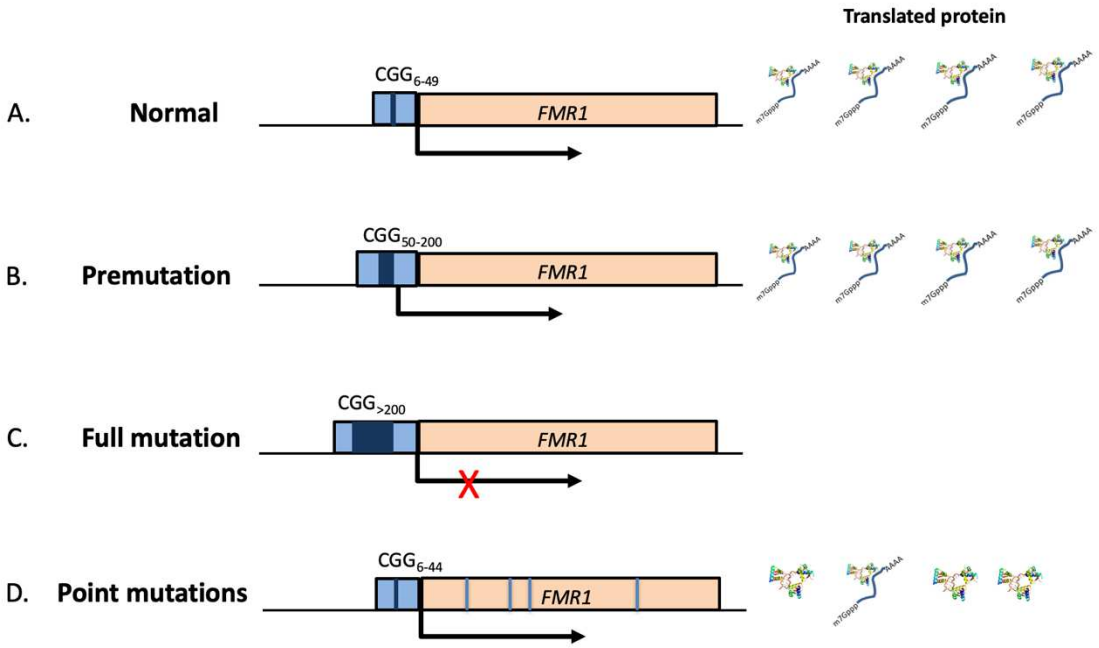

Figure 2. Fragile X Syndrome is caused by disruption of *FMR1* gene expression

(A) The *FMR1* gene on the X chromosome contains a CGG repeat expansion between 6-49 repeats within its 5'UTR. Under these circumstances, the *FMR1* gene is expressed, producing a fully functional FMRP protein. Repetitive sequences, such as CGG trinucleotide repeats, within the genome are susceptible to DNA-polymerase slippage, where it can drastically increase repeat number. (B) CGG repeat lengths between 50-200 are still able to express the *FMR1* gene normally and produce functional FMRP. However, males with this premutation have a higher probability of developing the neurodegenerative disorder Fragile X Tremor/Ataxia Syndrome and while females have a higher proclivity for Fragile X Associated Primary Ovarian Insufficiency. (C) The full, loss of function mutation occurs when CGG repeats expand beyond 200 repeats. This expansion causes hypermethylation at the *FMR1* locus inhibiting gene expression and resulting in loss of FMRP protein. (D) However, individuals with missense point mutations within the *FMR1* gene can develop FXS with normal CGG repeat numbers. These mutations are often hypomorphic alleles that produce FMRP with reduced function and stability.

1.1.4 *Drosophila* is an established model system to study FXS

In this study, we used the fruit fly *Drosophila melanogaster* as our model system to study the functions of fly FMRP. FMRP is a multivalent protein with several conserved functional domains (Figure 3A) (Siomi et al. 1993). FMRP and the related FXR1P and FXR2P proteins are evolutionarily conserved in mammals, with a single FMRP ortholog in *Drosophila*. The fly FMRP ortholog is 60% identical to human FMRP at the amino acid level (Wan et al., 2000). Most of the conserved sequence is found within the FMRP RBDs, suggesting their importance for FMRP function. Studying FXS and FMRP using flies as a genetic model is advantageous as there are no FXR paralogs, which have some redundant functions with FMRP and make it difficult to interpret results obtained from FMRP knock-down/-out experiments in mammalian models (Majumder et al., 2020). Additionally, many of the major neural, social and behavioral FXS phenotypes found in FXS patients also occur in the *FMR1-null* fly including: dendritic overelaboration, over-abundance of neurotransmitter containing vesicles in the presynaptic space, repetitive behaviors, courtship defects, and learning deficiencies (McBride et al., 2005, 2013).

1.1.5 FMRP domain structure and FXS-causing point mutations

1.1.5.1 FMRP contains DNA-binding tandem Tudor domains

At the amino-terminus (N-terminus) of FMRP are two DNA-binding Agenet domains, also referred to as tandem Tudor domains (Figure 3A). These domains are important for a nuclear function of FMRP in modulating the DNA damage response by directly interacting with chromatin (Alpatov et al., 2014). These interactions were found to

be important for regulating genomic stability by reducing susceptibility to double stranded breaks in DNA undergoing replication (Chakraborty et al., 2020).

1.1.5.2 FMRP contains three RNA-binding KH domains with elusive binding properties

Following the tandem Tudor domains are three structured hnRNP K homology (KH) domains KH0, KH1 and KH2 (Figure 3A). The KH1 and KH2 domains contain the highly conserved RNA-binding GXXG loop (Hollingworth et al., 2012). The more recently discovered KH0 domain, however, does not contain this conserved sequence suggesting that it may not interact with RNA (Hu et al., 2015; Myrick et al., 2015a). Before this region was identified as a non-canonical KH domain, it was reported that the KH0 domain was responsible for protein-interactions between FMRP and the cytoplasmic FMRP-interacting protein 1 (CYFIP1), the FMRP homolog FXR2P, and the polyribosome associated protein 82-FIP (82 kDa FMRP Interacting Protein) (Bardoni et al., 2003; Schenck et al., 2001; Siomi et al., 1996). Interestingly, KH0 has also been shown to bind the non-coding RNA, mammalian brain-specific cytoplasmic RNA 1 (BC1), which functions as a molecular adaptor linking FMRP with some mRNA targets within neurons (Zalfa et al., 2003).

An individual with developmental and intellectual disability in addition to intractable seizures was found to have an arginine to glutamine missense mutation within the KH0 domain (Arg138Gln) (Figure 3A). Studies have indicated this mutation disrupts FMRP association with nucleosomes and presynaptic BK channels (high conductance calcium- and voltage- dependent potassium channels), although this doesn't appear to be

occurring as a result of any significant structural changes in protein folding (Alpatov et al., 2014; Myrick et al., 2015a). Presynaptic BK channels are important for regulating action potential duration and neurotransmitter release, which is disrupted in Arg138Gln hippocampal CA3 pyramidal neurons (Myrick et al., 2015b). Interestingly, this mutation was not found to have any effect on some of the more well-characterized FMRP functions such as mRNA binding or translation regulation, suggesting this domain may control novel presynaptic FMRP function(s) (Myrick et al., 2015b).

Missense point mutations in the human KH1 and KH2 domains (Gly266Glu and Ile304Asn, respectively) have been identified in two individuals with FXS (De Boulle et al., 1993; Myrick et al., 2014). Although RNA-binding targets of the KH1 and KH2 domains remains largely elusive, these domains essential for polyribosome association which is significantly reduced in Ile304Asn and abolished in the (Gly266Glu) mutant (Darnell et al., 2005; Feng et al., 1997; Myrick et al., 2014). Interestingly, KH1 Gly266Glu introduces a large, hydrophobic residue which sterically clashes with neighboring side chains, and is predicted to disrupt KH1 domain structure (Myrick et al., 2014). The KH2 Ile304Asn mutation also results in a hydrophobic-to-hydrophilic residue mutation and occurs within the hydrophobic binding pocket of the KH2 domain, completely disrupting KH2 domain folding and is predicted to disrupt RNA-binding (Valverde et al., 2007).

One of the proposed mechanisms of FMRP-mediated translation regulation is via stalling translating ribosomes on target mRNAs (Darnell et al., 2011). The structure of the *Drosophila* FMRP-ribosome complex was solved using cryo-EM wherein the KH1, KH2,

and RGG domains were essential for this interaction (Chen et al., 2014). Interestingly, the KH domains dock on the 80S ribosome and overlap with the peptidyl site (P-site), which is hypothesized to prevent tRNA entry/departure and association of elongation factors, effectively halting translation. The two canonical KH domains may function in FMRP-mediated translation repression via this interaction, explaining how disruption of these domains via FXS-causing point mutations have detrimental effects in these individuals.

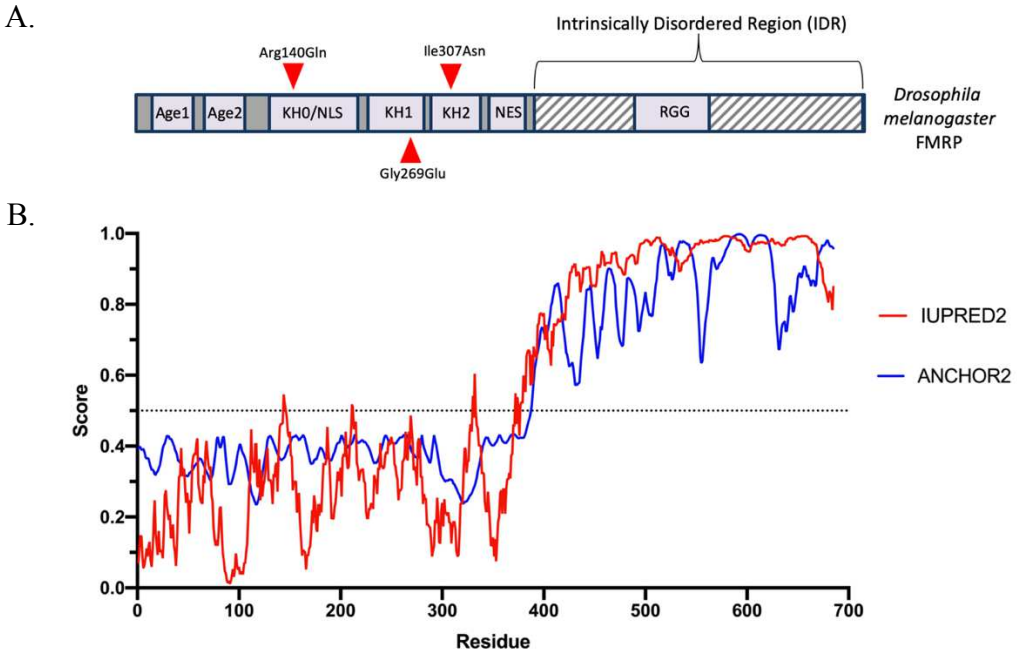

Figure 3. Schematic of *Drosophila melanogaster* FMRP

(A) All the functional domains and mutated amino acids are conserved in fly FMRP. FMRP contains several interaction domains including: Agenet 1 and Agenet 2 (Age1 and Age2) which are important for nuclear FMRP functions including chromatin binding (aka tandem Tudor domains). Three hnRNP K homology (KH) domains are conserved RNA-binding domains. The non-canonical KH0 domain also contains the nuclear localization sequence (NLS) which allows FMRP-nuclear localization. Locations of missense point mutations reported in three individuals with Fragile X Syndrome are indicated with red arrowheads and annotate the conserved amino acid residue substitution and position in the *Drosophila melanogaster* FMRP protein. A nuclear export sequence (NES) is positioned in between the KH2 and intrinsically disordered region (IDR) and permits nucleocytoplasmic shuttling of FMRP. The IDR makes up the entire C-terminus of FMRP and is shown in striped patterning. In the middle of the IDR is the arginine-glycine-glycine rich or RGG box. The RGG box binds G-quadruplex structures in mRNA targets. *Note: domain sizes and amino acid positions are approximate.* (B) Disorder plot aligned with the FMRP protein schematic show the C-terminus of FMRP is entirely disordered using IUPRED2. Unstructured binding domain predictions were made using ANCHOR2 (Mészáros et al., 2018). An IUPRED2A score of 0-0.5 is predicted to be structured, whereas scores between 0.5-1 is predicted to be unstructured.

Identifying mRNA targets and the RNA-recognition elements (RREs) to which the KH domains in FMRP are binding has been highly sought after, as FMRP is known to be a major translation regulator within neurons, and mutations within these domains cause severe FXS. Unfortunately, there has been much disagreement between studies using different high-throughput methods to identify FMRP-targeted mRNA motifs, specifically for the KH1 and KH2 domains. The RREs WGGA (where W = A or U) and ACUK (where K = G or U) were found to be enriched in FMRP RNA targets identified from photoactivatable ribonucleoside enhanced cross-linking and immunoprecipitation (PAR-CLIP) and RNA immunoprecipitation followed by microarray (RIP-ChIP) analysis (Ascano et al., 2012). WGGA is predicted to be targeted by the KH1 domain, while ACUK is the predicted RRE of the KH2 domain. In support of these findings, Tran and others identified an enrichment of ACUG motifs in FMRP targets (Tran et al., 2019). GACR (where R = A/G) RREs have also been identified as putative FMRP target motifs using the *in vitro* RNAcompete method (Ray et al., 2013). In this assay, the FMRP-KH domains were incubated with an assortment of RNAs in molar excess and bound targets were identified via microarray analysis. In 2014, Suhl and others conducted a comparative analysis on published FMRP RNA-target datasets to determine the degree of consensus of RREs enriched in targets identified in these studies (Suhl et al., 2014). Interestingly, they found that GACR was the only RRE enriched in all of these datasets, whereas WGGA was enriched to a lesser degree and only in some of these datasets. ACUK sequences which are found ubiquitously throughout the transcriptome, did not occur with any greater frequency

in FMRP targets in this comparative analysis. These previously identified sequences were pulled further into question by a recent study in 2020 which quantified FMRP-RNA binding affinities via fluorescence anisotropy (Athar and Joseph, 2020). Neither the KH0, KH1, nor KH2 domains were capable of binding the WGGA, ACUK, or GACR RREs, suggesting that the FMRP KH domains may be interacting instead with more complex RREs rather than these short sequence motifs. However, this analysis was performed *in vitro* using minimal FMRP domain-fusions which may not be physiologically relevant.

The lack of consensus between the different binding motifs identified for the KH domains could be due to differences in cell-type specific interactions that are being characterized. FMRP is expressed throughout the body and likely regulates different transcript populations in a cell-type dependent manner. It will be important to identify neuronal transcript targets and RREs identified by these KH domains using more consistent analyses in similar tissue/developmental stages in the future in order to gain a better understanding of their contribution to FMRP-mediated translation repression.

1.1.5.3 FMRP is a nucleocytoplasmic shuttling protein

Within the KH0 domain is a Nuclear Localization Sequence (NLS), which as the name suggests, is important for localizing FMRP to the nucleus (Kenny and Ceman, 2016). FMRP also contains a Nuclear Export Sequence (NES) between the KH2 domain and the C-terminal intrinsically disordered region (IDR), which together with the NLS, permits nucleocytoplasmic shuttling of FMRP (Eberhart et al., 1996). In addition to having a

function within the nucleus, FMRP is better known for its function in shuttling nascent mRNA targets out of the nucleus and into the cytoplasm (Hsu et al., 2019).

1.1.5.4 The C-terminal RGG box confers FMRP-target specificity

Following the NES, mammalian FMRP contains an arginine-glycine-glycine rich (RGG) box within its C-terminal intrinsically disordered region, or IDR (Figure 3A-B). The RGG box is an unstructured RBD that interacts with secondary structures in RNA targets such as stem loops and G-quadruplexes. These RREs are enriched in many FMRP-targets and are speculated to be one of the major features specifying FMRP-targets (Bechara et al., 2009; Brown et al., 2001; Darnell et al., 2001; Phan et al., 2011; Zhang et al., 2014). Interestingly, the RGG domain was recently shown to be important for the localization of transcripts containing G-quadruplex structures within their 3'untranslated regions (3'UTRs) to neurites (Goering et al., 2020). This supports previous findings reporting the enrichment of G-quadruplex structures within 3'UTRs of neuritically localized transcripts (Subramanian et al., 2011). Importantly, while the KH domains are important for translation repression, the RGG box is thought to contribute an mRNA-binding/localization function. However, the RGG domain is weakly conserved in *Drosophila*, and it is unclear whether it is capable of binding to G-quadraplex sequences in flies (Vasilyev et al., 2015).

1.1.5.5 The C-terminal half of FMRP is intrinsically disordered and is capable of promoting liquid-liquid phase separation *in vitro*

IDRs, also termed low-complexity domains (LCDs), are regions within a protein that have low amino acid complexity, and are typically deficient in bulky hydrophobic residues which drive large folding events within proteins (Yang et al., 2019). As such, these domains inherently lack a well-defined structure but are sometimes capable of adopting a 3D structure when the protein is bound to a substrate via other interaction domains. A substantial amount of evidence indicate that these sequences are capable of driving the formation of membraneless organelles (MLOs) in cells via the process of liquid-liquid phase separation (LLPS) (Brangwynne et al., 2009; Shin and Brangwynne, 2017).

LLPS is the reversible process by which a macromolecular solution spontaneously or actively demixes to form two distinct phases that can dynamically exchange material with one another (Berry et al., 2018; Boeynaems et al., 2018). This process can be likened to oil demixing from water and forming a dense liquid oil droplet within the dilute liquid water environment. This biological phenomenon is driven by weak inter- and intra-molecular interactions between proteins and nucleic acids, which upon reaching a "critical threshold" or "saturation limit" undergo a phase transition and form a non-membrane bound droplet (Figure 4A). These droplets have been coined many different names including, but not limited to, granules, bodies, condensates, MLOs, liquid droplets, foci, puncta, assemblies, and bodies. For the sake of simplicity, these will be referred to as "granules" or "MLOs" below. The formation of phase separated granules within a cell

serves as a means for the tight spatiotemporal regulation of diverse biomolecular processes such as ribosome biogenesis (Falahati and Wieschaus, 2017), gene expression (Al-Husini et al., 2018; Molliex et al., 2015), cell differentiation (Liu et al., 2020), and cell receptor assembly and signaling (Banjade and Rosen, 2014; Su et al., 2016).

Many proteins that drive LLPS contain IDRs. IDRs promote phase separation due to their propensity to form weak-intermolecular interactions with RNAs, folded proteins and other IDRs (Protter et al., 2018). The promiscuity of the interactions of IDRs within proteins are suggested to decrease the critical concentration of nucleic acid or protein interactors needed to phase separate, by enhancing the overall strength of multivalent interactions between molecules (Figure 4B) (Protter et al., 2018). Interestingly, IDR-containing proteins are common villains in neurodegenerative diseases due to their propensity to promote liquid-to-solid phase transitions which form pathological protein aggregates or amyloid fibrils (e.g. hnRNPA1, TDP-43 and FUS) (Babinchak et al., 2019; Lin et al., 2015; Molliex et al., 2015; Murthy et al., 2019). When mutated, these phase separating proteins commonly cause dominant-negative phenotypes and form irreversible fibrils or aggregates via homotypic or heterotypic interactions, respectively (Mathieu et al., 2020).

One model describing the composition and dynamicity of phase separated granules describes these structures as containing cores and shells, in which an initially heterogenous granule is remodeled into smaller dense “cores” surrounded by a more dynamic “shell” (Figure 4A) (Jain et al., 2016). This has been described particularly for stress granules

(SGs), but other biological MLOs are likely to be similarly organized. Molecules within the initial granule mature and form more stable interactions, nucleating cores which are synonymous with the immobile fraction of MLOs. This model also predicts that multiple separate cores can exist within a larger granule, all of which are surrounded by a dynamically exchanging shell. This shell contains molecules that make up the mobile fraction of MLOs. It's thought that mutations in stable core constituents may result in the formation of pathological aggregates, contributing to neurodegenerative disease (Lin et al., 2015).

Although IDRs are commonly thought to be the defining feature for a proteins ability to phase separate, multivalency of interaction domains is the actual driver for this process to occur *in vivo* (Boeynaems et al., 2018; Choi et al., 2020; Martin and Holehouse, 2020). The valency, or number of domains capable of undergoing inter- and intramolecular interactions in a protein is directly related to the critical concentration at which LLPS will occur, with a protein of higher valency phase transitioning at lower concentrations than a protein with lower valency (Figure 4B) (Li et al., 2012). Multivalency is crucial for this process by allowing multiple interactions to occur between a single molecule and multiple protein and/or RNA partners, effectively forming a biopolymer, or ribonucleoprotein complex (RNP). These RNPs are then often capable of interacting heterogeneously with other RNPs, greatly increasing protein and nucleic acid concentrations within a particular subcellular location. Upon reaching a particular saturation limit, interacting RNPs spontaneously form a droplet via LLPS.

Interestingly, the entire C-terminal half of mammalian and fly FMRP is intrinsically disordered (Figure 3B) (Tsang et al., 2019). This indicates that the IDR may have a substantial impact on how FMRP interacts with other biomolecules to form MLOs important for regulating gene expression. FMRP is a multivalent protein capable of interacting with DNA, RNA and proteins (Figure 3A. Interestingly, FMRP has been extensively documented as a component of many different phase separated granules within cells that function in modulating RNA translation and stability including: polyribosomes, RNA Processing bodies (P-bodies), SGs, and neuronal granules (NGs) (Barbee et al., 2006; El Fatimy et al., 2016; Gareau et al., 2013a; Stefani et al., 2004). Interestingly, the disordered C-terminus of human FMRP is sufficient to reversibly drive LLPS in a phosphorylation-dependent manner *in vitro* (Tsang et al. 2019). It has been proposed that this may serve as a mechanism for FMRP to regulate activity-dependent translation in neurons (Kim et al. 2019). **However, precisely how FMRP is able to interact with a diverse subset of cytoplasmic granules and what its functions are within them has yet to be elucidated.** In order to gain a better understanding of what the functions of FMRP within biomolecular condensates are, we need to first understand the breadth of known functions that FMRP has in the regulation of gene expression.

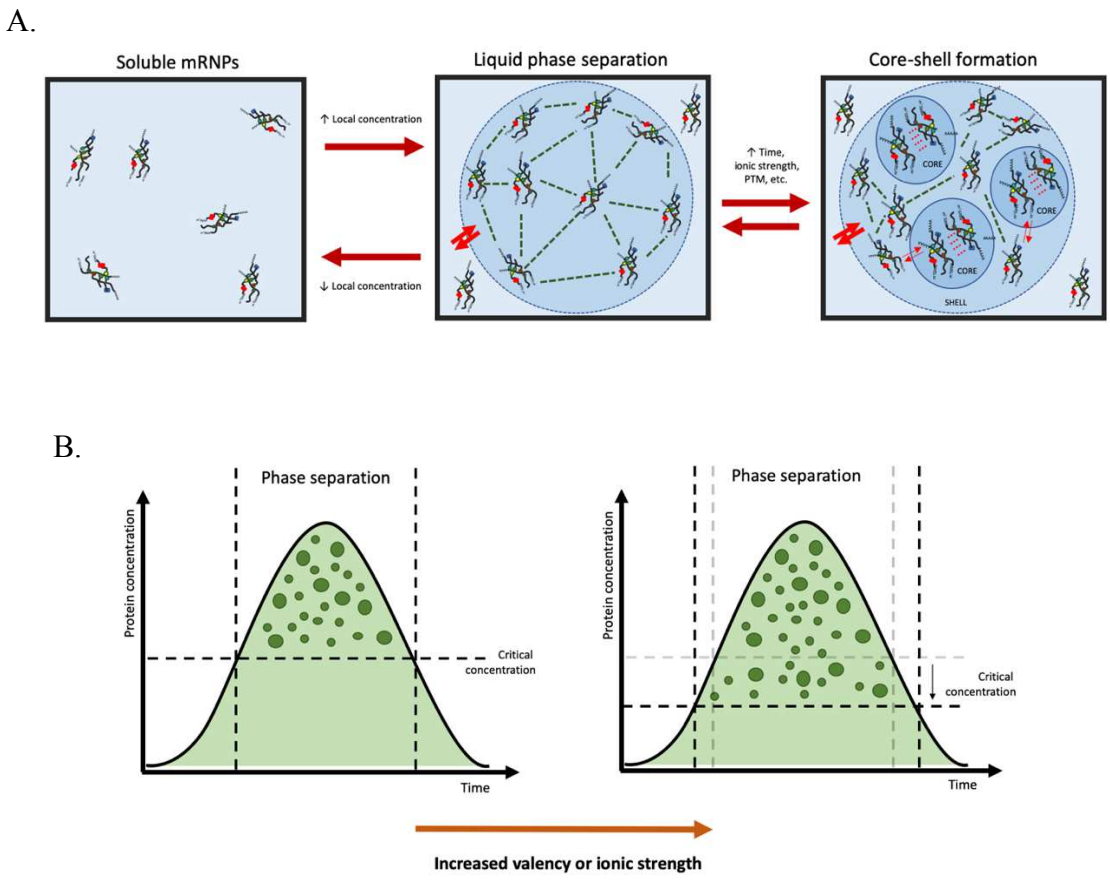

Figure 4. Liquid-Liquid Phase Separation

(A) Left: Proteins and RNAs form mRNP complexes that are soluble within the surrounding dilute liquid environment. Middle: Increased local protein and/or RNA concentration can cause phase separation to occur, forming a dense liquid droplet. These droplets are held together by weak multivalent interactions, are reversible and dynamically exchange with the surrounding dilute phase. Right: mRNP interactions within phase separated granules are capable of maturing over time and form stable cores within a more dynamic shell. These cores are formed by stably interacting mRNPs which minimally exchange with the more dynamic shell. Figure adapted from (Jain et al., 2016) (B) Left: Proteins are evenly distributed in a system and undergo phase separation above a critical concentration, forming liquid droplets. These droplets are stable so long as the protein concentration remains higher than the critical concentration. Liquid droplets dissolve if protein levels drop below the critical concentration. Right: The critical concentration for phase separation is reduced in proteins with higher valency or for proteins that interact more strongly. Figure adapted from (Alberti, 2017).

1.2 FMRP regulates translation and mRNA transport within granules

1.2.1 Models of FMRP-mediated translation regulation

FMRP has a clear function in regulating the translation of many proteins within neurons as indicated by the loss of FMRP causing significant alterations in protein expression (Richter and Zhao, 2021). Strong evidence showing the crucial role of FMRP in translation inhibition was the observation that proteins in FMR1-KO mice incorporated significantly more ^{35}S-methionine, reporting an up to 20% increase in protein synthesis (Dölen et al., 2007; Udagawa et al., 2013). FMRP is further implicated as a translation regulator as it binds over 1,000 transcripts predominantly within their coding sequences (CDS), and is found to be associated with stalled ribosomes in polyribosome fractions (Darnell et al., 2011; Li et al., 2020; Maurin et al., 2018; Sawicka et al., 2019; Das Sharma et al., 2019; Stefani et al., 2004). FMRP regulates mRNA translation and stability in both the pre- and postsynaptic space. These regulated transcripts encode proteins that are important for synaptic transmission, small GTPase signaling, dendritic outgrowth, and ionotropic glutamate receptor activity (Darnell et al., 2011; Tran et al., 2019). Moreover, FMRP is responsible for regulating multiple stages of the mRNA life-cycle including translation initiation and elongation, degradation inhibition, and translation repression of target mRNAs via the microRNA RISC (miRISC) pathway, within messenger RNP (mRNP) granules (Lai et al., 2020; Li et al., 2008; Richter and Zhao, 2021). Below, the focus will be on FMRP functions in repression of translational initiation and elongation, and its regulation of mRNA stability within different populations of mRNP granules.

1.2.1.1 Regulation of translation initiation

As previously mentioned, FMRP is responsible for differentially regulating a large subset of neuronal transcripts, and is able to do so at different points of the mRNA life cycle. Although it is not the major mechanism of FMRP-mediated translation repression, FMRP regulates translation initiation in an activity dependent manner (Napoli et al., 2008). FMRP interacts with the eukaryotic initiation factor 4E binding protein, CYFIP1 (Schenck et al., 2001). CYFIP1 is involved in targeted translation suppression and actin polymerization, two processes important for dendritic spine morphogenesis which is affected in FXS (De Rubeis et al., 2013). Within neurons, FMRP forms an mRNP complex with CYFIP1, and is able to recruit CYFIP1 to specific mRNAs such as the dendritically localized *Arc*, *camkii*, *Map1B*, and *APP* (Napoli et al., 2008). CYFIP1 then binds to the 5' 7-methylguanosine (m^7G) cap binding protein eIF4E, inhibiting the formation of the eIF4F complex at the m^7G cap. Without the eIF4F scaffold the 43S preinitiation complex with the small ribosomal subunit cannot be recruited to the transcript and cap-dependent translation initiation is inhibited (Hinnebusch, 2014). Following activation of mGluR at the PSD, CYFIP dissociates from eIF4E allowing translation to proceed (Napoli et al., 2008). Interestingly, CYFIP1 interacts with multiple genes associated with neurological disorders including ASDs, intellectual disabilities, attention deficit hyperactivity disorder (ADHD), schizophrenia, and Alzheimer's disease (AD), in addition to FXS, implicating its importance in regulating synaptic plasticity (De Rubeis et al., 2013). The FMRP-CYFIP1

initiation suppression complex may function to regulate only a particular subset of genes, as this is not the major mechanism of FMRP-mediated repression (Richter and Zhao, 2021).

1.2.1.2 Regulation of translation elongation

The observation that FMRP is found predominantly within polyribosome fractions and binds transcripts within their CDS, suggests that the major mechanism by which FMRP represses translation occurs at the level of elongation (Shah et al., 2020). Indeed, polyribosome runoff experiments have shown that FMRP associates with mRNAs and blocks ribosomal translocation as evidenced by high levels of ribosome-occupancy on FMRP-bound transcripts following puromycin treatment (Darnell et al., 2011). Puromycin stimulates premature termination of actively translating ribosomes, while having no impact on stalled ribosomes (Stefani et al., 2004). Ribosomal stalling as a mechanism of regulating translation was recently supported in a study showing a reduction of ribosomal pausing on FMRP-regulated transcripts in an *FMR1*-KO mouse model (Das Sharma et al., 2019). Additionally, over 300 mRNAs repressed by FMRP have been found to have increased ribosomal stalling (Shu et al., 2020). Although it's evident that FMRP regulates translation via ribosome stalling, how it's functioning as a molecular brake on specific subsets of neuronal transcripts has been debated throughout the years.

One model predicts that FMRP stalls ribosome translocation by blocking the association of tRNA and other elongation factors with the ribosome (Chen et al., 2014; Richter and Zhao, 2021). Using cryo-EM, the KH domains of *Drosophila* FMRP were

shown to interact directly with the ribosome near the ribosomal P-site, suggesting that it may block the addition of new amino acids to the elongating polypeptide chain (Chen et al., 2014). Additionally, the RGG box in FMRP bound near the A-site of the ribosome. This puts the RGG box in close proximity to putative G-quadruplex secondary structures in target mRNAs where it could be bound to the transcript. From this, it can be inferred that when FMRP is bound to G-quadruplex structures in target transcripts via the RGG-box, it is also able to bind translocating ribosomes via the KH domains and block elongation. However, these FMRP-ribosome interactions were shown *in vitro* and outside of the context of bound mRNA. Further studies on how FMRP interacts with translating ribosomes are required to gain a better understanding of this relationship.

Another model predicts that FMRP sterically hinders translocation via its ability to bind transcripts within and throughout their CDS via optimal codons (Darnell et al., 2011; Richter and Zhao, 2021). Within neurons, FMRP mRNA targets are enriched with optimal codons, which are codons that correspond with highly abundant tRNAs. FMRP preferentially interacts with and stabilizes transcripts with this optimal codons bias (Shu et al., 2020). In support of this model, transcripts with optimal codon bias are disproportionately down-regulated in FMRP-deficient mice (Sawicka et al., 2019; Thomson et al., 2017). It has been predicted that FMRP increases mRNA stability by binding and protecting mRNAs via these optimal codons and blocking an unidentified nuclease from degrading bound transcripts (Shu et al., 2020). However, the mechanism by which FMRP preferentially interacts optimal codons to control these processes has yet to

be elucidated and there are still a lot of questions that need to be answered for this recent model.

In summary, FMRP is able to repress translation of specific subsets of mRNA targets using vastly different mechanisms, which could enable cells to fine-tune expression at different stages in development, in different tissues, or even in spatially distinct areas within the cell (e.g. different populations of granules). However, how FMRP is able to differentially regulate translation is still unknown. We speculate that this is most likely determined by the particular mRNP complex with which FMRP is associated.

1.2.2 Regulation of mRNA in mRNP complexes

From the onset of transcription until decay, mRNAs are painted with RBPs, forming an mRNPs which choreograph mRNA fate within the cell. RBPs interact with transcripts via a number of RNA secondary structures or specific sequences located within the untranslated regions (UTRs), introns and exons. Motifs within the UTRs are typically important for directing cellular localization and increasing mRNA stability (Taliaferro et al., 2016). Interestingly, transcripts enriched within distal axonal and dendritic compartments of neurons, have considerably longer 3'UTRs which offers more RREs for miRNA and RBPs to interact with and promote stabilization during transport (Taliaferro et al., 2016; Tushev et al., 2018). FMRP is found within many different mRNP complexes which differ in protein content and molecular function including polyribosomes, SGs, P-bodies, and NGs. Polyribosomes contain mRNAs, ribosomes, translation factors, and other RBPs that can either promote or repress translation. As previously discussed, FMRP

associates with polyribosomes where it functions in ribosome stalling during translation elongation. Polyribosomes are the major mRNP granule which FMRP localizes to and functions within. However, FMRP is also able to stabilize and translationally repress mRNAs within other mRNP complexes.

1.2.2.1 FMRP promotes stress granule assembly

SGs are a type of MLO that form rapidly in response to cellular stress and contain transcripts that are stalled at the pre-initiation phase of translation. A number of stressors including heat/cold shock, oxidative stress, ER stress, osmotic stress, and UV irradiation can induce the formation of SGs where mRNAs are translationally stalled to reduce energy expenditure from protein production (Protter and Parker, 2016). SGs also serve as dynamic triage units within the cell where the fate of transcripts is determined and mRNAs are directed for repression, degradation, or storage. Depending on the type of stress, transcripts will either be stabilized and translationally repressed until the cell is no longer stressed and re-initiation of translation can resume, or targeted for degradation (Anderson et al., 2015).

FMRP has been identified as a core SG component and may be involved in shuttling translationally repressed transcripts from polyribosomes to SGs (Fu et al., 2020; Mazroui et al., 2002). Although FMRP is not required for SG nucleation, loss of FMRP reduces mRNA localization to SGs and reduces SG assembly (Didiot et al., 2009). FMRP maintains translation repression in its phosphorylated state. Interestingly, phosphorylation of residues within the C-terminal IDR of FMRP promotes its phase separation with CAPRIN1, a protein that promotes SG assembly (Kim et al., 2019). Assembly of the FMRP-CAPRIN1

complex may be a mechanism by which mRNAs are recruited to stress granules. However, the precise function of FMRP within SGs is largely unknown.

1.2.2.2 FMRP interacts with RNA Processing bodies within neurons

FMRP also interacts with P-bodies to regulate mRNAs (Barbee et al., 2006; Cougot et al., 2008; Zalfa et al., 2006). P-bodies are mRNP granules containing nontranslating mRNAs and RBPs involved in deadenylation, 5'→3' mRNA decay, mRNA storage and repression via the RNA-induced silencing complex (RISC) in somatic cells (Anderson and Kedersha, 2006; Standart and Weil, 2018). Some of the core components required for mRNA decay in P-bodies include the deadenylation complexes, decapping enzymes and enhancers of decapping (Coller and Parker, 2005; Eulalio et al., 2007; Ingelfinger et al., 2002; Luo et al., 2018; Parker and Sheth, 2007). In contrast to SGs, ribosomal subunits and most translation initiation factors are absent from these MLOs (Parker and Sheth, 2007; Teixeira et al., 2005). A subset of FMRP localizes to mRNP transport granules structurally related to P-bodies throughout neurons, illustrating yet another mechanism by which FMRP mediates translation repression and transcript stability (Barbee et al., 2006; Cougot et al., 2008). Although FMRP associates with P-bodies, its function within these structures has yet to be elucidated. FMRP associates with miRNAs and several components of the RISC pathway including Ago1, Ago2 and Dicer (Cheever and Ceman, 2009; Jin et al., 2004; Muddashetty et al., 2011). It has been speculated that FMRP may be involved in mediating translation repression in P-bodies via the RISC complex.

1.2.2.3 FMRP regulates RNA transport within neuronal granules

Neurons are able to control individual synaptic processes by fine-tuning the distribution and regulation of mRNAs within synapse-localized neuronal granules (NGs). NGs are a specialized MLO found throughout the brain and are enriched with cytoskeletal proteins, ribosomal subunits, translation regulators, RBPs and translationally repressed synaptic mRNAs (Antar et al., 2005; Banerjee et al., 2018; El Fatimy et al., 2016; Merrill et al., 2005; Miyashiro et al., 2003). Interestingly, in mouse brains these complexes also show a high degree of overlap with polyribosomes suggesting NGs may develop from stalled polyribosomes (El Fatimy et al., 2016).

Densely packaged NGs form within the soma and transport mRNAs in a translationally repressed state through dendrites and axons out to synaptic terminals (Figure 5). Forming a compact granule is necessary to prevent the loss of material due to hydrodynamic drag during rapid, motor-dependent transport through neurites (Alberti, 2017; Brangwynne et al., 2009). NGs are bidirectionally transported via microtubules between the soma and synaptic densities, revealing a recycling mechanism of NG components back to the cell soma, in addition to their delivery out to synapses (Bassell and Warren, 2008). Anterograde transport out to distal neurites occurs via the motor protein kinesin, while retrograde transport is dependent on the dynein motor protein (Carson et al., 2001; Kanai et al., 2004; Otero et al., 2002). At the synapse, NGs are maintained within the synaptic density and disassemble in response to local synaptic activation, permitting rapid protein synthesis in response to an acute stimuli (Buxbaum et al., 2014).

Within neurons, FMRP associates with NGs in the soma, neurites and at synaptic densities and it is proposed that FMRP regulates many mRNA targets within these structures (El Fatimy et al., 2016) However, FMRP occupies only a subset of NGs suggesting it may be essential for the spatiotemporal regulation of particular neuronal mRNAs (Barbee et al., 2006; El Fatimy et al., 2016). FMRP and the *FMR1* mRNA are both found within the PSD, suggesting the necessity for local translation of FMRP at these sites (Antar et al., 2004). Perhaps FMRP is not the major regulator of mRNAs during transport, but is instead required for translation repression out at the synapse. While studies using the MS2-tagging method show a requirement for FMRP in localizing target transcripts out to neurites, others indicate that FMRP is not required for NG transport (Dictenberg et al., 2008; Estes et al., 2008; Kao et al., 2010). Recently, Goering and others showed that the RGG box was required for the localization of mouse FMRP and G-quadruplex containing transcripts out to neurites using subcellular fractionation followed by high throughput sequencing (Goering et al., 2020). As indicated earlier, one of the major cellular defects in FXS is dendritic overgrowth due to aberrant protein synthesis at the synapse. This indicates that transcripts are localized out at synaptic densities even in the absence of FMRP, and that FMRP is not required for mRNA transport within NGs. Altogether, there is a general lack of understanding of what role FMRP has within NGs and how it interacts with these MLOs.

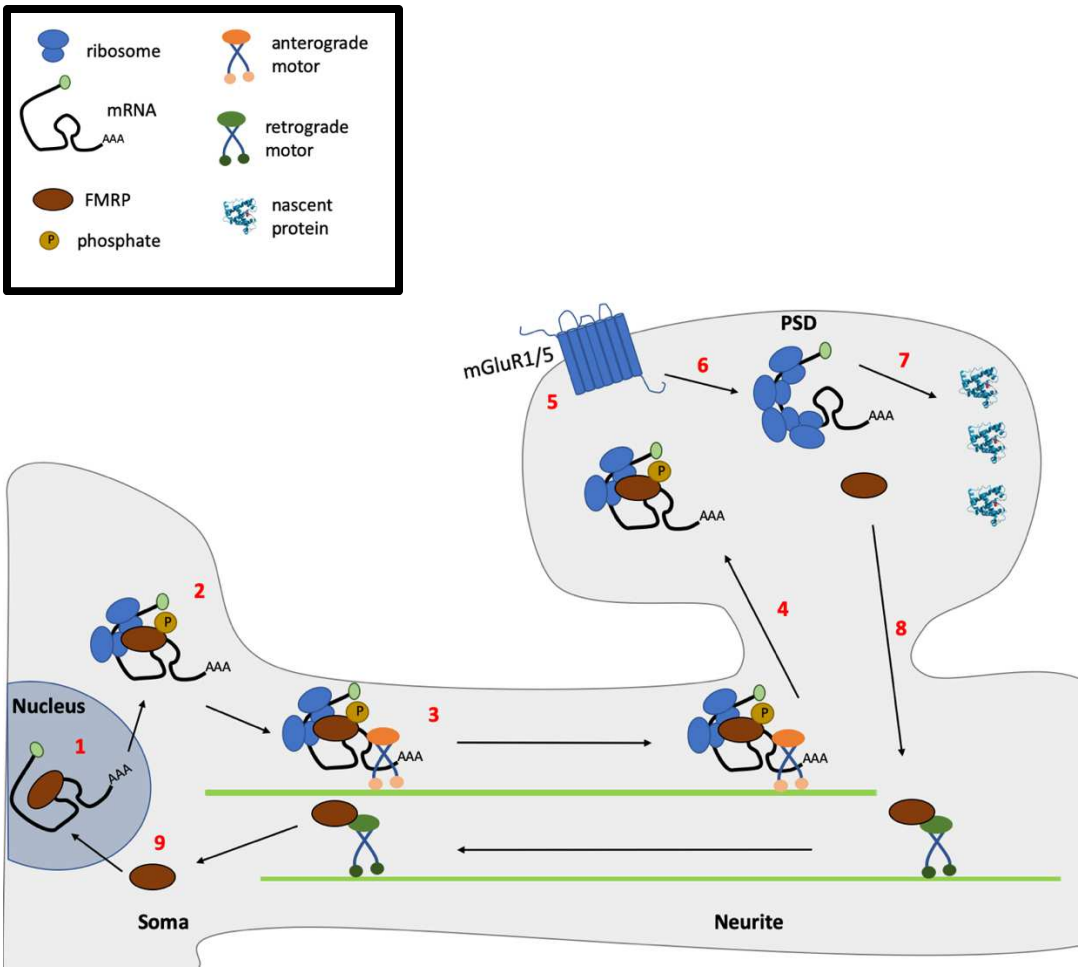

Figure 5. Model for FMRP function in NGs

1) FMRP binds target transcripts within the nucleus forming an mRNP. 2) This mRNP is shuttled out of the nucleus into the soma where ribosomes assemble on mRNAs and translate polypeptides until FMRP is phosphorylated which stalls translation. These translationally stalled complexes can then assemble with motor adaptors and other factors to form a NG. 3) The NG then associates with the kinesin motor protein and is translocated out to distant synaptic densities via microtubules. 4) After reaching a synaptic destination, the NG is released from the motor protein and maintained in the PSD. 5) Upon synaptic activation of the mGluR1/5, 6) FMRP is dephosphorylated and releases translation repression on its target transcript. 7) The transcript rapidly resumes translation, producing nascent protein in an activity dependent manner. 8) FMRP is either retained in the PSD or 9) transported back to the soma via dynein motor proteins. Figure adapted from (Bassell and Warren, 2008).

1.3 Summary

FMRP is an RBP important for regulating >1,000 mRNAs, many of which function in learning and memory formation. Even though its function as a repressor of translation is clear at both the initiation and elongation phase, how it is able to spatiotemporally regulate such a diverse population of transcripts has yet to be elucidated. One of the major cellular functions of FMRP is its ability to interact with distinct phase-separated granules. Organization by phase separation is speculated to be an important cellular phenomenon that allows for the compartmentalization of molecules important for specific processes while still permitting for dynamic exchange with the surrounding environment. The propensity of FMRP to localize to granules suggests that this is important for its function. Whether specific interaction domains of FMRP are required for recruitment to different granules is unknown. The specific RRE identified by the KH domains remains enigmatic, although the ubiquitous short sequences are the most likely candidate. We predict the KH domains are crucial for strengthening overall interactions within FMRP granules via these highly enriched RREs, while more specific interactions are contributed by the other domains. Here we present the **central hypothesis** that the KH domains of FMRP are required for FMRP granule formation. To test this hypothesis, we examine the impact of two FXS-causing missense point mutations in the KH domains on FMRP granule formation and function. We predict that multivalent interactions via these low specificity KH domains, promotes the formation of FMRP-interacting granules and more specifically, FMRP-positive NGs *in vivo*.

CHAPTER TWO: MULTIVALENT INTERACTIONS DRIVE FMRP GRANULE FORMATION IN DROSOPHILA S2 CELL CULTURE

2.1 The FMRP IDR functions cooperatively with the KH domains to form granules

FMRP has been well characterized in its ability to localize to different MLOs including SGs, P-bodies, Fragile X granules (FXGs), and NGs (Barbee et al., 2006; Christie et al., 2009; Gareau et al., 2013a; Lee et al., 2010; Li et al., 2009). Like human FMRP, the entire C-terminus of *Drosophila* FMRP is predicted to be disordered (Figure 3B). IDRs within RBPs have been shown to drive the formation of granules through the process of LLPS. Although the IDR of FMRP has been shown to promote droplet formation *in vitro,* the dependency of the IDR in granule formation *in vivo* has yet to be elucidated (Tsang et al., 2019). More specifically, little is known about what role the IDR plays in the context of the other RBDs in the ability of FMRP to localize to or form granules. To address this question, we first constructed a series of IDR and KH domain mutants with an N-terminal EGFP-tag (Figure 6A). We then expressed these constructs in transiently transfected *Drosophila* Schneider 2 (S2) cells to determine how they impact FMRP granules.

Similar to what has previously been shown by others, our EGFP-FMRP (WT-FMRP) construct forms numerous, characteristically small, spherical granules (Figure 6B; Gareau, Martel, et al. 2013; Gareau, Houssin, et al. 2013). We were initially interested in determining if the IDR of fly FMRP, referred to here as IDR, was necessary and sufficient to drive the formation of FMRP granules in S2 cells. As with its human ortholog, the IDR was sufficient to induce FMRP granules in transfected cells (Figure 6C). Interestingly, expression of the IDR alone is not capable of forming granules in all cells, with IDR-granules forming in approximately 25% fewer cells than WT-FMRP. This suggests that other domains within the N-terminus of FMRP likely contribute to the formation of (or the interaction with) granules *in vivo*. In support of this hypothesis, the structured N-terminus of FMRP (ΔIDR), which contains the DNA-binding tandem Tudor domains and the three protein- and RNA-binding KH domains, is also capable of forming granules, albeit at a significantly lower frequency (~26%). Interestingly, ΔIDR was able to form granules even at lower expression levels than WT-FMRP (Figure 6D). It's important to note, that we cannot conclude whether this indicates that FMRP is able to form granules without the IDR or if this construct is able to interact with already formed FMRP granules (or another MLO) via its N-terminal functional domains. Regardless, the loss of the either the N- or C-terminal domains significantly reduces the formation of FMRP granules *in vivo*.

Based on these observations, we speculated that the two major RBDs within the N-terminus, KH1 and KH2, may play an important role in promoting the formation of FMRP granules by working in cooperation with the IDR, as multivalent interactions are what drive

LLPS in the cellular context. Indeed, we found that by adding back both KH domains (KH+IDR) this granule phenotype was rescued, with over 90% of cells forming granules (Figure 6C). These data support recent evidence suggests that although IDRs are important for the biogenesis of MLOs, multivalent interactions contributed by other interaction domains is required for more physiological granule formation (Banani et al., 2016). More specifically, this suggests that the KH1 and KH2 domains cooperate with the IDR to form FMRP granules, *in vivo*.

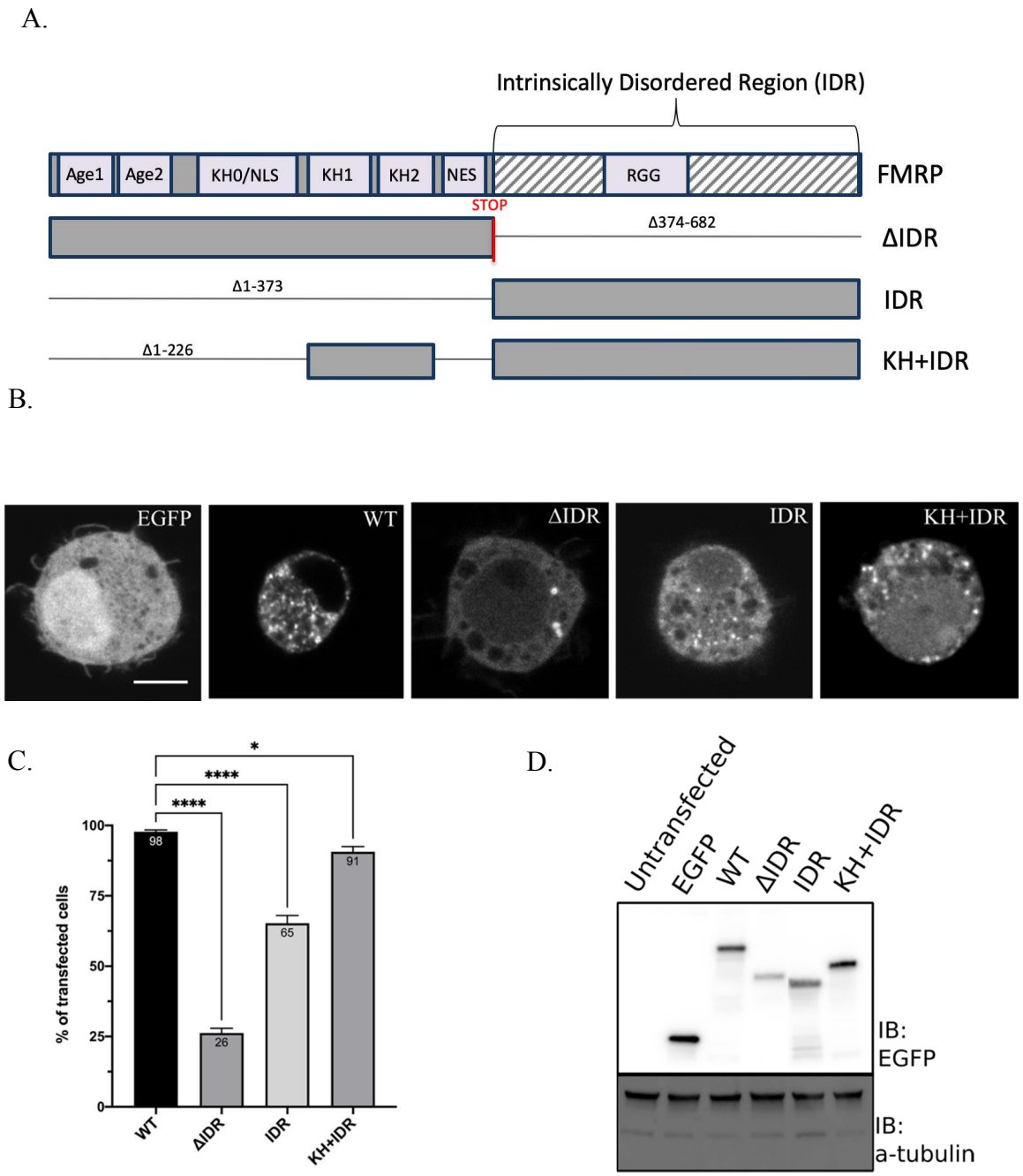

Figure 6. The IDR functions cooperatively with the KH domains to form FMRP granules in S2 cells

(A) Schematic of FMRP showing each of the RBDs in light blue boxes and its IDR which is indicated by grey and white stripes (top). IDR mutants that were made in this study are shown below WT-FMRP and amino acid deletions are annotated with thin lines. Premature stop codon was added before the IDR domain (amino acids 374-682) in ΔIDR construct. For IDR, the first 373 amino acids were deleted from FMRP. Both KH1 and KH2 domains are fused to the IDR in the KH+IDR mutant. The first 226 amino acids up to KH1 domain were deleted as well as the region between the KH2 and IDR domains (336-373). Each of these constructs were made within an N-terminally tagged EGFP vector. (B) Representative images of EGFP-FMRP mutant granule phenotypes in S2 cells. These images show the major FMRP phenotype produced by these mutants. Scale bar: 2μm. (C) Quantification of the percentage of transfected cells forming FMRP granules (mean ± S.E.; n≈100 cells in triplicate). (D) Western blot analysis of *EGFP* protein levels in untransfected cells or cells transiently transfected EGFP and EGFP-FMRP mutant constructs. *α-tubulin* was used as a loading control. IB= immunoblot. Statistical analysis was done by ordinary one-way ANOVA followed by Holm-Šídák's multiple comparisons test.

2.2 FXS-causing missense mutations in the KH domains disrupt granule formation

Disease-causing missense mutations in the KH1 and KH2 domains of hsFMRP (Gly266Glu and Ile304Asn, respectively) are predicted to disrupt proper folding of KH domains via steric disturbance. Disruption of protein structure by these mutations results in the loss of several important FMRP functions including mRNA-binding, AMPA receptor trafficking and polysome association (Darnell et al., 2005; Myrick et al., 2014; Valverde et al., 2007). To better understand what role(s) the KH1 and KH2 domains have in FMRP granule formation, we made the analogous point mutations in the evolutionarily conserved residues of the *Drosophila* FMRP ortholog, Gly269Glu and Ile307Asn, hereafter referred to as KH1* and KH2*, respectively (Figure 7A) (Valverde et al., 2007).

First, we transfected S2 cells with these EGFP-tagged point mutants to see what impact this had on FMRP granule formation (Figure 7B). Interestingly, we observed a two-fold decrease in the ability of cells transfected with KH1* to form granules, while KH2* had no effect (Figure 7C). This suggests that the KH1, but not the KH2 domain, is required for *de novo* assembly or recruitment to pre-existing granules. We also saw a significant reduction in the ability to form granules in cells expressing the KH1*KH2* double mutant which disrupts both KH domains. KH1*KH2* did not have as robust of an effect on granules as KH1*, instead representing an intermediate between the mutants. Higher local concentrations of protein drive granule formation, and lower expression of the KH1* and KH1*KH2* mutants could explain why we saw fewer granules in these cells (Bolognesi

et al., 2016; Li et al., 2012). However, these mutants were each expressed at similar levels suggesting this is not the reason we see fewer granules in these mutants (Figure 7D).

As a control, we also made a construct called ΔKH in which both the KH1 and KH2 domains were removed (Figure 7A). This has been used in previous studies looking broadly at the role of functional domains in FMRP granule formation and dynamics in S2 cells (Gareau et al. 2012). Consistent with published results, ΔKH had no effect on the ability of FMRP to form granules *in vivo* (Figure 7C). Together, these data suggest that the KH1, but not KH2, domain is required for FMRP granule formation in S2 cells.

A.

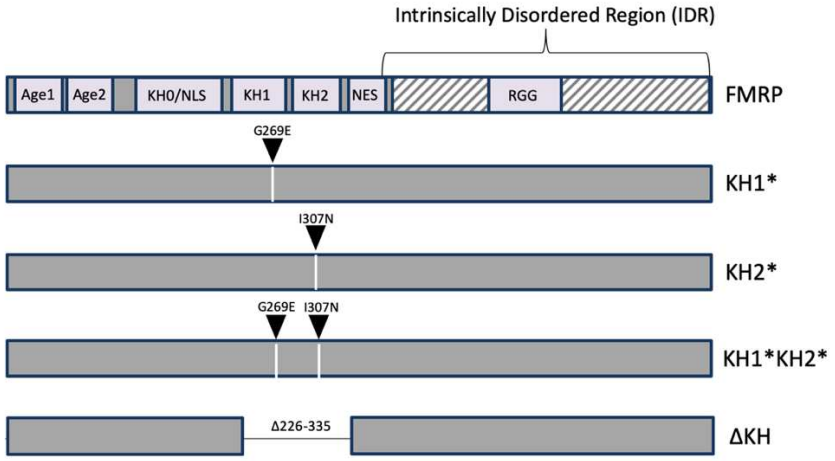
Intrinsically Disordered Region (IDR)
Age1
Age2
KH0/NLS
KH1
KH2
NES
RGG
FMRP
G269E
KH1*
I307N
KH2*
G269E
I307N
KH1*KH2*
Δ226-335
ΔKH

B.

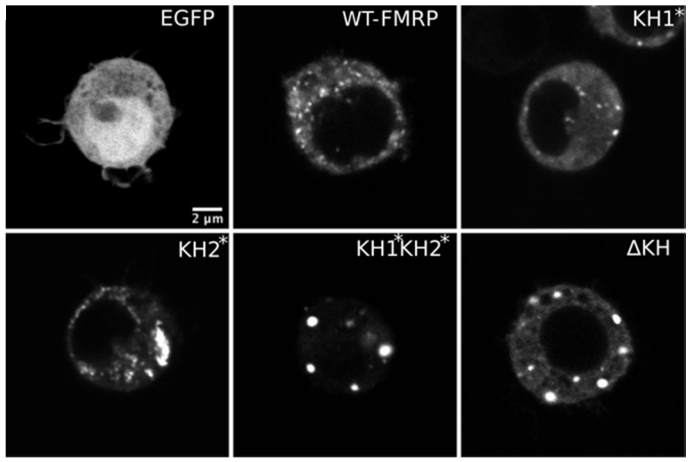
EGFP
WT-FMRP
KH1*
2 μm
KH2*
KH1*KH2*
ΔKH

C.

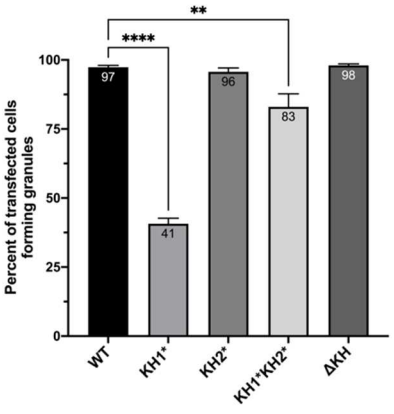
**
****
Percent of transfected cells forming granules
100
75
50
25
0
97
41
96
83
98
WT
KH1*
KH2*
KH1*KH2*
ΔKH

D.

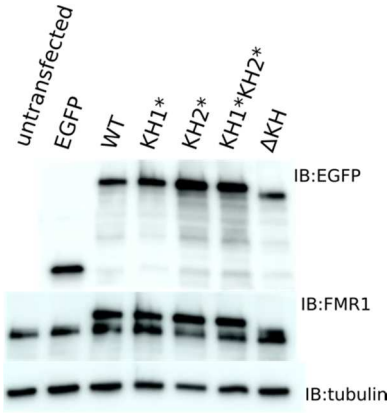
untransfected
EGFP
WT
KH1*
KH2*
KH1*KH2*
ΔKH
IB:EGFP
IB:FMR1
IB:tubulin

Figure 7. The KH1 FXS-causing point mutation disrupts FMRP granule formation

(A) Schematic representation of FMR1 variants used in this study. Arrow heads point to location on a Drosophila melanogaster FMRP protein where the analogous FXS-causing missense mutation is located at the conserved residues. Deletion of the two adjacent KH domains is annotated with a break in the FMR1 gene between amino acids 225-236. (B) Representative confocal images of transiently transfected EGFP or EGFP-FMRP constructs in S2 cells. Scale bar: 2μm. (C) Quantification of the percentage of transfected S2 cells that formed EGFP-FMRP granules. Average is shown in the top of each bar (mean ± S.E.; n≈100 cells in triplicate). (D) Western blot analysis of *FMR1* and *EGFP* protein levels in untransfected cells or cells transiently transfected EFGP and EGFP-FMRP mutant constructs. *α-tubulin* was used as a loading control. IB= immunoblot. Statistical analysis was done by ordinary one-way ANOVA followed by Holm-Šídák's multiple comparisons test.

In addition to differences in their ability to form granules, we noticed distinctive morphological phenotypes in several of our constructs. We classified these morphological differences into two categories: 1) "normal" granules, which were generally round in shape with diameters of ~ 200-1,000 nm, and 2) amorphic granules, which were considered to be any type of non-round granule. Although each construct could induce the formation of amorphic granules, this typically occurred in less than 10% of cells (Figure 8A-B). EGFP-tagged IDR, KH+IDR, KH1*, KH1*KH2*, and ΔKH resulted in the formation of granules that were morphologically indistinct from WT-FMRP granules. In contrast, 70% of ΔIDR (Figure 8A) and ~ 50% of KH2* (Figure 8B) granule forming cells contained amorphic granules that took up large volumes within the cell, oftentimes with diameters greater than 1,000 nm. This suggests that the IDR and KH2 domain may be involved in forming interactions with additional factors that restrict the size and shape of FMRP granules. Interestingly, round granules in KH1*KH2* and ΔKH were very large, reminiscent of liquid-like droplets that have fused into larger structures (Figure 7B) (Brangwynne et al., 2009). This further suggests that the KH domains may be regulating granule size in S2 cells.

We also noticed differences in the number of granules present within these cells which led us to quantify the average number of granules each mutant was able to form. To our surprise, neither the IDR (Figure 8C) or KH mutants (Figure 8D) were able to recapitulate WT granule numbers, with an at least three-fold reduction in each mutant. However, KH2* formed more granules than any of the other constructs. This further

indicates that this mutation does not substantially impact FMRP granule formation *in vivo* (Figure 8D). Altogether, these data suggest that the KH domains and IDR are cooperating to regulate FMRP granule formation *in vivo*. Loss of any single domain alters but does not abrogate granule formation, morphology or number, suggesting that FMRP granule formation is dependent on multivalent interactions.

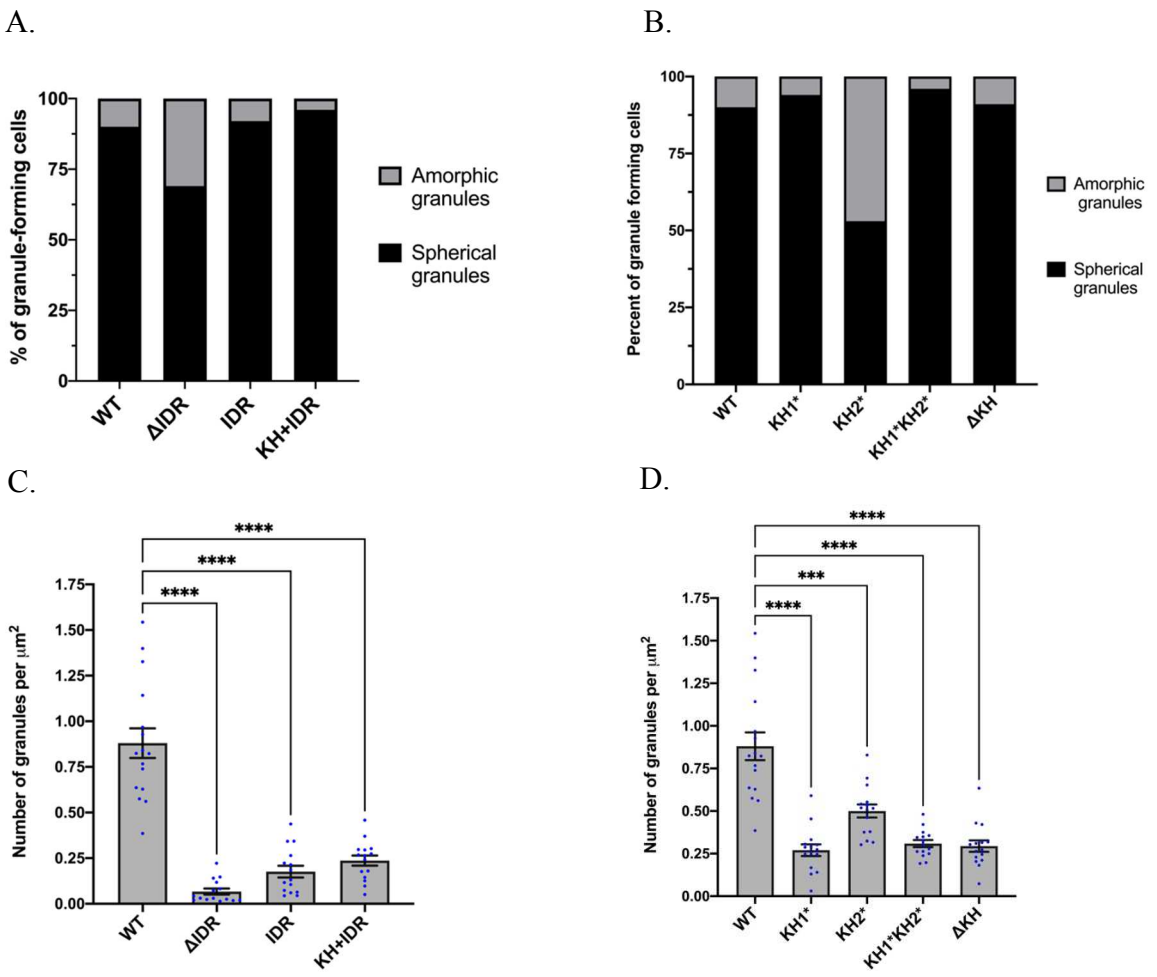

Figure 8. The KH2 domain and IDR regulate FMRP granule morphology

Comparisons of the two major morphological phenotypes observed in the (A) FMRP-IDR mutants and the (B) FMRP-KH mutants. Spherical granules (black bars) were always present in cells, although some also coincided with non-spherical, amorphic granules (grey) that often took up much larger volumes of the cell. Cells were categorized as amorphic if at least one granule within the cell was amorphic. A small percentage of all cells formed amorphic granules. Spherical granules ranged in size from ~200-1,000 nm (n=100 cells). Comparison of the average number of granules per cell in the (C) FMRP-IDR mutants and the (D) FMRP-KH mutants, normalized to cell area, μm^2 (mean ± SE; n=15 cells). Statistical analyses were done by Brown-Forsyth ANOVA followed by Dunnett's T3 multiple comparisons test.

2.3 The IDR promotes FMRP-core formation, while the KH domains alter the dynamics of the outer shell in FMRP granules

Thus far, we have demonstrated that the formation of FMRP granules is driven, in part, by multivalent interactions involving the modular N-terminal RBDs and the C-terminal IDR. FMRP is able to undergo LLPS *in vitro* (Tsang et al., 2019). FMRP granules in our study share some classic features with phase separated droplets. Droplets are characterized by forming round structures, which we see with our FMRP granules (Figure 6A & 7A). Another common feature is their propensity to coalesce into a single larger droplet upon contact with one another (Brangwynne et al., 2009). Although FMRP granules move throughout the cell and come into contact with one another, we rarely saw them remain fused together, and rather would interact briefly and then split off (data not shown). Liquid droplets are also characterized by their dynamic ability to rapidly reorganize and exchange with their surrounding environment (Shin and Brangwynne, 2017). It has previously been shown that deletion of the KH domains in FMRP significantly reduces the ability of FMRP to exchange between granules and the cytosol (Gareau et al., 2013b). Thus, we predicted that one important function for the individual KH domains may be to modulate FMRP granule dynamics (Goering et al., 2020; Tsang et al., 2019).

To study the dynamics of FMRP in granules in transfected S2 cells, we conducted Fluorescence Recovery After Photobleaching (FRAP) experiments. First, we examined the independent and collaborative roles of the IDR and KH domains in FMRP granules dynamics. Interestingly, WT-FMRP formed relatively stable granules (Figure 9A). The

IDR and ΔIDR in contrast rapidly recovered their exchangeable pools, suggesting that domains within the N-terminus and C-terminus may somehow cooperate to stabilize WT granule dynamics (Figure 9A-D). In support of this, fusing the KH domains to the IDR helped stabilize granule interactions, recovering somewhat more slowly following photobleaching (Figure 9A-B and 9D). However, these granules were still significantly more dynamic than WT, suggesting additional N-terminal domains are also contributing to stabilizing FMRP-interactions within granules.

A current model suggests that membraneless SGs are made up of stable cores from which there is little or no exchange, and are surrounded by a highly exchangeable shell-like structure (Jain et al., 2016). In FRAP experiments, it is predicted that proteins within the non-recovering immobile fraction represent stable cores, whereas the mobile fraction represents the dynamic shell (Figure 4C). Approximately 30% of WT makes up these stably interacting cores, while the other ~70% resides within the exchangeable pool (Figure 9C). In the IDR only, FMRP shifts significantly into the exchangeable pool. The mobile fraction for IDR (86.4%) is significantly larger than WT and adding the KH domains back does not increase core occupancy (86.5%) (Figure 9C). Interestingly, the immobile fraction is completely absent in ΔIDR (Figure 9C). These data suggest that the ΔIDR granules that form are completely lacking the stable core associated with WT-FMRP granules.

In addition to a large immobile pool, the mobile fractions within WT granules have a relatively slow recovery time (recovery half-time or $t_{1/2}$= 12.1s; Figure 9D). The IDR and ΔIDR formed granules that shared ~ 10-fold more rapid exchange rates ($t_{1/2}$= 1.7s and 1.6s,

respectively). KH+IDR significantly increased recovery time ($t_{1/2}$= 3.6s) relative to the IDR and ΔIDR, suggesting the KH domains are contributing some stability to interactions within the dynamic shell of FMRP granules. Altogether, these data support the hypothesis that the IDR and KH domains are collectively contributing to granule stability.

A.

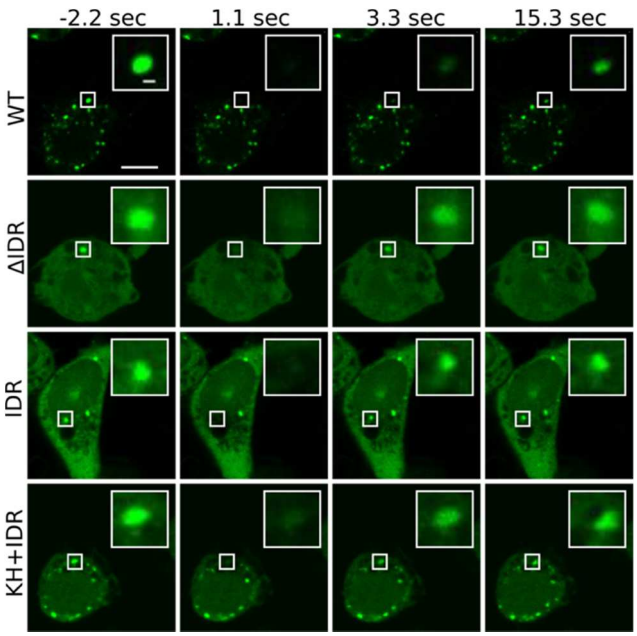
-2.2 sec
1.1 sec
3.3 sec
15.3 sec
WT
ΔIDR
IDR
KH+IDR

B.

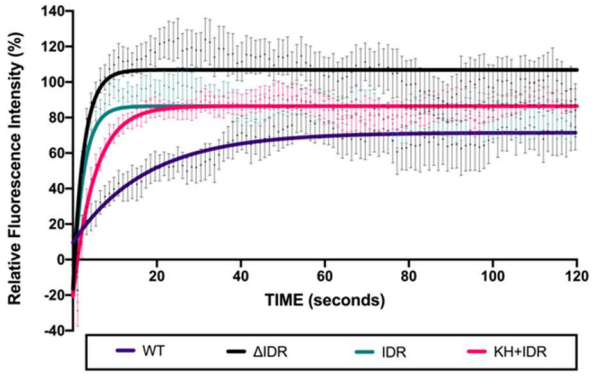
Relative Fluorescence Intensity (%)
TIME (seconds)
WT
ΔIDR
IDR
KH+IDR

C.

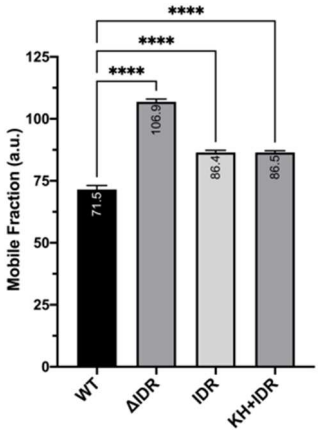
Mobile Fraction (a.u.)
71.5
106.9
86.4
86.5
****
WT
ΔIDR
IDR
KH+IDR

D.

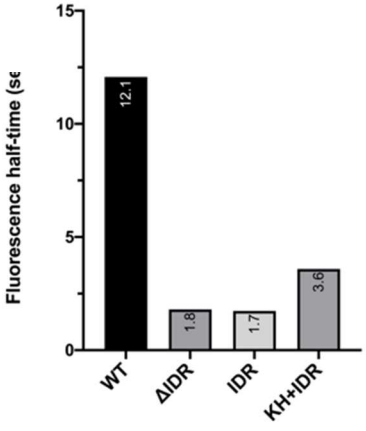
Fluorescence half-time (se
12.1
1.8
1.7
3.6
WT
ΔIDR
IDR
KH+IDR

Figure 9. Loss of the IDR abolishes the immobile fraction of FMRP granules

Representative time-lapse images of FMRP-mutant FRAP pre-bleach and at 1, 3 and 15 seconds following the bleaching event. Scale bar in whole cell image: 5μm. Scale bar in zoomed in granule image: 0.5μm. Images show differences in recovery rates in the first 15 seconds of recovery. (B) Nonlinear one-phase association curves of FRAP experiments representing fluorescence intensity of granules relative to initial intensity over 120 seconds (mean ± SE; n=17-23 granules). Figure legend on the bottom indicate the different mutants. (C) Comparison of the average mobile fraction of FMRP mutant granules. Average mobile fraction for genotype is annotated at the top of each bar (mean ± SE; n=17-23 granules). a.u.=arbitrary units. (D) Quantification of the average time for granules to recover half their mobile fraction, or final intensity in seconds. Average $t_{1/2}$ is annotated at the top of each bar (n=17-23 granules). Statistical analyses were done by Brown-Forsyth ANOVA followed by Dunnett's T3 multiple comparisons test.

We next wanted to determine how the KH point mutants affected FMRP granule dynamics, predicting that they may contribute to FMRP exchange rates. To test this, we analyzed dynamics of the KH1* and KH2* mutants in S2 cells using FRAP. Mutating either or both of the KH domains caused FMRP granules to recover much more rapidly than WT, similar to the IDR and ΔIDR mutants (Figure 10A-B). Notably, ΔKH had the opposite effect and significantly reduced exchange rates of the mobile pool, similar to what has been previously shown (Figure 10B; Gareau, Martel, et al. 2013). The immobile fractions of KH1* and KH2* FMRP granules were no different from WT, whereas *KH2* reduced the exchangeable pool roughly 15%, similar to ΔKH (Figure 10C). This suggests that disruption or deletion of both KH domains severely disrupts FMRP granule dynamic, potentially in a non-physiological manner. As expected, KH1* and KH2* impacted the rate of recovery of the dynamic shell which recovered much more rapidly ($t_{1/2}$= 4.3 and 13.1s for KH1* and KH2*, respectively), than WT ($t_{1/2}$= 21.9s; Figure 10D). This supports our previous findings that the KH domains function in stabilizing homotypic or heterotypic interactions between FMRP and constituents of the mobile fraction of granules. As with granule formation (Figure 7C), the effects of the KH1* and KH2* mutations do not appear to be additive, as KH1*KH2* represents an intermediate between the individual mutations (Figure 10D). Collectively, these data are consistent with the model suggesting multivalency is the driving force underlying granule formation and that reducing valency of FMRP increases dynamics by destabilizing overall protein interaction strength (Shin and Brangwynne, 2017). Most notably, we provide evidence showing that not all interaction

domains are created equal in FMRP, and the KH1 and IDR are more essential for this process.

A.

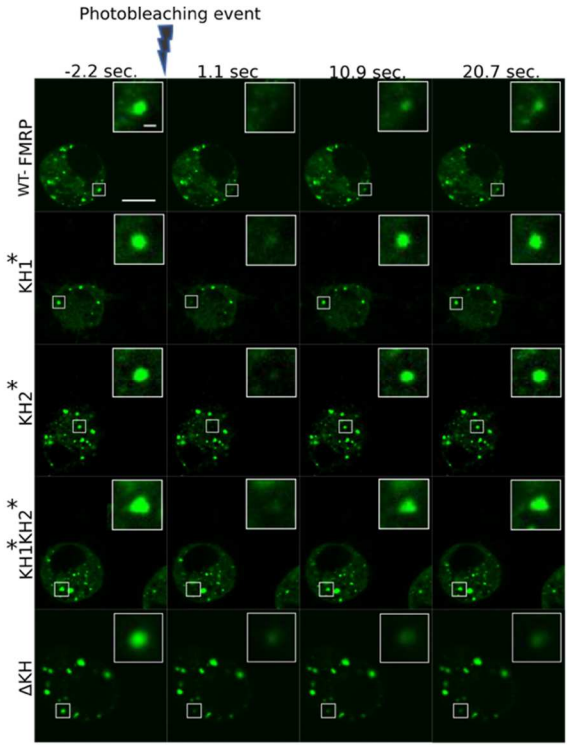
Photobleaching event
-2.2 sec.
1.1 sec.
10.9 sec.
20.7 sec.
WT- FMRP
KH1*
KH2*
KH1*KH2*
ΔKH

B.

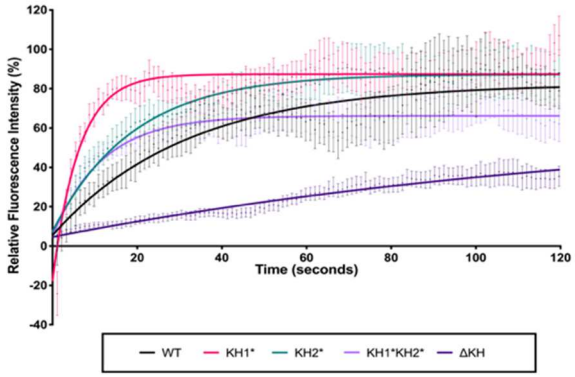
Relative Fluorescence Intensity (%)
Time (seconds)
WT
KH1*
KH2*
KH1*KH2*
ΔKH

C.

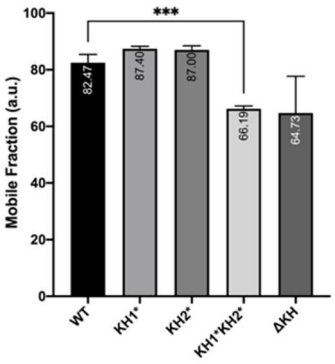
***
Mobile Fraction (a.u.)
82.47
87.40
87.00
66.19
64.73
WT
KH1*
KH2*
KH1*KH2*
ΔKH

D.

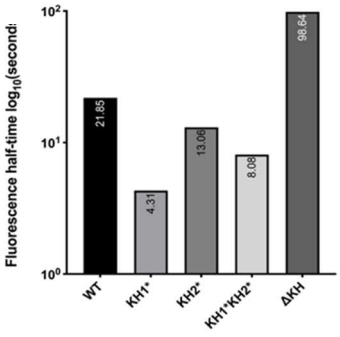
Fluorescence half-time log10(second
21.85
4.31
13.06
8.08
98.64
WT
KH1*
KH2*
KH1*KH2*
ΔKH

Figure 10. FXS-causing point mutants increase the exchange rate of mobile fraction in FMRP granules

(A) Representative time-lapse FRAP images showing differences in recovery rates between WT, FXS-causing point mutations and ΔKH up to 20 seconds following the photobleaching event. Scale bar in whole cell: 5μm. Scale bar in zoomed-in granule image: 0.5μm. (B) Nonlinear one-phase association regression recovery curves of FMRP-mutants representing fluorescence intensity of granules relative to initial intensity over 120 seconds (mean ± SE; n=17-21 granules). (C) Average mobile fraction of FMRP mutant granules (mean ± SE; n=17-21 granules). a.u.=arbitrary units. (D) Quantification of the average time in $\log_{10}$(seconds), it takes for granules to recover half of their exchangeable pool. Average $t_{1/2}$ is annotated at the top of each bar (n=17-21 granules). Statistical analyses were done by (C) Brown-Forsyth ANOVA followed by Dunnett's T3 multiple comparisons test.

2.4 FXS-causing mutations alter the liquid-like nature of stress granules

FMRP is a constituent of several different RNP populations in cells including P-bodies and SGs (Kapeli and Yeo, 2012; Sossin and DesGroseillers, 2006). As we show above that the KH domains regulate FMRP granule formation and dynamics, we were curious whether the disease-causing mutations in the KH domains had an effect on the interaction of FMRP with these RNP populations or on their formation.

To examine interactions with SGs, we co-transfected S2 cells with EGFP:FMRP constructs and mCherry-tagged Rasputin (Rin), the fly ortholog of G3BP1, a highly conserved SG marker (Yang et al., 2020). First, we were interested in whether KH1* and KH2* induced SG formation prior to the introduction of a stressful stimuli. We found that a subset of cells formed SGs prior to the introduction of a stressor in all cases, which is likely the result of Rin overexpression, which is known to induce SG formation (Matsuki et al., 2013) (Figure 11A-B). Strikingly, we noticed that all cells forming KH1* granules significantly overlapped with the population of cells forming SGs (Figure 11A). While each of the FMRP constructs usually overlapped with the Rin granules, KH1* granules only formed when Rin granules were also present. Due to diffuse cytoplasmic staining in unstressed cells overlapping with punctate granules, quantifying this was not possible (data not shown). This suggests that KH1* preferentially localizes to pre-formed SGs and is likely dysfunctional in its ability to assemble granules on its own.

To see if these mutants altered the liquid-like properties of SGs that formed in unstressed cells, we quantified the number of cells that formed Rin-positive SGs after

treatment with 1,6-hexanediol (Figure 11B). 1,6-hexanediol is an aliphatic alcohol that disrupts weak hydrophobic protein-protein (π-π) and protein-RNA (π-cation) interactions required to form dynamic MLOs (Itoh et al., 2021; Kroschwald et al., 2015, 2017). Overexpressing Rin and FMRP induced SG formation in approximately 20% of transfected cells and similar results were observed with KH1*, KH2*, KH1*KH2*, and ΔKH (Figure 11B, left). Interestingly, the population of Rin-positive granules observed in these cells did not disappear after treatment with 1,6-hexanediol, suggesting these non-stress-induced SGs are less liquid-like in nature, and may be forming stable structures (Figure 11B, right). Although this may be indicative of the overexpression of Rin or the FMRP constructs as causing aggregate formation in a small subset of cells which could be toxic, it's likely to be mild as these cells showed no significant defects in viability (Figure 11D).

To gain further insight into the biophysical properties of FMRP granules, we treated co-transfected cells with 1,6-hexanediol and looked at the impact on FMRP (Figure 11C). As expected WT, KH1* and KH2* mutant FMRP granules readily dissociated upon treatment, suggesting that they are forming liquid-like assemblies in S2 cells (Figure 11C-right). However, ΔKH and KH1*KH2*, do not show as robust of a response to 1,6-hexanediol implying that these are forming granules with solid-like characteristics. These results support our FRAP data and indicate that ΔKH, and to a lesser extent KH1*KH2*, is inducing the formation of non-physiological solid-like aggregates in cells and are not behaving similarly to the single missense mutations.

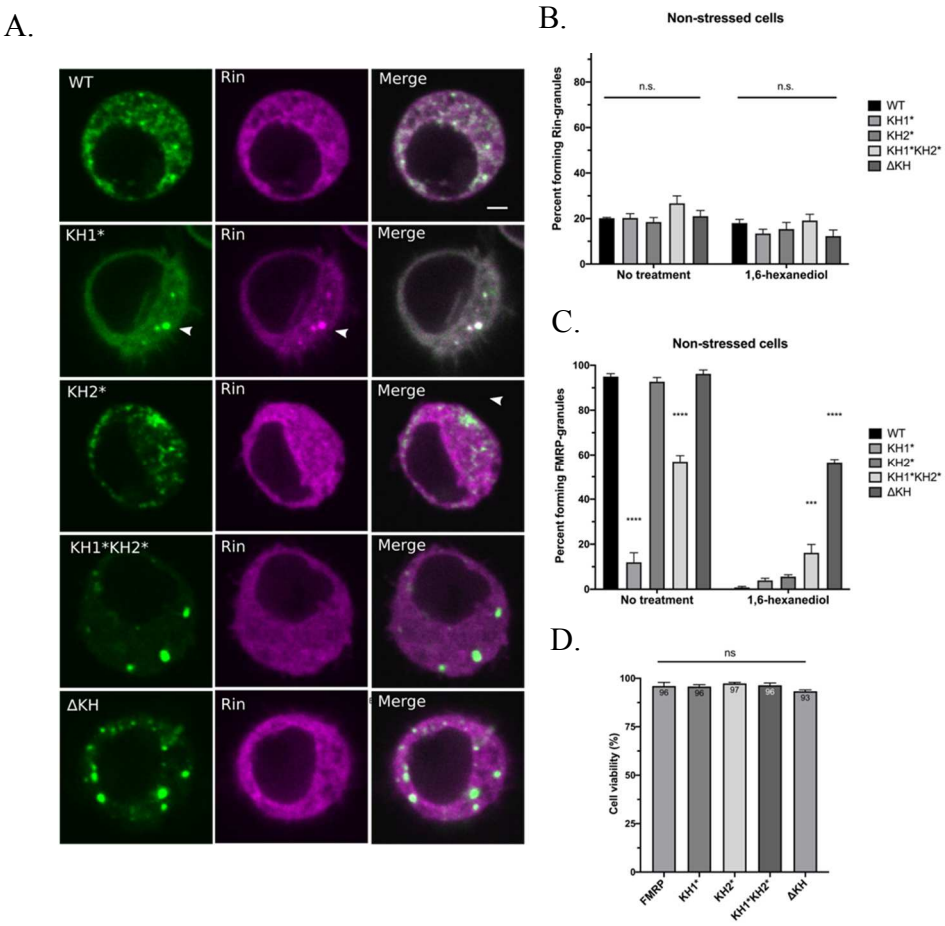

Figure 11. KH1* is only capable of interacting with pre-existing Rin+ SGs

(A) Representative images of the intracellular localization of transiently transfected FMRP mutants (green) and Rin (magenta). Constructs shown are indicated in the top left corner of each image. FMRP and Rin merged images are shown in the right column. White arrowheads point to colocalized FMRP and Rin granules which only occurred in KH1*. Scale bar: 2µm. Comparison of the percent of co-transfected cells forming (B) Rin-granules or (C) FMRP granules without (left) or with (right) the addition of 10% 1,6-hexanediol. Cells were incubated with 1,6-hexanediol or with media (no treatment) for up to 20 minutes to count the number of cells forming granules. Approximately 100 cells were manually analyzed in triplicate for each genotype per treatment group and compared to WT (mean ± SE). (D) Trypan Blue stain was used to determine percent viability of cells ectopically expressing each of the FMRP-mutants in triplicate (mean ± SE). Statistical analyses were done by (B-C) ordinary two-way ANOVA followed by a Šídák's multiple comparisons test and (C) ordinary one-way ANOVA followed by Holm-Šídák's multiple comparisons test.

FMRP is a core component of SGs and has been shown to readily shift into SGs following stress induction (Gareau et al., 2013a). As expected, under arsenite-induced stress, we see that most of the FMRP and Rin proteins shift out the cytoplasm and sink into granules (Figure 12A). Rin almost always overlapped with WT, KH1*, KH2*, and KH1*KH2* while ΔKH modestly reduced this colocalization (Figure 12B). These data suggest the KH domains are not required for FMRP localization to SGs. However, co-transfection with KH1* or KH2* modestly but significantly reduced arsenite-induced SG formation (Figure 12C, left). Moreover, dissolution of these SGs following 1,6-hexanediol treatment was significantly reduced in these mutants, revealing that the KH mutations are shifting these SGs from liquid-like to more solid structures (Figure 12C, right). Together, these data suggest that SG dynamics are significantly impacted by these FXS-causing point mutations.

We next asked whether these mutations altered how FMRP associated with arsenite-induced SGs. Although stress is not required to induce the formation of FMRP granules, it shifts FMRP from the cytoplasm, polyribosomes, or other RNPs into SGs (Gareau et al., 2013a). Interestingly, fewer cells expressing KH1* and KH1*KH2* formed FMRP granules in response to arsenite stress compared to WT (Figure 12D, left). This is consistent with the reduced ability of KH1* to form granules in unstressed cells. As with Rin-positive granules, FMRP granules in stressed cells did not dissolve as readily when treated with 1,6-hexanadiol suggesting that they are forming solid-like structures (Figure 12D, right). KH1*, KH1*KH2*, and ΔKH granules most notably only mildly dissolved

following the addition of 1,6-hexanediol (Figure 12D). This further implicates the KH domains in initiating the transition from a liquid to a solid-like assembly, particularly in the case of ΔKH granules. Altogether, these data show that while the KH domains are not required for SG formation or FMRP recruitment to SGs, they contribute important dynamic interactions within these structures, as mutating either or both KH domains causes both SGs and FMRP granules to transition from dynamic liquid-condensates to more stable solid-like structures.

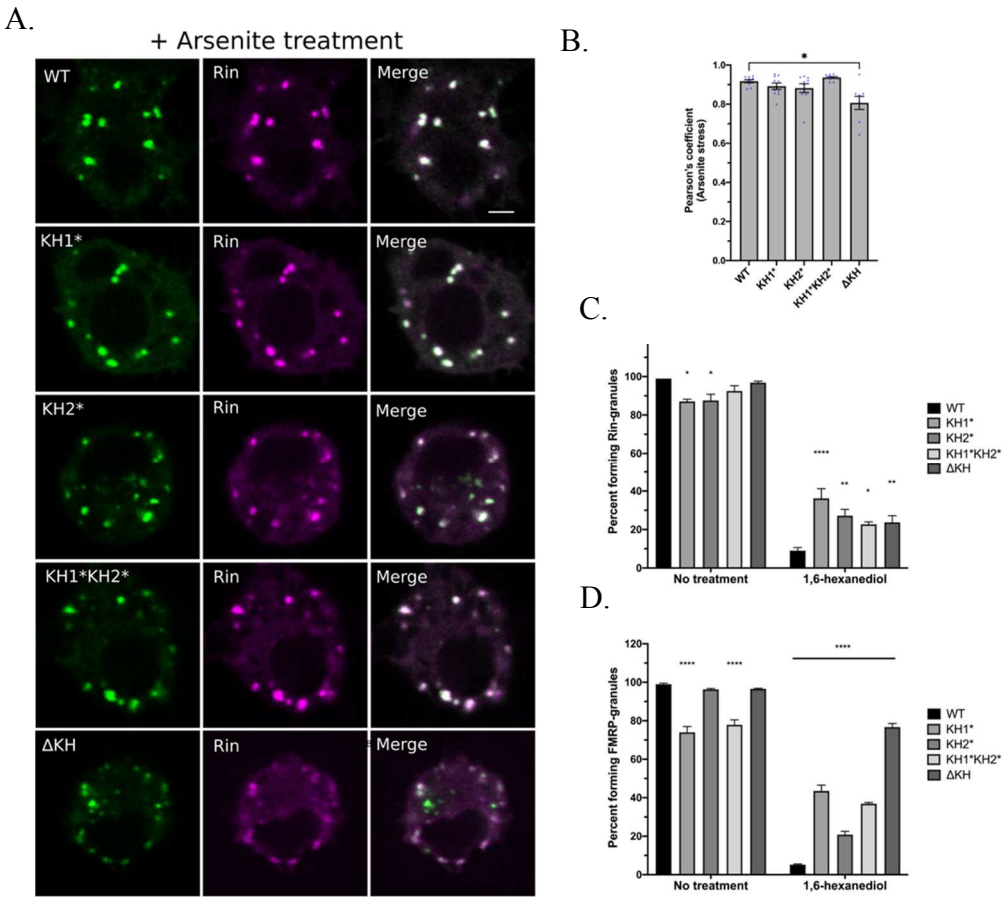

Figure 12. Loss of either KH domain shifts causes the formation of solid-like granules in arsenite stressed cells

(A) Representative images of the intracellular localization of transiently transfected FMRP mutants (green) and Rin (magenta) treated with 0.5mM sodium arsenite for 45 minutes. Constructs shown are indicated in the top left corner of each image. FMRP and Rin merged images are shown in the right column. Scale bar: 2μm. (B) Comparison of the average Pearson correlation coefficient between FMRP-mutants and the stress granule marker, Rin, in arsenite treated cells (mean ± SE; n=8-10 cells). Comparison of the percent of transfected cells treated with 0.5 mM sodium meta-arsenite for 45 minutes forming (C) Rin-granules or (D) FMRP granules with or without 10% 1,6-hexanediol treatment. Approximately 100 cells were manually analyzed in triplicate for each genotype per treatment group and compared to WT. (mean ± SE). Statistical analysis was done by (B) ordinary Brown-Forsyth ANOVA followed by a Dunnett's T3 multiple comparisons test and (C & D) ordinary two-way ANOVA followed by a Dunnett's multiple comparisons test.

2.5 The KH1 domain is essential for FMRP localization to P-bodies

In addition to SGs, FMRP has been shown to associate with P-bodies in fly and mammalian neurons (Barbee et al., 2006; Cougot et al., 2008). Thus, we were next interested in whether the KH mutants affected P-body assembly or colocalization. To address this question, we used HPat, a highly conserved P-body component in yeast and flies, as our P-body marker (Pilkington and Parker, 2008). HPat-positive P-bodies formed in each of the mutants constitutively, suggesting that the KH domains are not required for P-body assembly (Figure 13A). As expected, we found that some P-bodies did not have any FMRP present within them (white arrowheads in Figure 13A and Figure 13B), although most punctate FMRP colocalized with punctate HPat (Figure 13C). As FMRP is not present in all P-bodies, this suggests that it is not required for P-body assembly. Interestingly, we never saw KH1* granules overlapping with HPat granules, implying that the KH1 domain may be required for FMRP recruitment to P-bodies (yellow arrows in Figure 13A). Indeed, quantification of the average Pearson's colocalization coefficient shows a significant reduction in KH1* when compared with WT (Figure 13B). It must me noted that, although the Pearson's coefficient for KH1* is positive (which would suggest an interaction between these proteins), this may be biased as this analysis does not differentiate between diffuse FMRP and HPat fluorescence within the cytoplasm and granules. Alternatively, reduced colocalization could be due to the lower number of FMRP granules observed in the KH1* mutant (Figure 8D). In contrast, KH1*KH2* and ΔKH led to the formation of large spherical granules that colocalized more strongly with HPat

(Figure 13C), suggesting that FMRP and HPat may be sinking into these larger solid-like structures. Collectively, we found that the KH1 domain is important for FMRP association with P-bodies and disrupting this domain may be abolishing the transference of FMRP from other granules such as SGs, into P-bodies.

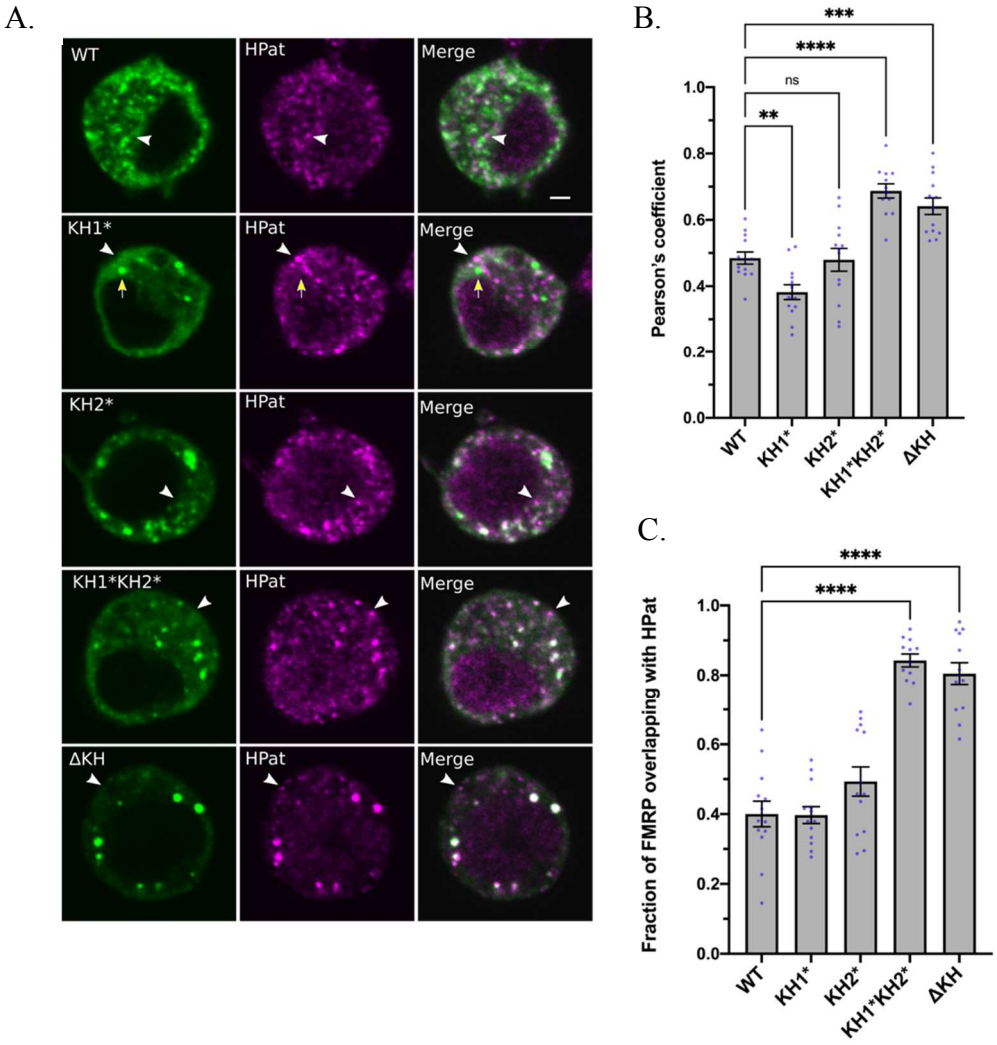

Figure 13. The KH1 domain is required for P-body association

(A) Representative images of the intracellular localization of transiently transfected FMRP (green) and HPat (magenta). Arrowheads show HPat-positive granules that do not overlap with an FMRP-positive granule. Arrows indicate KH1 induced stress granules that do not overlap with P-bodies. Scale bar: 2µm. (B) Quantification of the average Pearson correlation coefficient between FMRP-mutants and the P-body component, HPat, compared to WT (mean ± SE of 12-13 cells). (C) Average Mander's coefficient showing the fraction of FMRP overlapping with HPat fluorescence. Statistical analyses were done by ordinary one-way ANOVA followed by a Holm-Šídák's multiple comparison test.

CHAPTER THREE: THE FMRP KH DOMAINS ARE REQUIRED FOR THE FORMATION AND STABILIZATION OF NEURONAL GRANULES IN MOTOR NEURONS

3.1 The KH1 domain is required for NG formation in primary motor neurons

FMRP plays a critical role in neurodevelopment by assembling into neuronal RNA transport granules (NGs). These granules are important for the transport of FMRP, translation machinery and specific mRNA cargo important for synaptic growth and maintenance from the soma into distal neuronal processes (Antar et al., 2004, 2005, 2006; Davidovic et al., 2007; Dictenberg et al., 2008; El Fatimy et al., 2016). FXS is caused by loss-of-function of FMRP within neurons and presumably the subsequent loss of transport and translation repression within NGs and at synapses. Patients with missense mutations in the KH1 and KH2 domains present with severe FXS-phenotypes. Based on this, we were next interested in exploring whether either of the KH domains played a role in assembly or function of FMRP-containing NGs. Here, we took advantage of an established system used to examine NG composition and dynamics in primary cultures of *Drosophila* larval

motor neurons (Barbee et al., 2006). To study FMRP granules *in vivo*, we generated a series of transgenic flies that allowed for their inducible expression under control of the UAS/Gal4 system (Brand and Perrimon, 1993). To normalize expression levels, all transgenes were inserted into the same locus on the 3rd chromosome near the endogenous *dFMR1* gene. All were also recombined with the *FMR1Δ50* null allele to reduce levels of endogenous protein. Unless otherwise noted, experiments were done in a heterozygous null mutant background (*FMR1Δ50/+*). We drove the expression of our EGFP-tagged FMRP mutants using a restrictive motor neuron-specific *Gal4* driver (*C380-Gal4, cha-Gal80*). Primary motor neurons were harvested from 3rd instar larva in order to study FMRP granule formation and dynamics *in vivo* (hereafter referred to as *WT,Δ50/+*, *KH1*,Δ50/+*, etc.).

We first asked whether these mutants were capable of forming somatic and neuritic NGs in primary motor neurons. Similar to what we saw in S2 cells, *WT,Δ50/+* and *KH2*,Δ50/+* formed numerous round granules within the cell body (Figure 14A). In contrast, *KH1*,Δ50/+* and *KH1*KH2*,Δ50/+* fluorescence was almost entirely diffuse and cytoplasmic, with few or no granules forming within the soma or neurites. While we observed only a slight reduction in the number of *KH2*,Δ50/+* MNs containing NGs, *KH1*,Δ50/+* and *KH1*KH2*,Δ50/+* only formed NGs in ~2% and 10% of neurons, respectively (Figure 14B) This is not likely to be due to reduction in protein expression in either KH1* or KH1*KH2* as expression levels are similar among all constructs (Figure 14C). As with S2 cells, this signifies that the KH1 domain is essential for NG assembly within neurons. The *FMR1Δ50/Δ113* null background is viable through adulthood (Bushey

et al., 2009). Ectopically expressing these mutants in the *FMR1* loss-of-function, instead of the *FMR1* heterozygous background would be ideal in order to eliminate all endogenous FMRP protein. However, expression of KH1* and KH1*KH2* causes embryonic lethality when expressed in the *FMR1Δ50/Δ113* background (data not shown). Notably, lethality occurs even when expression of the mutants is driven by the restrictive motor neuron-specific driver, *C380-Gal4,cha-Gal80*. This suggests that the KH1* mutation may have some unknown dominant-negative effect, particularly within motor neurons.

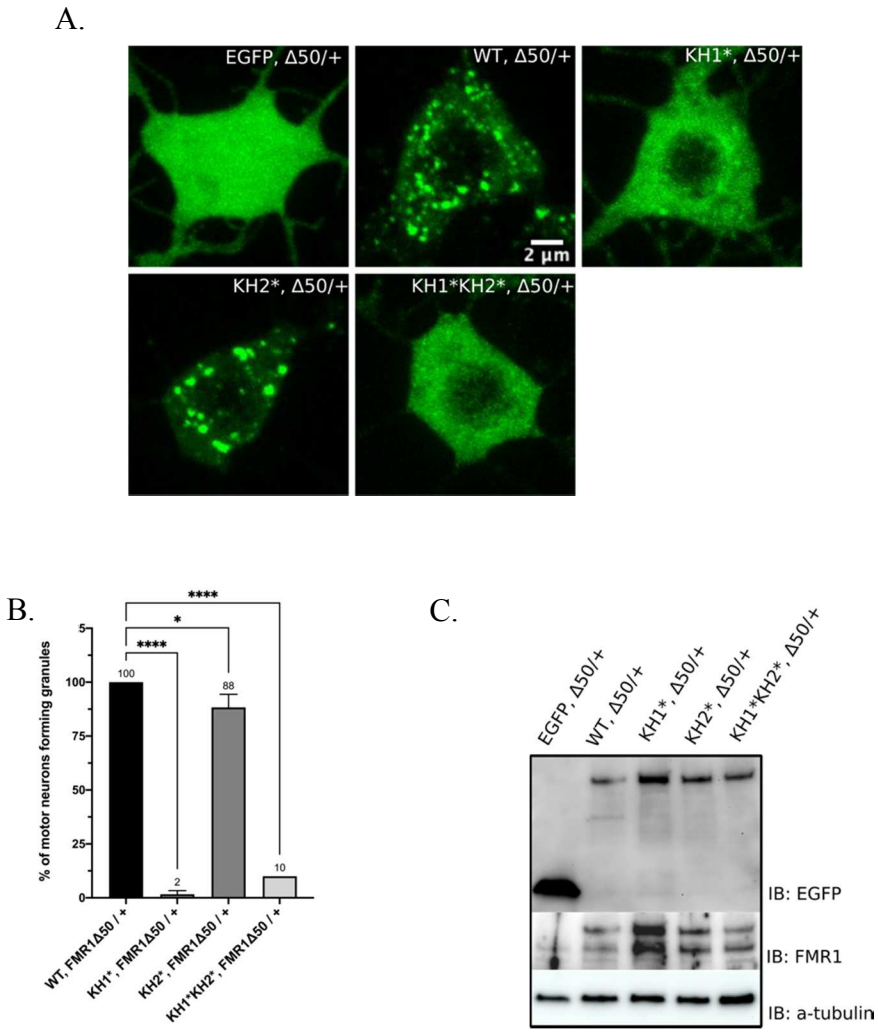

Figure 14. The KH1 domain is essential for NG formation in motor neurons

(A) Representative Z-projections of major granule phenotype in *Drosophila* primary motor neuron cell bodies. *C380-cha-Gal80* was used to drive expression of the EGFP: FMRP constructs (green) in a subset of primary motor neurons in the *FMR1Δ50/+* heterozygous background. Scale bar: 2µm. (B) Comparison of the percent of EGFP-expressing motor neurons forming granules in *FMR1*-heterozygous background. Mean percentage is shown above respective bar (mean ± SE; n=20 cells in triplicate). (C) Western blot analysis of *EGFP* (top) and *FMR1* (middle) expression of UAS-EGFP and UAS-EGFP-FMRP mutants under the *C380-Gal4, cha-Gal80* selective motor neuron driver in the larval CNS. *a-tubulin* was used as a loading control. Statistical analysis was done by ordinary one-way ANOVA followed by a Holm-Šídák's multiple comparison test.

3.2 The KH2 domain stabilizes the dynamic shell of NGs

Thus far, we have shown that the KH1 and KH2 domains, although similar in predicted function, have substantially different effects on NG phenotypes. Abrogation of NGs due to the KH1* mutation coincides with embryonic lethality in *FMR1* nulls. The KH1 domain therefore appears to be contributing some essential function which correlates with NG formation. *KH2*,Δ50/+* on the other hand, only mildly disrupts NG formation and has no negative impact fly viability. As we have previously shown that the point mutants disrupt granule dynamics in S2 cells, we were curious whether KH2* similarly impacted NGs.

We predicted that NGs are more stable within neurites than in the soma which could prevent the loss of granule constituents during active transport. To determine whether there was a difference between these populations, we photobleached individual round granules in either the soma (top panel-Figure 15A) or neurite (top panel-Figure 15B) and compared recoveries over a 3-minute span. Extending FRAP analysis beyond 200s was not possible due to excessive photobleaching (data not shown). Contrary to what we predicted, there was not an increased immobile fraction of WT granules in the soma vs. neurites (black bars-Figure 15E). Instead, we saw a the mobile fraction in neurites recovered two times slower than in somatic granules (black bars-Figure 15F). This suggests that, while WT FMRP is not reorganizing into stable "cores" within neuritic NGs, FMRP within the dynamic shell is instead forming more stable interactions which is maintaining NG structure during transport.

We next compared the recovery curves of somatic and neuritic populations of *KH2*,Δ50/+* NGs to determine whether the KH2* mutation disrupted stability. Somatic and neuritic recovery curves for *WT,Δ50/+* and *KH2*,Δ50/+* were quite similar, although *KH2*,Δ50/+* mobile fractions recovered much more rapidly than *WT,Δ50/+* in both the soma (Figure 15C) and neurites (Figure 15D). Interestingly, we observed dramatic alterations to both the mobile and immobile pools of *KH2*,Δ50/+* NGs. In contrast to WT granules, we saw a significant shift of *KH2*,Δ50/+* into the immobile fraction in both NG populations (immobile fraction increased by 5.6% ± 1.19 in soma and 12.9% ± 1.06 in neurites; Figure 15E). Strikingly, mobile fractions of *KH2*,Δ50/+* NGs recovered ~7 times more rapidly than *WT,Δ50/+* in soma and ~15 times more rapidly in neurites (Figure 15F). This highlights the importance of the KH2 domain in contributing stabilizing interactions within the dynamic shell of NGs. Altogether, these data suggest that the KH2 domain moderates NG granule shell/core organization by 1) causing more KH2* to shift into the nondynamic core and 2) destabilizing the remaining KH2* in the shell.

A.

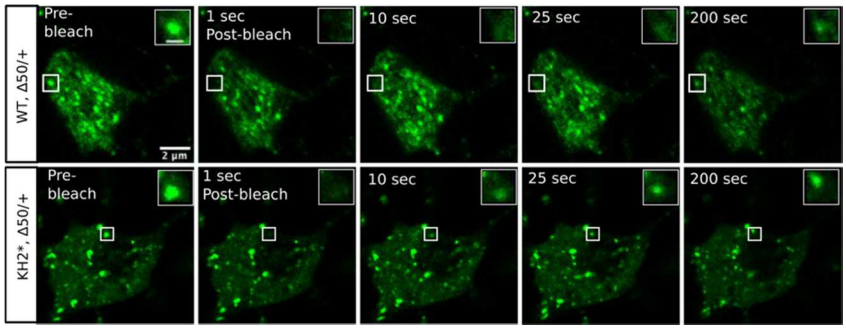
WT, Δ50/+
KH2*, Δ50/+
Pre-bleach
1 sec Post-bleach
10 sec
25 sec
200 sec
2 μm

B.

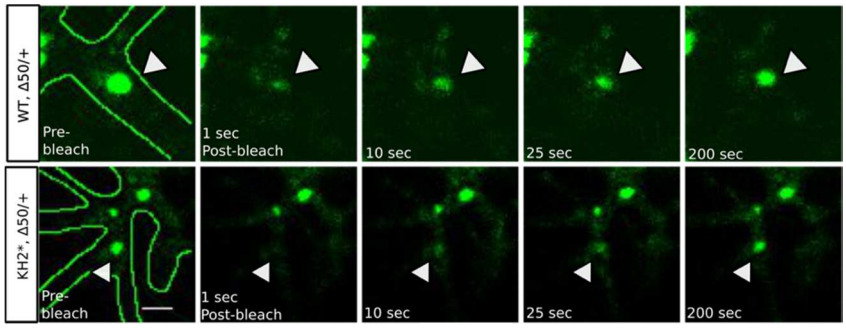
WT, Δ50/+
KH2*, Δ50/+
Pre-bleach
1 sec Post-bleach
10 sec
25 sec
200 sec

C.

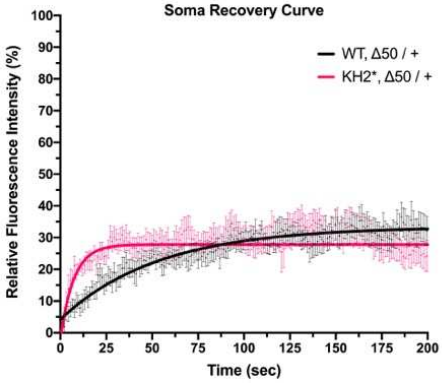
Soma Recovery Curve
WT, Δ50 / +
KH2*, Δ50 / +
Relative Fluorescence Intensity (%)
Time (sec)

D.

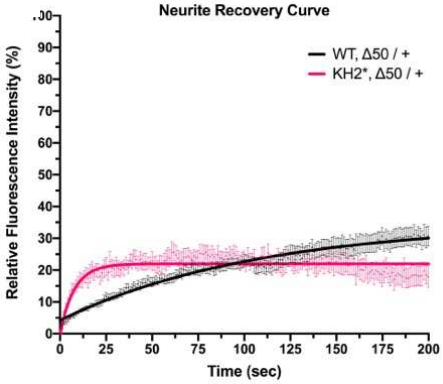
Neurite Recovery Curve
WT, Δ50 / +
KH2*, Δ50 / +
Relative Fluorescence Intensity (%)
Time (sec)

E.

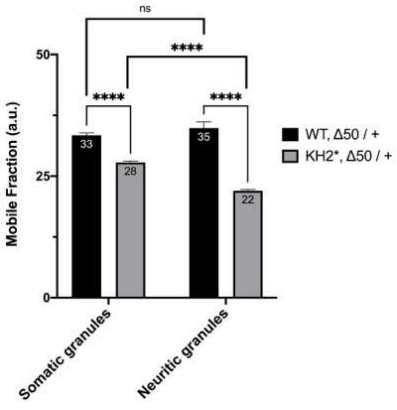
ns
****
****
****
Mobile Fraction (a.u.)
33
28
35
22
WT, Δ50 / +
KH2*, Δ50 / +
Somatic granules
Neuritic granules

F.

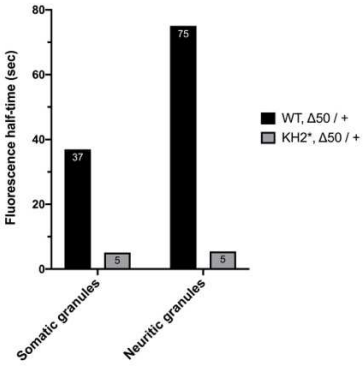
Fluorescence half-time (sec)
37
5
75
5
WT, Δ50 / +
KH2*, Δ50 / +
Somatic granules
Neuritic granules

Figure 15. The KH2 domain stabilizes NG interactions

(A) Representative time lapse images of somatic FRAP NGs pre-bleach, 1 second post-bleach and then at 10, 25, and 200 seconds following the bleaching event. Scale bar in whole cell image is 2 μm. Scale bar in zoomed-in granule image is 1 μm. (B) Representative time-lapse images of neuritic FRAP NGs pre-bleach, 1 second post-bleach and then at 10, 25, and 200 seconds following the bleaching event. Neurites are outlined in green in the pre-bleach image, arrow heads point to the photobleached granule. Scale bar: 1μm. Nonlinear one-phase association regression curves of NGs representing fluorescence intensity of (C) somatic NGs and (D) neuritic NGs relative to initial intensity over 200 seconds (mean ± SE; n ≥ 9 granules). (E) Comparison of the average mobile fractions of somatic and neuritic mobile fraction of WT and KH2* NGs (mean ± SE; n ≥ 9 granules). a.u.=arbitrary units. (F) Comparison of the average fluorescence recovery half-time of somatic and neuritic mobile fraction of WT and KH2* NGs (mean; n ≥ 9 granules). Statistical analysis was done by ordinary two-way ANOVA followed by Šídák's multiple comparison test.

3.3 The KH2 domain is important for neuritic transport

We were next curious as to whether biophysical alterations observed in *KH2*,Δ50/+* NGs, had any impact on NG transport as this could impact FMRP function and mRNA trafficking out to the synapse. We noticed conspicuous differences in NG number and distribution between *WT,Δ50/+* and *KH2*,Δ50/+* in neurites (Figure 16A). Although we previously saw minimal defects in *KH2*,Δ50/+* NG formation (Figure 14B), we found 30% fewer granules out in neurites when compared with *WT,Δ50/+* (11.2 ± 3.30 fewer granules in *KH2*,Δ50/+*; Figure 16B). Although, it is possible that this simply due to a reduction in the number of granules in neurons this is potentially indicative of transport defects in these mutant granules. To determine whether this was true we calculated the percentage of granules in neurites proximal (<10μm) and distal (≥10μm) from the soma. We found a significant reduction in the proportion of neuritic *KH2*,Δ50/+*NGs in distal neurites, further supporting that this mutation results in NG transport defects (Figure 16C).

We next asked whether *KH2*,Δ50/+* displayed altered neuritic transport of NGs. Similar to what others have found, the majority of *WT,Δ50/+* NGs were static with ~20% actively transported through neurites (Kao et al. 2010; Cioni et al. 2019; Figure 16D). KH2* had no impact on directionality of NG transport (X^2 = 0.581, p= 0.748; data not shown). However, KH2* did impact the kinetics of NGs. We observed a significant increase in the anterograde velocity *KH2*,Δ50/+* granules (Figure 16E). Increased velocities would be expected to increase shear force on liquid droplets caused by hydrodynamic drag which could account for the reduction of observable *KH2*,Δ50/+*

granules out in distal neurites. Additionally, this increased velocity could also reduce NG docking to synaptic compartments, preventing granules and their constituents from entering synapses, although this typically results in an accumulation of granules out in neurites which we did not see with *KH2*,Δ50/+* (Kao et al., 2010; Yoshimura et al., 2006). Altogether these data suggest that the KH2* mutation is disrupting FMRP granule transport out towards distal regions of neurites.

A.

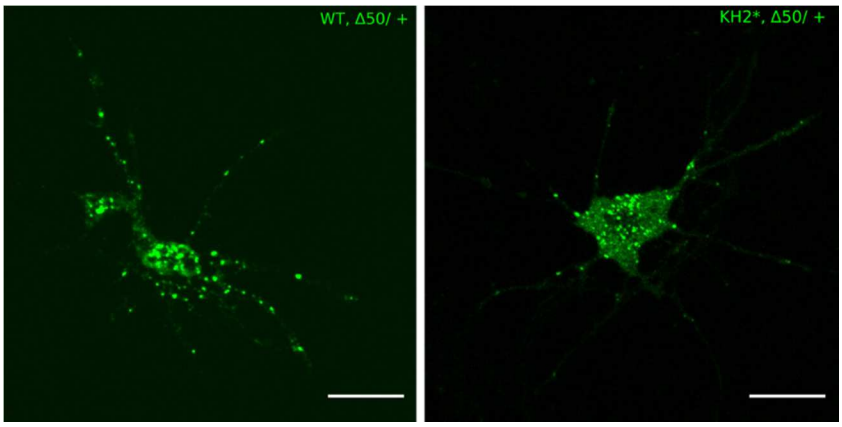
WT, Δ50/ +
KH2*, Δ50/ +

B.

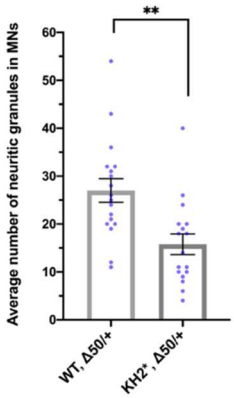
Average number of neuritic granules in MNs
**
WT, Δ50/+
KH2*, Δ50/+

C.

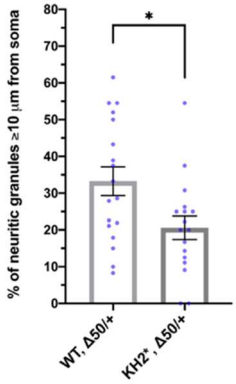
% of neuritic granules ≥10 μm from soma
*
WT, Δ50/+
KH2*, Δ50/+

D.

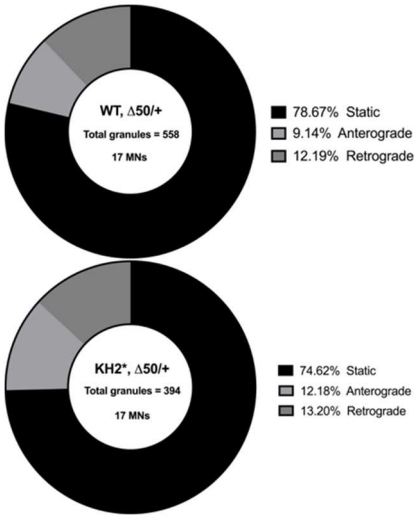
WT, Δ50/+
Total granules = 558
17 MNs
78.67% Static
9.14% Anterograde
12.19% Retrograde
KH2*, Δ50/+
Total granules = 394
17 MNs
74.62% Static
12.18% Anterograde
13.20% Retrograde

E.

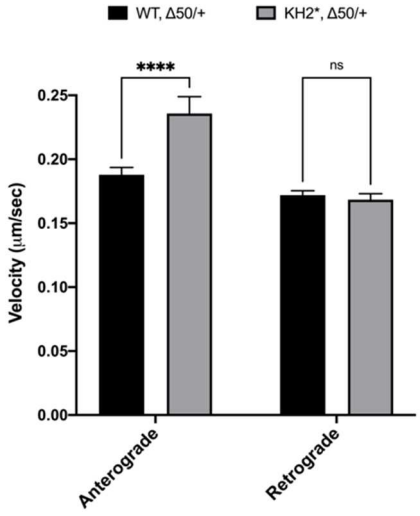
WT, Δ50/+
KH2*, Δ50/+
****
ns
Velocity (μm/sec)
Anterograde
Retrograde

Figure 16. KH2 domain is necessary for NG transport into neurites

(A) Representative images of *FMRP, FMR1Δ50/+* (left) and *KH2*, FMR1Δ50/+* (right) primary MNs. WT and KH2* GFP granules can be visualized in the soma (cell body) and neurites (branching off of cell body). Scale bars: 10μm. (B) Box and whisker plot comparing the average total number (box) of NGs within neurites of primary MNs. Range of neuritic granule number is represented by dots. (mean ± SE; n=17-18 MNs). (C) Box and whisker plot showing the average (box) percentage of neuritic granules that are distal (≥10 μm) from the motor neuron cell body. Range of distances is represented by dots. (mean ± SE; n=17-18 MNs). (D) Pie charts representing fraction of neuritic granules that remain stationary (static) or move in the anterograde or retrograde direction (relative to the cell body). Percentages are annotated in the legends. Total number of granules counted in 17 MNs are indicated within each pie chart. (E) Comparison of anterograde and retrograde velocities of motile *FMRP, FMR1Δ50/+* and *KH2*, FMR1Δ50/+* neuritic NGs (mean ± SE; n=46-75 granules per category). Statistical analyses were done using unpaired t tests.

CHAPTER FOUR: FUNCTIONAL IMPACTS OF FXS-CAUSING POINT MUTATIONS ON FMRP IN *DROSOPHILA MELANOGASTER*

4.1 The KH1 domain is required for FMRP-mediated translational repression

FMRP has been shown to interact with about 4% of neuronal mRNAs, although the mechanism by which it is able to bind and regulate such a large subset of mRNAs is still unclear (Ashley et al., 1993; Brown et al., 2001). Recent evidence suggests that the RGG box of mammalian FMRP contributes target specificity by binding to G-quadruplex structures in mRNAs and that these interactions are important regulating mRNA neuritic transport (Goering et al., 2020). In contrast, the KH domains which bind to short, ubiquitous sequences, are important for polysome association and are implicated in suppressing translation elongation via ribosome stalling in flies (Chen et al., 2014; Darnell et al., 2005; Feng et al., 1997). Previous studies show that KH1* is defective in binding three known mRNA targets *CaMKII, PSD95,* and *Map1B* using RNA-coimmunoprecipitation followed by qPCR in mouse cortical neurons (Myrick et al., 2014). However, loss of binding does not directly indicate that KH1* is non-functional in

translation repression. In contrast, KH2* which has been better characterized, disrupts both RNA-binding and translation repression of several known FMRP targets (Ascano et al., 2012; Darnell et al., 2005; Siomi et al., 1994).

To determine the role of the KH domains in regulating translation in S2 cells, we examined the ability of these FXS-causing mutations to repress translation in a modified λN-based tethering assay (Rehwinkel et al., 2005). In this set of experiments, λN-FMRP was artificially tethered to the 5X BoxB sequence in the 3'UTR of the luciferase reporter (Figure 17A). This allowed us to study translation repression of each of the FMRP mutants in an mRNA-binding independent manner. In λN-FMRP we see repression of the firefly luciferase (FLuc) reporter, indicating that λN-FMRP is able to inhibit translation when tethered to a transcript in the 3'UTR (Figure 17B). Interestingly, λN-KH2* was similarly able to repress reporter translation, which was surprising given that the KH2 domain is expected to repress translation by interacting with the elongating ribosome (Darnell et al., 2011). In contrast, significant de-repression was observed with the λN-KH1* and λN-KH1*KH2* mutants (Figure 17B). This suggests that the KH1 domain is important for translation inhibition, consistent with published data (Chen et al., 2014).

A.

B.

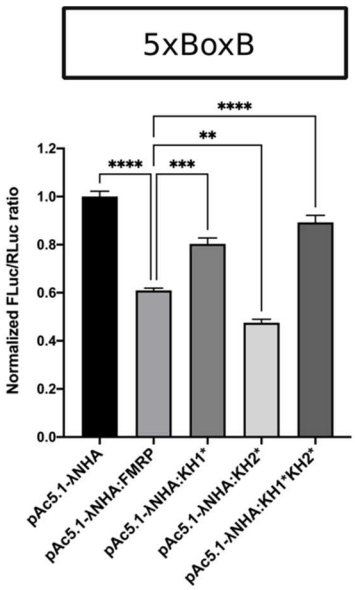

Figure 17. The KH1 domain is required for FMRP-mediated translational repression

(A) Diagram of the FLuc reporter fused to a 5xBoxB 3'UTR. Luciferase assays of (B) λN:HA-tethered FMRP-mutants repression of the 5xBoxB FLuc reporter FLuc/RLuc ratios were normalized to empty vector ratios. Graph shows repression of the FLuc reporter by empty vector or FXS-causing point mutants compared to *pAc5.1-FMRP* (mean ± SE). Statistical analysis was done by ordinary one-way ANOVA followed by a Holm-Šídák's multiple comparison test.

4.2 The KH domains are required to regulate translation of known target mRNAs

Next, we were interested in addressing whether untethered FMRP could repress the translation of the FLuc reporter by binding to the 3'UTRs of known mRNA targets of FMRP and whether the KH domains were required for this to occur (Figure 18A). To test this, we cloned the 3'UTR of *camkii, FMR1,* the degenerin/epithelial sodium channel (DEG/ENaC) family protein, *pickpocket* (*ppk*), and the gene encoding the *Drosophila* homolog of the actin-binding protein profilin, *chickadee (chic)* into the FLuc reporter vector replacing the BoxB 3'UTR (Hou et al., 2006; Reeve et al., 2005; Rehwinkel et al., 2005; Schaeffer et al., 2001; Xu et al., 2004). It is not known precisely how FMRP binds to these targets although *FMR1* and *chic* are predicted to contain G-quadruplexes (Kikin et al., 2006). Similar to the 5X BoxB assay, KH2* did not disrupt repression of the *ppk*, *FMR1,* and *chic* luciferase reporters, suggesting that the KH2 domain may not be required for translational repression of these specific reporter mRNAs (Figure 18B-D). In contrast, we saw significant de-repression with KH1* and KH1*KH2*, implying that the KH1 domain is required for translation repression of this subset of reporters. Interestingly, the KH1 domain appears to be dispensable for repression of the *camkii* reporter, while KH2* slightly, but significantly de-represses translation (Figure 18E). These data suggest that the individual KH domains regulate the translation of distinct mRNA populations and supports previous work that these domains are important for FMRP function in translation regulation. Importantly, the loss of repression in KH1* correlates with the failure to form FMRP granules.

A.


FLuc
ppk 3'UTR
AAAAA...
FLuc
chic 3'UTR
AAAAA...
FLuc
fmr1 3'UTR
AAAAA...
FLuc
camkii 3'UTR
AAAAA...

B.

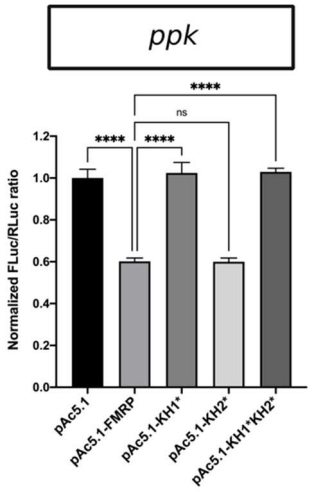
ppk
Normalized FLuc/RLuc ratio
pAc5.1
pAc5.1-FMRP
pAc5.1-KH1*
pAc5.1-KH2*
pAc5.1-KH1*KH2*

C.

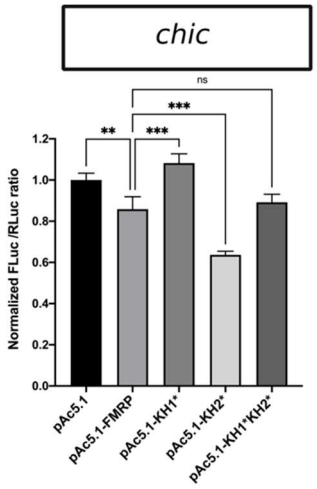
chic
Normalized FLuc /RLuc ratio
pAc5.1
pAc5.1-FMRP
pAc5.1-KH1*
pAc5.1-KH2*
pAc5.1-KH1*KH2*

D.

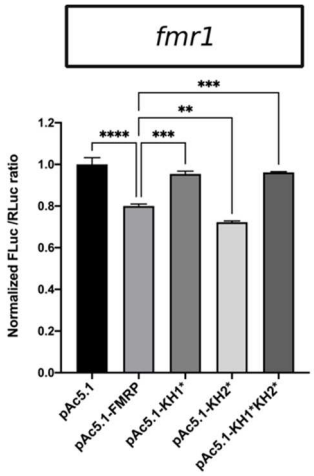
fmr1
Normalized FLuc /RLuc ratio
pAc5.1
pAc5.1-FMRP
pAc5.1-KH1*
pAc5.1-KH2*
pAc5.1-KH1*KH2*

E.

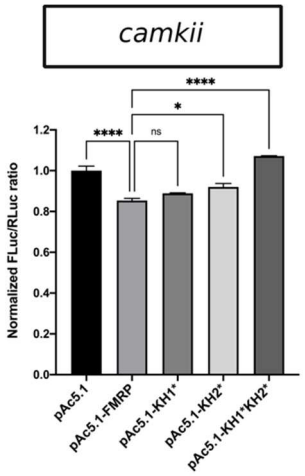
camkii
Normalized FLuc/RLuc ratio
pAc5.1
pAc5.1-FMRP
pAc5.1-KH1*
pAc5.1-KH2*
pAc5.1-KH1*KH2*

Figure 18. The KH domains regulate translation of different mRNA targets

(A) Diagram of the FLuc reporters used in this study fused to the 3'UTR of certain known targets of FMRP. Luciferase assays comparing repression of FLuc fused with (B) *pickpocket (ppk)* 3'UTR, (C) *chickadee (chic)* 3'UTR, (D) *fragile x mental retardation 1 (FMR1)* 3'UTR or (E) *calcium/calmodulin kinase ii (camkii)* 3'UTR by untethered FMRP mutants. FLuc/RLuc ratios were normalized to empty vector ratios. Graph shows repression of the FLuc reporter by empty vector or FXS-causing point mutants compared to *pAc5.1-FMRP* (mean ± SE). All statistical analyses were done by ordinary one-way ANOVA followed by a Holm-Šídák's multiple comparison test.

4.3 FMRP KH domains are important for modulating synapse formation

The *Drosophila* larval neuromuscular junction (NMJ) has been used extensively as a model synapse to study FXS in flies. The fly NMJ contains a simple glutamatergic synapse, resembling those found in the mammalian CNS and *Drosophila* FMRP has a well-established presynaptic function in the control of NMJ development (Drozd et al., 2018; Zhang et al., 2001). To study how the FXS-causing KH mutations affect the function of FMRP at this synapse, we analyzed the number of synaptic specializations or "boutons" that formed at the larval NMJ of the well-characterized body wall muscles 6/7 in abdominal segment 3 when FMRP was overexpressed using the motor neuron-specific driver, *C380-Gal4* (Figure 19A). This NMJ is innervated by two neurons which form type 1 "big" (1b) and "small" (1s) motor neurons which can be easily distinguished from each other by size and immunostaining. Synaptic boutons of these MNs are visualized using antibodies against *discs large*, or DLG, which is the *Drosophila* ortholog of the post synaptic markers PSD-95/SAP70 and the neuronal membrane marker, HRP (Lahey et al., 1994; Menon et al., 2013). While 1b boutons are much larger in area and contain more DLG-containing active zones in the juxtaposed postsynaptic space, 1s boutons are characterized by their relatively small size and association with significantly fewer active zones.

FMRP negatively regulates synaptic growth in motor neurons and overexpression of FMRP in the *UAS-FMR1* fly has been shown in previous studies to significantly reduce synaptic terminal growth at the larval NMJ (Zhang et al., 2001). Here we were able to recapitulate the reduction of 1s (Figure 19B) and 1b (Figure 19C) boutons normalized to

muscle area (μm) at the *UAS-FMR1* NMJ (Zhang et al., 2001). We also saw a reduction in synaptic complexity in these flies assayed by the number of "tips" of strings of boutons (Figure 19D). Overexpression of EGFP-tagged FMRP (*UAS-EGFP-FMRP*) at the fly NMJ only affected 1b boutons, in which we saw a reduction relative to our overexpression control (*UAS-EGFP*) (Figure 19C). This indicated to us that our *UAS-EGFP-FMRP* construct was functional within fly motor neurons. Interestingly, although overexpression of *UAS-EGFP-KH1*, UAS-EGFP-KH2*,* and *UAS-EGFP-KH1*KH2** had no effect on 1s or 1b bouton numbers, each of these mutants reduced complexity of the NMJ (Figure 19D). Taken together, this suggests that bouton number and arborization are not necessarily linked processes. While the KH domains may be required to regulate RNAs involved in bouton growth they may not be required to regulate RNAs involved in branching.

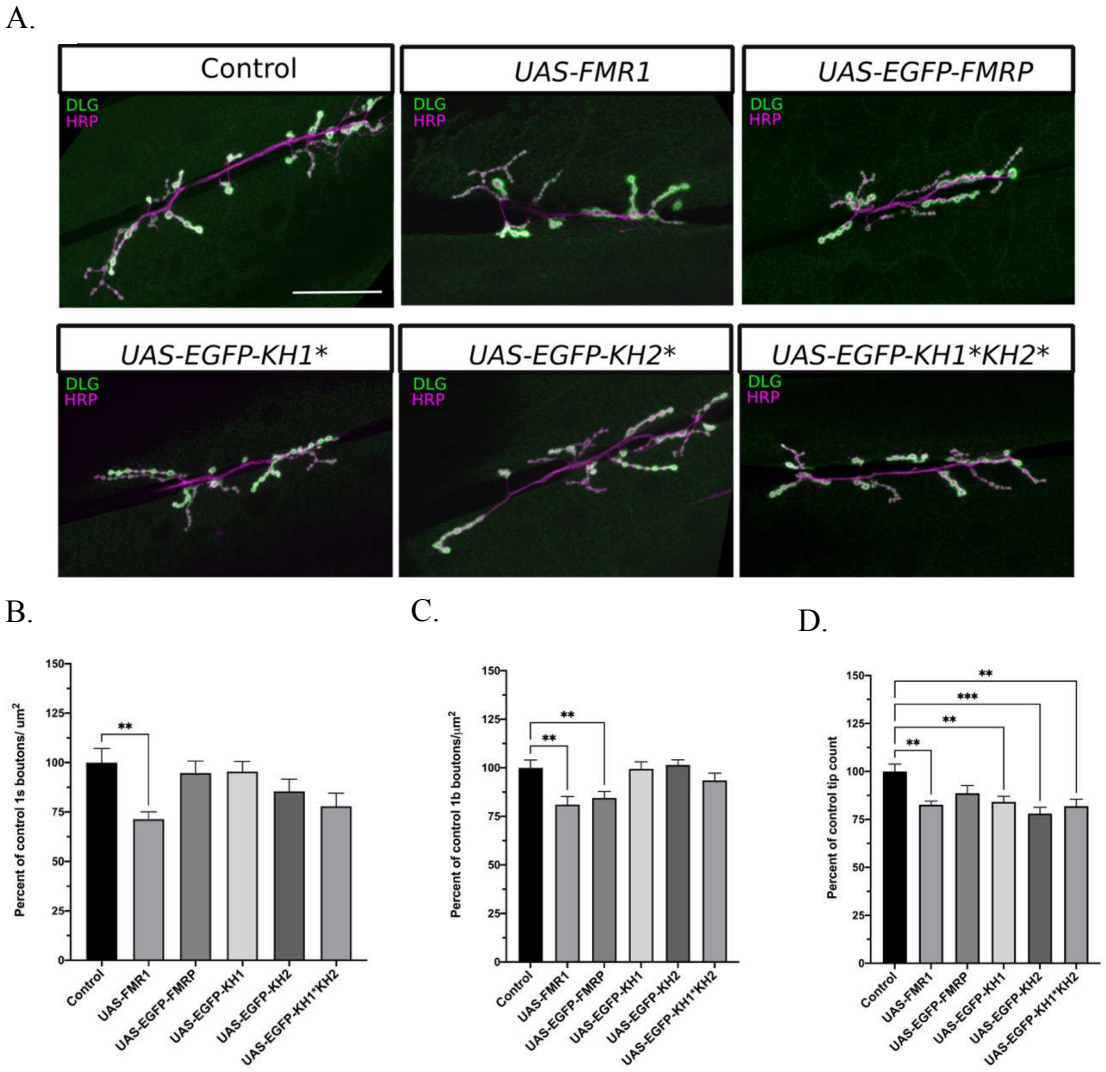

Figure 19. FXS-causing point mutants disrupt FMRP function in synapse formation

(A) Wandering third instar larval NMJs from *C380-Gal4/+;;UAS-EGFP/+* controls, FMRP overexpression, *UAS-FMR1* and *UAS-EGFP-FMRP*, and FXS-causing point mutant overexpression, *UAS-EGFP-KH1*, UAS-EGFP-KH2*,* and *UAS-EGFP-KH1*KH2** in *C380-Gal4* motor neurons. Maximum Z-projections of NMJs in abdominal segment 3 innervating body wall muscles 6/7 were stained with antibodies targeting the postsynaptic density marker DLG (green) and the neuronal membrane marker, HRP (magenta) for analysis. Scale bar: 50µm. (B) 1s bouton number/muscle area (µm) and (C) 1b bouton number/muscle area (normalized to control were manually counted and compared with the control NMJ ($n \geq 11$ NMJs, mean ± SE). All statistical analysis was done by Brown-Forsyth ANOVA followed by a Dunnett's multiple comparison test.

4.4 FXS-causing point mutants do not cause localization defects of a target mRNA

As previously stated, NGs are a specialized type of RNP granule within neurons which function in transporting translationally arrested mRNAs between the cell body and dendrites/axons (Kiebler and Bassell, 2006; Krichevsky and Kosik, 2001; Lai et al., 2020). As the KH domains are essential in regulating distinct mechanisms involved forming FMRP granules, we were interested in whether the loss or reduction of FMRP granules in neurites, as seen with in *KH1*,Δ50/+* and *KH2*,Δ50/+*, had any impact on the transport of a known mRNA target. Using single molecule Fluorescence *in situ* hybridization (smFISH) we were able to address this question by quantifying *camkii* transcripts in the soma and neurites in our *EGFP-FMRP, Δ50/+* primary motor neurons.

CamKII is a kinase critical for regulating synaptic plasticity and memory formation. Its mRNA is spatially localized to both pre- and postsynaptic densities where it's regulated by FMRP (Kao et al., 2010; Zalfa et al., 2003). In fly primary motor neurons, FMRP has been shown to colocalize with a MS2-tagged *camkii* RNA within FMRP granules (Estes et al., 2008). Using smFISH we were able to detect single *camkii* transcripts throughout the cell soma and out in neurites (Figure 20A). We did not include the KH1*KH2* double mutant in these analysis as we do not believe this construct is physiologically relevant (based data shown throughout Chapter 2). Interestingly, we found that all of the *FMR1* mutants, including controls had significantly fewer transcripts in the soma compared with the *C380-Gal4,cha-Gal80* controls, suggesting that any reduction of endogenous FMRP impacts total transcript number (Figure 20B). Interestingly, we found that there was a

significantly higher percentage of *camkii* transcripts out in the neurites of *WT,Δ50/+* MNs relative to the *FMR1*-nulls (Figure 20C). This suggests that FMRP can promote the transport of *camkii* mRNA in neurites. Although the percentage of neuritic transcripts was lower in the KH mutants compared to *WT,Δ50/+* MNs, the results were not statistically significant. This indicates that the KH domains are not required to regulate transport. Moreover, normal localization of *camkii* in KH1* suggests that FMRP granule formation is not a prerequisite for transport. This cannot be explained by the presence of one copy of FMRP in these experiments because *Δ50/+* results are similar to *Δ50/Δ113*. In summary, these data indicate that FMRP can promote, but is not required for, *camkii* transport in neurites. Moreover, neither of the KH domains are required to control this process.

A.

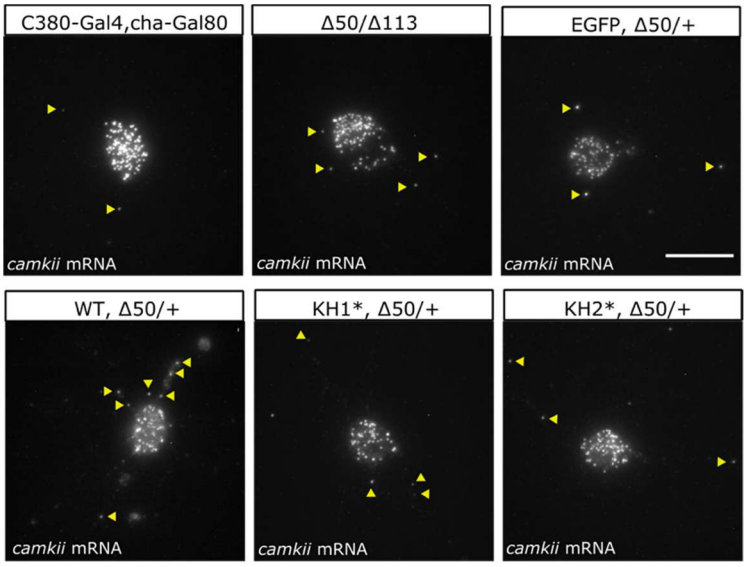

B.

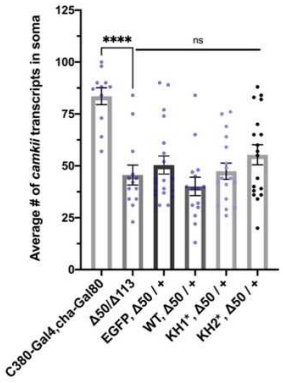

C.

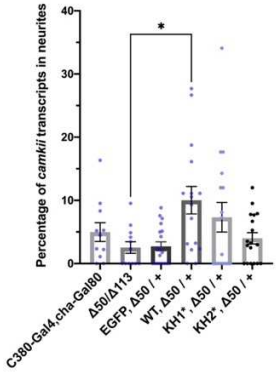

Figure 20. The KH domains are not required for *camkii* transport in MNs

(A) Representative images of *camkii* mRNA smFISH in MNs. Yellow arrowheads in images are distinguishing *camkii* transcripts out in neurites. Scale bar: 10μm. (B) Comparison of the average number of *camkii* transcripts in soma and (C) comparison of the average percentage of *camkii* transcripts in neurites in C380-Gal4, cha-Gal80, FMR1Δ50/Δ113 nulls, EGFP, FMR1Δ50/+ control and each of the FMRP, FMR1Δ50/+ mutants relative to the Δ50/Δ113 control (mean ± SE of 11-20 MNs). Statistical analyses were done using a (B) one-way ANOVA followed by the Holm-Šídák's multiple comparisons test and (C) Kruskal-Wallis test followed by the Dunn's multiple comparisons test.

CHAPTER FIVE: DISCUSSION

5.1 Multivalency drives FMRP granule formation *in vivo*

Here, we show that the IDR and KH domains cooperate with each other to promote FMRP granule formation *in vivo*. Granule formation is driven by LLPS, a biophysical process wherein densely packed molecules spontaneously form a membraneless condensate upon reaching a critical concentration (Alberti, 2017). These condensates loosely confine the proteins and RNAs required for a biological process to occur in a particular space and time. This spatial and temporal regulation is important for diminishing off-target interactions that could occur within the cytoplasmic environment. In the context of RNA granules, these condensates can be important for removing particular mRNAs from the cytoplasmic environment to reduce expenditure of energy on costly processes such as translation during times when energy conservation is a priority (e.g. during stress).

IDRs have a high propensity to phase separate *in vitro* and are enriched in other IDR-containing proteins, which has led to an overestimation of their function within biological systems (Lin et al., 2015; Pechstein et al., 2020). A common misconception is that the IDRs within phase separating proteins are the only domains contributing to these

phase transitions. However, more studies are coming out and have illuminated weak, multivalent interactions as the drivers of this process *in vivo* (Banjade and Rosen, 2014; Li et al., 2012). Increased valency (i.e. more interaction domains) of a protein provides a scaffold of *cis*-acting binding sites by which interactions with multiple protein or RNA species can occur (Martin and Holehouse, 2020). These *trans*-acting binding partners are then capable of interacting with more proteins or RNAs, enabling these biomolecules to stack and concentrate within a small area (Banani et al., 2016; Li et al., 2012).

In our study we found that the FMRP IDR was alone capable of forming granules *in vivo* although, it was able to do so in only ~65% of cells (Figure 6C). IDR-granules were also quite different phenotypically from WT granules, suggesting that even though granules are forming via this domain they are unlikely to be functioning properly (Figure 6B). These results indicate that the IDR is not the sole domain required for FMRP granule formation and may function cooperatively with domains in the N-terminus to control this process. This perhaps is not surprising as the other interaction domains within FMRP are likely facilitating interactions with other core components of MLOs.

Further supporting this hypothesis, we found that adding back the KH1 and KH2 domains (KH+IDR) significantly increased granule formation in cells (Figure 6C). Perhaps increasing the stability of interactions within these granules via increasing valency reduces the critical concentration of FMRP needed to optimize phase separation. Further studies could confirm this. As overall expression levels between these constructs were similar, we

can conclude that the reduced propensities of mutants to form granules was not due to lower protein concentrations, which could be influencing this process (Figure 6D).

In addition to affecting FMRP granule formation, the FMRP-IDR mutants drastically altered its distribution within the cytoplasm. The IDR-mutants were conspicuously much more diffuse within the cytoplasm further implicating the exclusion of a large fraction of these mutants from granules. This exclusion is also likely to be caused by reduced valency of FMRP. In support of this conclusion, we saw that when we increased the number of interaction domains, granule occupancy increased and coincided with a reduction in the cytoplasmic fluorescence intensity (Figure 6B & 8C). Altogether, we found that the KH domains and IDR function cooperatively to promote FMRP granule assembly (Figure 6-7). Our results thus support the model that multivalency is playing a significant role in the ability of FMRP to form liquid-like granules *in vivo*.

5.2 The KH1 domain promotes FMRP granule formation in *Drosophila*

FXS is normally caused by a complete loss of FMRP expression. However unique cases have occurred from single missense mutations within the KH domains, implying that these domains are essential for normal FMRP function (De Boulle et al., 1993; Myrick et al., 2014). KH1* was predicted to be a hypomorphic allele due to the loss of several major FMRP-functions including polyribosome association and mRNA binding (Myrick et al., 2014). Here, we show that KH1* also substantially diminishes FMRP granule assembly in S2 cells (Figure 7C). This mutation also reduced SG-formation (Figure 12D) and FMRP localization to P-bodies (Figure 13B). Even more striking, was the absence of KH1*

granules in motor neurons (Figure 14A-B). Although we report KH1* granules in ~2% of motor neurons, these cells were only able to form a single granule, suggesting that even in the limited cases where granules are able to form, FMRP is not localizing normally (data not shown). From this, we can infer that the KH1 domain promotes formation of SGs and is essential for FMRP to form (or interact with) SGs, P-bodies, and NGs.

Interestingly, we found that in the *FMR1* null mutant fly, KH1* and KH1*KH2* caused embryonic lethality, even when expressed only in a subset of motor neurons (data not shown). This was surprising, as loss of *FMR1* expression in and of itself is not lethal. This suggests that the KH1* mutation may have a quasi-dominant phenotype within motor neurons which is causing lethality. We did not try expressing this mutant in other cell types to see if this was a global phenomenon. Further studies looking into how KH1* increases embryonic lethality will be important for gaining a better understand of how this domain is disrupting FMRP function within neurons and how this mutation is causing FXS.

Our results beg the question: what's so special about the KH1 domain? As we've shown, valency and not individual interaction domains drive granule formation *in vivo.* However, when we disrupt the KH1 domain by expressing the KH1* mutant, we see a loss of FMRP-positive P-bodies and NGs. One explanation for the loss of KH1* granules is that the KH1 domain could normally be increasing the valency of FMRP in granules by binding ubiquitous sequence motifs in mRNAs, such as WGGA, nonspecifically (Ascano et al., 2012). Arguing against this, the ACUK sequence, which is recognized by the KH2 domain is more highly enriched within the transcriptome than WGGA, specifically within

genes linked with autism spectrum disorders (Ascano et al., 2012; Tran et al., 2019). If this was the mechanism by which the KH1 domain affected granule formation, we would predict that disrupting the KH2 domain would produce similar (or perhaps stronger) defects. However, we do not see these same phenotypes in KH2* granules, suggesting this may not be the mechanism by which KH1 contributes to granule formation.

Alternatively, KH1 domain interactions may be shifting the concentration threshold required to promote FMRP granule formation (Figure 4B). Presumably, KH1 contributes to granule formation by its associations with RREs in target mRNAs (Li et al., 2020). RNA promotes LLPS of FMRP and other proteins such as hnRNPA1 and FUS, by shifting the phase boundary and requiring lower protein concentrations to initiate phase separation (Molliex et al., 2015; Schwartz et al., 2013; Tsang et al., 2019). Transcripts targeted by the KH1 domain in particular may be recruiting FMRP to mRNPs, thereby bringing FMRP in proximity with other protein/RNA species that it can then interact with via its other interaction domains. However, the specific RNAs targeted by the KH1 domain remains elusive. Future studies identifying the mRNAs targeted specifically by the KH1 domain are needed to address this possible mechanism of granule formation. Additionally, addressing whether these RNAs contain multivalent RREs are also needed to show if these RNAs can seed granule formation more efficiently than other RNAs. Regardless of what the particular mechanism is, our data unambiguously show that the interactions contributed by the KH1 domain are essential for FMRP to form NGs and assemble to P-bodies.

5.3 The KH2 domain stabilizes FMRP within granules, and loss of KH2 domain function in the KH2* mutant disrupts NG dynamics and transport

The KH2 domain in FMRP is required for association with polyribosomes and stalls translation elongation presumably through this association (Feng et al., 1997; Zang et al., 2009). Here we show that translation repression and ribosome association via the KH2 domain are not required for granule assembly *in vivo.* In contrast, disruption of the KH2 domain has substantial impacts on the associative properties of FMRP within granules.

In S2 cells and primary MNs, we found that KH2* was destabilized within the mobile fraction of granules, indicated by KH2* rapidly recovering after photobleaching (Figure 10B). Protein valency is one of the mechanisms regulating mobile fraction dynamics (Van Treeck and Parker, 2019). This is due to the increased propensity of a protein with higher valency to come into contact with another binding partner before exchanging. We believe that loss of KH2 domain function destabilizes the dynamic shell of granules as a result of reduced valency, particularly because of the loss of a domain that participates in binding to a highly prevalent RRE. The KH2 domain interacts with the short sequence motif ACUK and loop-loop pseudoknot kissing complexes in transcripts (Ascano et al., 2012; Darnell et al., 2005). ACUK is found ubiquitously throughout the transcriptome (Suhl et al., 2014). It is therefore likely that KH2-ACUK interactions increase FMRP valency by enabling FMRP to interact weakly with essentially any transcript it comes into contact with. Although we did not test this hypothesis here, future

studies looking at KH2* propensity to phase separate with different RNA species containing varying numbers of ACUK sequences *in vitro* would be valuable.

While we saw destabilization of KH2* within mobile fractions, we simultaneously observed a substantial shift of KH2* into the nondynamic core, particularly in neuritic NGs (Figure 15C-F). Although a loss of valency could explain the increased exchange rate of the mobile fraction, this does not explain why this mutation causes FMRP to shift into stable cores. Immobile fractions are thought to be formed within granules via strong intermolecular interactions, energy dependent processes or protein chaperones, and posttranslational modifications (Banani et al., 2016; Jain et al., 2016; Van Treeck and Parker, 2019). Mutations within granule-forming RBPs have a high propensity to potentiate protein aggregation, which could account for what is occurring to KH2* in MNs. Indeed, FMRP has a high propensity to aggregate *in vitro,* and *in silico* analyses have identified multiple putative aggregation prone sequences within the FMRP CDS (Sjekloća et al., 2009, 2011) Interestingly, one of these aggregation prone sequences occurs within the KH2 domain, just outside of the RNA-binding pocket in which the KH2* mutation occurs. Thus, the Ile307Asn mutation within this domain could potentially elevate aggregation propensity by disrupting domain folding and increasing aggregation-sequence site exposure.

In addition to altering the molecular dynamics of FMRP within granules, we found that the KH2* mutation disrupted NG transport within neurites, in contrast to what has been shown previously in rat PC12 cells (Castrén et al., 2001; Schrier et al., 2004).

Interestingly, Schrier et al. found that the KH2 Ile304Asn mutation in human FMRP was unable to form granules in PC12 cells, but was still able to localize out in neurites via microtubules—potentially within sub-microscopic mRNPs (Schrier et al., 2004). However, this lack of granule formation could be due to the relatively low expression level of their Ile304Asn mutant in comparison to endogenous FMRP (i.e. mutant expression level was reduced to half of endogenous FMRP). As granule formation is dependent on protein concentration, this could explain the lack of observable granules in their study.

In agreement with previous literature, we provide evidence that the KH2* mutant functions in, but is not required for neuritic transport of NGs (Schrier et al., 2004). However, we did find that this mutation increased the kinetics of anterograde NGs (Figure 16E). Kinesins are a family of proteins that function as molecular motors for anterograde transport and can mediate fast and slow transport, depending on the particular kinesin with which the granule attaches (Arpag et al., 2014). Although the KH2 domain has not been implicated in FMRP attachment to molecular motors, this mutation could potentially enhance association of FMRP with adaptor proteins for different motors. These findings may also explain why we see an overall reduction of KH2* granules in neurites, particularly in distal neurites (Figure 16B-C). As destabilized KH2* granules are being transported out in neurites more rapidly, we predict that these granules are falling apart during transport. Future studies identifying which adapters and kinesin motors FMRP attaches and how this is potentially disrupted in KH2* mutants will be important for gaining a better understanding of NG transport kinetics.

5.4 The KH domains are not required for *camkii* transport in motor neurons

We found that while FMRP promotes *camkii* transport in MNs, it was not required for this process (Figure 17C). Moreover, we found that neither the loss nor disruption of NG transport caused by KH1* and KH2*, respectively, had any effect on *camkii* transport out in neurites. This coincides with a recent study implicating the requirement of the RGG box, and not the KH2 domain of mammalian FMRP, for the localization of neuritic mRNAs (Goering et al., 2020). Interestingly, RNA-seq analysis from their study determined that translationally repressed transcripts did not overlap with transcripts dependent on FMRP for their localization, suggesting an uncoupling of these two FMRP functions. However, this may not be the case in flies. The fly RGG-box is only weakly conserved and has not been shown to bind G-quadruplexes like the RGG-box in mammalian FMRP (Vasilyev et al., 2015). Additionally, *camkii* is predicted to contain two weak G-quadruplex structures throughout the entire transcript (Kikin et al., 2006). Perhaps *camkii* is being shuttled through neurites via the IDR or other N-terminal interaction domains in this system.

Another surprising finding was the underwhelming degree of colocalization between the *camkii* smFISH probes and FMRP (data not shown). There were only a few instances of overlap that we saw between these molecules, which could indicate that *camkii* may largely be transported via an FMRP-independent mechanism. Previous studies showing FMRP colocalization with target transcripts in NGs, including *camkii,* have been largely performed using the MS2-tagging system (Dictenberg et al., 2008; Estes et al., 2008; Kao et al., 2010). Incorporating MS2-targeted stem loop structures into target

mRNAs allows for transcript visualization when bound by MS2-GFP (Bertrand et al., 1998). Our lab has shown that fly FMRP is capable of directly binding to MS2 stem loop structures, which could explain why our results are in opposition to previous literature using this system (Kaul et al., unpublished data).

Another explanation of the lack of *camkii* transcripts in FMRP granules could be due probe inaccessibility in these RNPs. It has been previously shown that smFISH probe hybridization is capable of being hindered for transcripts confined within tightly packaged granules (Buxbaum et al., 2014). Thus, their occupancy within granules can effectively "mask" the identification of these transcripts by blocking probe hybridization. We are currently continuing our smFISH analysis with other transcripts predicted to be dependent on FMRP granule transport to see if these findings are pervasive amongst multiple targets.

5.5 Granule formation may be a functional consequence of translational repression

Using tethered and untethered translation reporter assays we were able to determine whether either of the KH domains were required for translation repression in an RNA binding-dependent or independent manner. It's predicted that the RGG box confers specificity for mRNA targets by binding to higher-order structures within the CDS or 3'UTR in mammalian FMRP (Vasilyev et al., 2015). When bound to these transcripts via the RGG box, the KH domains are then predicted to stall elongating ribosomes when they come into proximity of FMRP (Harigaya and Parker, 2014). As RNAs are flexible polymers, the KH domains could potentially stall translation by FMRP binding virtually anywhere on the transcript. Many G-quadruplex structures in FMRP-targets are located in

the 3'UTR, which was the reasoning behind the design of our luciferase reporters containing putative RNA binding sites in the 3'UTR (Zhang et al., 2014). Using the QGRS Mapper, we were able to identify putative G-quadruplex structures in the 3'UTRs of the different FMRP target transcripts (Kikin et al., 2006). The *FMR1* and *chic* 3'UTRs contain G-quadruplex structures, which could be targeted by the RGG box. However, *camkII* and *ppk* 3'UTRs are not predicted to contain these structures and thus are likely to either depend on RGG binding to other RNA structures or on the other RNA binding domains within FMRP.

In our study, we found that the KH1* mutant significantly impaired FMRP-mediated translation repression of several FMRP targets (Figure 19). The KH1* mutation disrupts mRNA binding and polysome association supporting our results (Myrick et al., 2014). Our work here adds to these previous studies by showing that the KH1* mutation can perturb translation repression independent of RNA-binding (Figure 18B). In contrast, KH2* did not disrupt translation repression of most of the luciferase reporters used in this study. This was surprising as the KH2 mutation has been shown to disrupt FMRP translation repression *in vitro* (Laggerbauer et al., 2001). The KH1 domain, and to a lesser extent the KH2 domain, inhibits ribosome translocation by directly binding the ribosome (Chen et al., 2014). We argue that FMRP may function in translationally repressing our luciferase reporters in a ribosome-binding and stalling-dependent manner, as we see a greater effect when we disrupt the KH1 domain. It's important to note that we were not

able to distinguish whether the FXS-causing mutants were disrupting RNA-binding or translation repression in our untethered luciferase reporter assays (Figure 19).

From these findings, we provide a model describing the functional consequence of reduced granule formation by the KH1* mutation. Loss of RNA-binding, and thus valency, through the KH1* mutation significantly destabilizes FMRP within granules. This reduction in valency causes the phase transition boundary of these granules to shift upward, requiring higher local FMRP concentrations to initiate this process. Loss of granules indirectly reduces FMRP-mediated translation repression by reducing the propensity of corralling particular interactors that may enhance repression. Although translation repression is able to occur outside of granules, it is likely that within distinct cytoplasmic foci all the required components are contained and primed for action. Thus, although loss of granule formation does not abrogate this process, it can significantly inhibit it.

5.6 Disease-causing mutations in FMRP increase granule dynamics in contrast to promoting the formation of pathological inclusions

Many proteins associated with neurodegenerative diseases including Alzheimer's disease, amyotrophic lateral sclerosis (ALS), and multiple sclerosis (MS) undergo phase separation, linking MLOs to pathological inclusions which are a hallmark of these diseases (Ryan and Fawzi, 2019). Neurons are particularly susceptible to the formation of these pathological MLOs as they are post-mitotic cells that rely heavily on protein degradation pathways which function less efficiently in aged neurons (Lim and Yue, 2015). Interestingly we found in our study that FXS-causing point mutations in FMRP mostly

form more dynamic condensates, in contrast to these solid aggregates. To our knowledge this is the first time anyone has shown an MLO-associated protein linked to disease that doesn't have a propensity to form toxic insoluble aggregates when mutated.

What makes FMRP different from other phase separating proteins? Most other proteins produce gain-of-function mutations that make them form more "sticky" interactions within MLOs (Patel et al., 2015). This causes protein entrapment within granules, incapable of exchanging with the surrounds environment and thus unable to carry out normal functions. In the case of FMRP, we might be seeing the opposite effect. If FMRP is unable to stabilize interactions between RNAs, translation machinery or other RBPs within MLOs for long enough to carry out its normal function (in translational repression or RNA transport) it may cause a significant reduction in function. Further work needs to be done to determine whether altered dynamics of FMRP granules has a direct effect on NG function. **However, our study creates an interesting new framework for understanding how disrupting stable interactions and multivalency effect granule dynamics and formation and how some MLOs are more susceptible to these perturbations.**

5.7 Conclusions and future directions

FMRP is an important regulator of mRNA translation and transport within neurons. It is enriched within multiple distinct cytoplasmic foci, in which it is predicted to regulate these processes. Disruption of FMRP function due to single missense point mutations with the RNA-binding KH domains produces severe FXS. Unraveling how these mutations alter

FMRP-associated granules will aid in understanding what functions these domains have in their interaction with particular MLOs and how this may impact their associated disease states. The work presented here gives us a better understanding of the functions the structured RNA-binding domains and IDR have in FMRP recruitment to FMRP granules, SGs, P-bodies and NGs, and provides a model describing the functional consequence of granule formation in the context of translation repression. Future studies looking the differential interaction with the neuronal transcriptome in KH1* and KH2* are needed to better understand which and how targets are regulated by these domains.

CHAPTER SIX: MATERIALS AND METHODS

6.1 Experimental model and subject details

6.1.1 Fly stocks and husbandry

In all experiments, both male and female flies were used. *Drosophila* stocks were incubated at 25°C with 12-hour light/dark cycles and 60% humidity on standard Bloomington medium. Fly lines used and made in this study are listed in Appendix 1.

pUAST:attB:EGFP flies were generated via restriction cloning *EGFP* and each *EGFP-FMRP* mutant into the multiple cloning site of *pUAST-attB* for directional cloning into the 5'-*KpnI* and 3'-*XbaI* cloning sites. *pUAST:attB:EGFP* and *pUAST:attB:EGFP-FMRP* mutants were sent to *BestGene* where these constructs were injected into fly strain #24485 for *PhiC31* integration into chromosome III. *pUAST:attB:EGFP-FMRP* mutant flies were recombined with w^{1118};; $FMR1^{\Delta 50M}$ / *TM6B,* Tb^{+} FMR1 mutant flies for FMRP primary motor neuron experiments. Final recombinants were genotyped for the $FMR1^{\Delta 50M}$ deletion by knocking out a single adult in a PCR tube on ice for 5 minutes. Flies were squished with a 200 µL pipette tip in 5µL of squishing buffer (10 mM Tris-Cl pH 8.0, 1 mM EDTA, 25 mM NaCl, and 0.2 mg/mL proteinase K) and incubated at room temperature

for 20 minutes. Samples were then boiled at 95°C for 5 minutes, cooled on ice for 3 minutes and then spun down at 16,000X G for 5 minutes in benchtop centrifuge. For genotyping, 5 μL of the supernatant (genomic DNA prep) was used in a standard NEB One Taq Polymerase PCR reaction using the *FMR1* deletion forward and reverse primers which were annealed at 60°C and elongated for 7 minutes as described by Zhang et al. (Zhang et al., 2001). PCR products were ran in a 1% agarose gel following standard DNA gel electrophoresis procedures and probed for the presence of a 4.2 kbp (deletion) or 6.8 kbp (*wildtype*) PCR product.

2.1.2 Schneider's S2R+ and S2 cell culture

S2 and S2R+ cells were maintained at 24°C with ambient humidity in a dark incubator and maintained on Shields and Sang M3 media (Sigma-Aldrich; S8398) containing bactopeptone and yeast extract, and supplemented with 10% fetal bovine serum (Gibco; 16000044), 1% penstrep (Invitrogen; 15070-063) and fungizone (Invitrogen; 15290-026), also known as M3+BPYE media. DNA transfections were performed with Qiagen's Effectene Transfection Reagent kit (Qiagen; 301425) (see below). Most experiments were conducted on S2R+ cells due to their higher propensity to adhere to and flatten out on cover slips, making imaging stationary cells more reliable.

6.1.3 *Drosophila* third-instar primary larval motor neuron tissue culture

Primary motor neurons were cultured from wandering 3rd instar larvae using a tissue culture protocol adapted from Barbee et al. 2006. For each genotype, 10 larvae were washed briefly in 70% ethanol, followed by five one-minute washes in 1xPBS pH 7.4.

CNS's were dissected from 3rd instar larvae in supplemented media, or M3+BPYE media supplemented with 50 μg/mL insulin (Sigma-Aldrich; I6634), from which optic lobes were also removed leaving only the ventral ganglia (VG). VG were washed briefly in supplemented media five times, then transferred to a sterile microfuge tube containing ~1 mL of Rinaldini's solution (800mg NaCl, 20mg KCl, 5mg NaH2PO4*H2O, 100mg NaHCO3, 100mg glucose, and 1mL penstrep to final volume of 100 mL). VG were spun for 5 minutes at 300 x G. Supernatant was carefully removed, and fresh Rinaldini's solution was added, vortexed, spun down and removed a total of five times to wash off residue yeast and other contaminants. In a sterile hood, supernatant was removed and 1mL of Liberase (Roche; LIBDH-RO; containing collagenase and dispase) supplemented Rinaldini solution was incubated with VG for 1 hour. The dissociated tissue was then spun down for 5 minutes at 300 x G. Supernatant was discarded and VG were washed another 4 times with supplemented M3+BPYE media. Following this, the supernatant was removed and VG were resuspended in 200μl of supplemented media. The dissociated VG were titrated with a fire-polished, glass Pasteur pipette 56 times and then 175 times with a medium coated P200 tip. The MN cell suspension was then seeded onto a single Concanavalin-A (Sigma-Aldrich; C2010) and Laminin (Corning; CB-40232) coated 35mm glass bottom dish (Cellvis; D35-10-1-N). Once plated, cells were incubated at 24°C with ambient humidity in a dark incubator 3-5 days before imaging. Media was carefully aspirated and replaced every 2 days.

6.2 Method details

6.2.1 Molecular cloning and Site directed mutagenesis

For S2 cell fluorescence imaging, *pAc5.1B:EGFP-FMRP-IDR* and *ΔKH* mutants were cloned into the multiple cloning site of *pAc5.1B-EGFP* following PCR amplification of the target open reading frame(s) from *pAc5.1B:EGFP-FMRP*. Amplification primer sequences and sites are listed and described in the Appendix 1. The human KH1 Gly266Glu and KH2 Ile367Asn point mutations are orthologous to *Drosophila* Gly269Glu and Ile307Asn, respectively. To generate these Fragile X Syndrome causing point mutants in *Drosophila* FMRP, SDM primers were designed using the "substitution" feature in NEBaseChanger v1.2.9 (New England BioLabs Inc.). Mutagenesis was designed to occur at nucleotide 805-807 (GGA→ GAA) and nucleotide 868-870 (ATC→ AAC) in the KH1 and KH2 domain, respectively. NEB's Q5 Site-Directed Mutagenesis Kit Protocol (E0554) was conducted on the *pAc5.1B:EGFP-FMRP* vector to introduce the KH1 and KH2 missense mutations. The following modifications were made to NEB's mutagenesis PCR reaction: KH1 mutagenic primers Ta=62℃, elongation at 72℃ for 4 minutes; KH2 mutagenic primers Ta= 64℃, elongation at 72℃ for 4 minutes.

To clone the SG protein, Rasputin, into a C-terminally tagged mCherry vector, we constructed a $(Gly_4Ser)_3$ linker-mcherry pAc5.1 vector. The mCherry-tag was amplified from *pAc5.1B-mCherry* which included 5'-*HindIII* and 3'-*BamHI* restriction sites for directional cloning into *pAc5.1B* with an in-frame stop codon following the mCherry sequence. Primers for cloning the $(Gly_4Ser)_3$ linker upstream of mCherry were also

designed to allow for ligation of the three fragments (pAc5.1 + $(Gly_4Ser)_3$ + mCherry) in the correct orientation. To amplify Rasputin (Rin) to clone into the mCherry vector, total RNA was extracted from four BL Canton S adult males using the Zymogen RNA extraction kit and following the manufacturer's protocol (Zymo Research Corporation; R2060). RT-PCR was then conducted on total RNA using Clontech's RNA to cDNA EcoDry™ Premix (Oligo dT) kit (#639543). Rasputin cDNA was amplified using primers that added 5'-*HindIII* and 3'-*EcoRI* restriction sites for directional cloning into the mCherry vector to make the final pAc5.1B:Rasputin-$(Gly_4Ser)_3$-mCherry.

The Fluc reporters used in the translation reporter assays were all sourced from the *pAc5.1C:FLuc:Stop:5BoxB* backbone vector (Addgene #21301). The 5BoxB 3'UTR was replaced with the 3'UTRs of *FMR1* and *camkii* by Restriction or Gibson cloning methods. We cloned the *camkii* isoform with the long 3'UTR, so that all possible binding sites were conserved in the reporter. DNA from 4 adult male BL Canton S flies was extracted and purified using the E.Z.N.A Tissue DNA kit (Omega Bio-Tek #D3396-01). From the extracted DNA, the long 3'UTR of *camkii* was amplified using the CaMKIIUTRFwdGA and CaMKIIUTRRvsGA primer set, then purified using Zymogen's DNA Clean and Concentrator-5 Kit (#11-302C). *pAc5.1C:FLuc:Stop:5BoxB* was digested with *EcoRI*-HF and *XhoI* following NEB's general protocol for restriction enzymes to remove the 5xBoxB 3'UTR. The *camkii* 3'UTR was then cloned into the luciferase destination vector via Gibson Assembly (#E2611) following NEB's protocol. The *FMR1* 3'UTR was similarly amplified using the FMR1Fwd and FMR1Rvs primer set and then

cloned into the *pAc5.1C:FLuc:Stop:5BoxB* destination vector using the 5'*EcoRI* and 3'*XhoI* restriction sites while removing the 5xBoxB sequence.

6.2.2 S2R+ and S2 cells transient transfections and cell viability assay

Transient transfections were performed following Qiagen's standard Effectene reagent protocol in which 0.5 μg of each construct was optimized, except for *pAc5.1B-EGFP:FMRP:KH1* in which 0.75 μg was transfected per 1 million cells in a 12-well plate. Transfected cells were grown for approximately 72 hours before used in assays.

To determine whether any of the ectopically expressed FMRP mutants were lethal to cells, we used trypan blue to identify differences in viability. Three days post-transfection, a 1:1 dilution was made of each cell suspension and 0.4% Trypan Blue solution. Approximately 10μl of this solution was loaded onto a hemocytometer and incubated for 2 minutes at room temperature. Viable cells remained unstained and translucent in appearance, whereas non-viable cells were stained blue. All unstained and blue cells within a 1 x 1 mm square were manually counted in triplicate experiments. Data were plugged into Excel to determine % viability and analyzed using Prism.

6.2.3 Live cell imaging and analysis of granule

For granule formation, morphology and count assays, live cell imaging was conducted on transiently transfected S2R+ cells. Cells were plated on poly-d lysine coated imaging dishes 72 hours post-transfection and imaged within 2 hours of plating. In all experiments, images were obtained using an Olympus FV3000 confocal laser scanning

microscope and cells were visualized with a 100x (NA 1.4) objective digitally zoomed to 2.95x for best resolution.

To count the number of transfected cells able to form granules, approximately 100 cells were manually identified at the microscope. The total number of cells that formed granules out of all EGFP-expressing cells were counted. Cells were scanned through in Z to make sure that granules in any plane were identified. The number of granule-forming cells was divided by total number of transfected cells in three separate experiments.

To compare the propensity of the different mutants to form spherical granules, approximately 100 granule-forming transfected cells were identified at the microscope. The number of cells forming spherical and amorphic (non-spherical) granules were counted. In most cases, cells that formed amorphous granules also contained spherical granules-- cells that formed any number of amorphous granules were categorized as amorphic.

Finally, to count granules formed by each FMRP-mutant, 15 cells were analyzed in a single experiment. The z-plane where the nucleus took up the largest cell area was examined. Punctate areas of fluorescence intensity above background were considered to be granules and counted using ImageJ's cell counter plugin. For each image, both cell diameter (through the longest axis in the same z-plane) and granule number were collected. From this, the number of granules per cell area (μm^2) was plotted.

Data from each of these experiments was entered into Excel for initial analysis. These data were then entered into Prism for statistical analysis.

6.2.4 Fluorescence Recovery After Photobleaching

For FRAP experiments, 17-21 EGFP positive granules were viewed with a 100x (NA 1.4) objective digitally zoomed to 2.95x and photobleached with the lowest laser intensity necessary to completely bleach ROI, ranging from 2.44-10% 488nm laser power for 500-1,000 milliseconds. Two pre-FRAP images were collected and images were captured every 1.0878 seconds pre and post bleaching for a total of 200 frames.

To set up the FRAP analysis, images were initially processed in ImageJ2/FIJI (Rueden et al., 2017; Schindelin et al., 2012). Data were analyzed essentially as described in (Cheney et al., 2017). A ROI was manually traced in each FRAP movie for 1) the bleached granule, 2) an unbleached granule, and 3) diffuse cytoplasmic staining for background. To ensure that fluorescence was accurately measured, ROI was moved throughout the movie if/when granules moved in x/y out of the initially set ROI to maintain consistency. From these movies, the mean fluorescent intensity was obtained for each frame and plugged into an excel sheet. Using these data, the following was calculated: 1) Photobleach Correction Value (PCV), in which the initial pre-bleach unbleached granule average fluorescence intensity was divided by each subsequent unbleached granule average intensity, 2) Corrected Average Intensity (CAI), where the bleached granules mean intensity was multiplied by the PCV, 3) Background Corrected Fluorescence Intensity (BCFI), where the CAI was subtracted by the average intensity of the background ROI, and 4) the Final Corrected Value (FCV) which was calculated by dividing each BCFI by the initial BCFI value and multiplying by 100 to get a normalized fluorescence intensity

profile. The FCV's from each movie were then plugged into a nonlinear fit in Prism to calculate the fluorescence recovery curve, mobile fraction, and half-life.

For the IDR FRAP analysis, WT-FMRP Relative Fluorescence was adjusted post-hoc. For some unknown reason, WT granules were bleached to an average fluorescence intensity of -20 following photobleaching, which caused a shift in the recovery curve. As this did not occur in WT in our FXS-causing point mutant WT, we did not believe this was the true representation of these data. To adjust for this, each data point was increased by 20 to account for this deviation.

6.2.5 Immunocytochemistry, arsenite and 1,6-hexanediol treatments

The following immunocytochemistry procedure was followed for all S2R+/S2 cell imaging, unless indicated otherwise. Cells were plated, immunostained and imaged on 35 mm glass bottom dishes with 10mm #1 cover glass (Cellvis; D35-10-1-N). After allowing cells to settle on imaging dishes for at least 20 minutes, they were fixed with 4% PFA for 10 minutes followed by a 5-minute incubation with ice cold methanol at -20°C. Cells were washed three times for 5 minutes in 1xPBS (pH 7.4), permeabilized in 1xPBST (pH 7.4) for 10 minutes, and then blocked in 1xPBST with 2% BSA (w/v; Sigma-Aldrich, A9647) and 5% normal goat serum (v/v; Sigma-Aldrich, S26-M) for 30 minutes. Cells were incubated with primary antibodies overnight at 4°C, washed in 1xPBS, and then incubated for 1 hour in secondary antibodies at room temperature. Cells were washed with 1xPBS and then mounted in DAPI-Fluoromount-G Clear Mounting Media and sealed by adhering a #1 coverslip to the dish.

For FXS-causing point mutants/HPat colocalization experiments, immunostaining was conducted on cells transfected with *pAc5.1B:EGFP-FMRP* and FXS-causing point mutants. For this assay, rabbit anti-HPat (1:1,500) primary and goat anti-rabbit Alexa-567 (1:500) secondary antibodies were used.

To induce stress, cells were co-transfected with *pAc5.1B:EGFP-FMRP* mutants and *pAc5.1B-Rasputin(Gly$_4$Ser)$_3$mCherry*. At 72 hours post transfection, cells were treated with 0.5mM sodium meta-arsenite in M3+BPYE media for 45 minutes. For colocalization analysis, cells were immediately fixed in 4% PFA for 10 minutes, incubated with ice cold methanol at -20°C for 5 minutes and then washed 3 times for 5 minutes in 1xPBS (pH 7.4). Preparations were then mounted in DAPI-Fluoromount-G Clear Mounting Media (Southern Biotech).

For analysis of granules with 1,6-hexanediol transfected cells were co-transfected with *pAc5.1:EGFP-FMRP* mutants and *pAc5.1-Rasputin(Gly$_4$Ser)$_3$mCherry*. Non-stressed cells were imaged via CLSM on either fresh cell culture media or 10% 1,6-hexanediol (w/v) in media. Cells were imaged within 20 minutes of the addition of hexanediol, as cells start to bleb and stress granules begin to form after long exposure times (Wheeler et al., 2016). Stressed cells were treated with 0.5 mM sodium arsenite for 45 minutes before the addition of fresh 0.5 mM arsenite, or 0.5 mM arsenite + 10% 1,6-hexanediol. In all conditions, approximately 100 live transfected cells were analyzed for the presence of FMRP or Rin granules, in triplicate. Data from each of these experiments was entered into

Excel for initial analysis. These data were then entered into Prism where we performed statistical analysis and created graphs.

6.2.6 Colocalization analysis

To determine the degree to which FMRP mutants colocalized with SG or P-body components, 12-13 images were analyzed in ImageJ/FIJI using the Just Another Colocalisation Plugin, JACoP (Bolte and Cordelières, 2006). In all cases, images were cropped to the smallest area possible to eliminate colocalization events outside of the cell of interest and images for FMRP/HPat colocalization were background subtracted to a rolling ball radius of 50 pixels to account for the higher degree of HPat background staining. In JACoP, Pearson's coefficient analysis was performed between the FMRP and SG or P-body channels which were recorded in Excel and analyzed in Prism.

6.2.7 Western blotting

Western blots were generally carried out as follows. Samples were boiled at 95°C for 10 minutes, chilled on ice for 5 minutes and sonicated for three one second pulses, with one second pauses in between at 50 mW on ice. Samples were chilled on ice for 5 minutes before clarification at 15,000X G for 15 minutes at 4°C. Supernatants were carefully transferred to a fresh microfuge tube on ice, and then 15-25 µL of sample was added per well in a 4-20% Mini-PROTEAN TGX Precast Protein Gel (Bio-Rad, #4561094). Gels were run at 250V for 35 minutes or until adequate separation was achieved. Prior to protein transfer, the SDS-PAGE gel and nitrocellulose membrane were equilibrated in 1x transfer buffer for 10 minutes with agitation. Gel transfer to nitrocellulose membrane was run at

120V for 45 minutes on a stir plate with an ice pack to keep the solution cool. The nitrocellulose membrane was then incubated in blocking solution (5% non-fat milk in 1X TBST pH 7.4) for 30 minutes at room temperature with agitation. Primary antibodies were diluted in blocking solution (indicated below) and incubated with membrane for either 2 hours at room temperature or overnight at 4°C with agitation. Membranes were washed 5 times in 1X TBST with agitation. Secondary antibodies were diluted in blocking solution and incubated with membrane for 45 minutes to 1 hour at room temperature with agitation. Membranes were washed in TBST for 5 minutes 3 times with agitation. Approximately 1 mL of Thermo Scientific SuperSignal West Dura Chemiluminescent Substrate (Thermo Scientific; 34075) was incubated with membrane before imaging on a FluorChem R (ProteinSimple).

For westerns conducted on *EGFP-FMRP* mutant ectopic expression assays in S2R+ cells, transfected cells were harvested at three days post-transection from a 6-well plate. Cells were scraped and resuspended by pipetting up and down and 1.5 mL of cells were spun down at 1,000x G for 5 minutes at 4°C. Cells were then resuspended in 400 µL of 2x Laemmli sample buffer + **β**-mercaptoethanol on ice.

For westerns conducted on C380, cha-Gal80/+ ; ; UAS:EGFP-FMRP, $FMR1^{\Delta 50M}$/+ larvae ectopically expressing the FXS-causing point mutants, 5 CNS's were diluted in 100µL of 2x Laemmli sample buffer + **β**-mercaptoethanol on ice. CNS's were homogenized in a 1.6 mL microcentrifuge tube for 30 seconds on ice using a hand-held

homogenizer. Homogenate was incubated on ice for 3 minutes, and then processed as indicated above.

For both of these assays, the primary antibodies used were mouse anti-*dFMR1* (1:3,000), rabbit anti-*EGFP* (1:2,000), and mouse anti-*a-tubulin* (1:1,000). Secondary antibodies used were horse anti-mouse HRP or goat anti-rabbit HRP which were diluted 1:1,000 in block.

6.2.8 Primary motor neuron imaging and neurite transport analysis

Primary motor neurons were cultured from flies as indicated in section 6.1.3. At 3-5 days post-harvest, live primary motor neurons were imaged using an Olympus FV3000 scanning confocal microscope with a 100x (NA 1.4) objective. For soma imaging, images were digitally zoomed to 2.95x for optimal resolution and a z-stack was obtained with 0.39μm slices through the entire soma. Images were presented as Z-projections which were made using Fiji/ImageJ.

For neurite transport movies, live cells were imaged with the 100x objective digitally zoomed to 1.79x so most branching neurites were imaged. Movies were collected containing four 0.39μm z-slices, over 100 frames (8:04 minutes). Movies were then analyzed using the Kymolyzer plugin in FIJI/ImageJ from which granule velocities and directionality were obtained, using a lower speed limit set to the pixel size, 0.138μm. (Basu et al., 2020).

To calculate the average number of neuritic granules in primary motor neurons, the max-intensity Z-projection of the first time point imaged was used (Frame 1). The Cell

Counter plugin was used to manually count the number of granules within neurites for each of the movies used for tracking neuritic granules. Additionally, the proportion of neuritic granules 10μm or further from the cell body was determined from these images. The scale of these images was globally set and a symmetrical circle was drawn tightly around each cell using the Oval selection tool in ImageJ, containing as much of the cell as possible. The diameter of each cell body was recorded in μm. The center of each circle was determined and marked using the Pencil tool. From this point, a line was drawn to the center of each granule within neurites and crude distance from the cell body was recorded in μm. The distances recorded were subtracted by the radius for their respective cell body to obtain the final distance used in analysis. Data were recorded in Excel and statistical analyses were performed in Prism.

6.2.9 Single molecule FISH and FISH-quant image analysis

Primary motor neurons were cultured from flies driving expression of *UAS-EGFP:FMRP, FMRΔ50* under the control of the *C380,cha-Gal80* driver as described in section 6.1.3. Custom Stellaris® FISH Probes were designed against *Drosophila melanogaster fmrI, camkII, futsch,* and *chic* by utilizing the Stellaris® FISH Probe Designer (Biosearch Technologies Inc., Petaluma, CA) available online at www.biosearchtech.com/stellarisdesigner. Primary motor neurons were hybridized with the indicated Stellaris FISH Probe set labeled with either Quasar-570 or 670 (Biosearch Technologies, Inc.) following the manufacturer's instructions available online at www.biosearchtech.com/stellarisprotocols. Essentially, at 3-4 days post culturing, cells

growing on #1.5 cover glass were washed in 1X PBS (pH 7.4). Cells were then incubated in fixation buffer (3.7% formaldehyde in 1X PBS) for 10 minutes at room temperature, then washed twice in PBS. To permeabilize cells were immersed in 70% ethanol at 4°C for at least 1 hour and up to a week. Ethanol was aspirated and cells were washed in Stellaris Wash Buffer A for 5 minutes, then hybridized with the indicated probe(s) in a dark, humid hybridization chamber at 37°C for 5-16 hours. Probes were used at a final molarity of 0.125μM in Stellaris Hybridization buffer. Hybridization buffer was aspirated and cells were incubated with Wash Buffer A twice at 37°C for 30 minutes, then washed with Stellaris Wash Buffer B for 5 minutes at room temperature. Buffer was aspirated and Vectashield Mounting Medium was added to the #1.5 cover glass in the imaging dish and a clean coverslip was placed on top and sealed with clear nail polish. Imaging dishes were stored in the dark at -20°C for up to 2 days before imaging on an ONI Nanoimager S.

Approximately 15 cells were imaged per genotype using the widefield microscopy application on the ONI Nanoimager S for imaging smFISH probes. In order to detect smFISH probes, cells were exposed to 7% 570- or 640-laser power for 1,500 milliseconds. Z-projection was obtained with 0.2 μm slices through the entire cell. EGFP-FMRP was imaged sequentially which allowed us to distinguish the soma and neurites from background.

To analyze smFISH images, we used the FISH-Quant Matlab application to detect, localize and quantify mRNA in primary motor neurons (Mueller et al., 2013). Motor neuron soma and neurites were outlined individually, which allowed us to differentiate

mRNAs residing within the soma and neurites. Data were compiled in Excel and statistical analyses were performed in Prism.

6.2.10 Luciferase reporter assays

Transfections were performed in three biological replicates in 24-well plates. For a single well, 0.025 μg of the *firefly* luciferase (FLuc) 3' UTR mRNA reporter plasmid, 0.1 μg of the *Renilla* luciferase (RLuc) transfection control plasmid, and 0.25 μg of either the empty λN vector or the λN: FMRP mutant vector was transfected. At three days post transfection, cells were thoroughly scraped and resuspended and 75 μL of cells were added in three technical replicates to a 96-well white, flat bottom polystyrene assay plate (Costar). Following the Dual-Glo Luciferase Assay System kit protocol (Promega), an equal volume of Dual-Glo Reagent and then Dual-Glo Stop & Glo Reagent were added to each well and incubated for 15 minutes before measuring FLuc and RLuc luminescence, respectively. Luminescence was measured using a Synergy™ HTX Multi-Mode Microplate Reader (BioTek).

6.2.11 Larval NMJ immunohistochemistry and morphological analysis

Third instar larval body wall preps for NMJ analysis were dissected in ice cold calcium-free Jan and Jan buffer (130 mM NaCl, 5 mM KCl, 36 mM sucrose, 5 mM HEPES [pH 7.3], 4 mM MgCl2, and 0.5 mM EGTA) within 30 minutes on sylgard plates. Dissection buffer was removed and preps were fixed in 4% PFA for 20 minutes, then washed 3x 5 minutes in 1X PBS (pH 7.4) and permeabilized in 1X PBS (pH 7.4) + 0.1% Triton X-100 for 10 minutes. Preps were blocked in 1X PBS with 2% BSA and 5% normal

goat serum with shaking for 30 minutes. Block was removed and primary antibody (mouse anti-DLG, 1:200) diluted in block was incubated overnight at 4°C. Preps were washed 6x 5 minutes in PBS and then incubated for 1 hour with secondary antibodies diluted in block at room temperature (goat anti-mouse Alexa 488 or 567 at 1:500 & Dylight 649-conjugated anti-HRP at 1:500). Preps were washed in 1xPBS and then mounted on slides in DAPI-Fluoromount-G Clear Mounting Media.

All imaging was done on an Olympus FV3000 scanning confocal microscope using 20X and 60X objectives to image the NMJ at muscles 6/7 in abdominal section 3 (N.A. 0.85 and 1.42, respectively). When shown, maximum Z projections were assembled from 0.4µm optical sections. All post-hoc image processing was done using Fiji in ImageJ2. For morphological analysis of larval NMJs, between 10-17 images were examined per experiment, in which 1s, 1b and axon terminals were manually counted at muscles 6 and 7 (m6/7) in abdominal segment 3 (A3) using the Cell Counter plugin in Fiji. To account for muscle area differences between genotypes which effects NMJ size, synaptic bouton numbers were normalized to muscle surface area (MSA). MSA was calculated by outlining both m6/7 using the freehand selection tool in ImageJ2/Fiji and recording the calculated muscle area. 1s and 1b bouton numbers were divided by the corresponding muscle area. These data were then normalized to the *C380-Gal4/+;; UAS-EGFP/+* overexpression controls. Data were collected and calculations were conducted in Excel and statistical analyses were performed in Prism.

6.2.12 Quantification and statistical analysis

All data were initially recorded in Excel (Microsoft) and then graphed and analyzed in Prism version 9.0.2 (GraphPad). Results were considered statistically significant if $p<0.05$. Error bars throughout the study indicate mean ± SEM. n.s. = not significant, * $p<0.05$, ** $p<0.01$, *** $p<0.001$, and **** $p<0.0001$. Outliers were identified and removed using ROUT method in Prism, where necessary. Statistical tests and sample sizes for each experiment are indicated within the corresponding figure legend and/or in methods section.

REFERENCES

Abbeduto, L., McDuffie, A., and Thurman, A.J. (2014). The fragile X syndrome--autism comorbidity: what do we really know? Front. Genet. *5*, 355.

Al-Husini, N., Tomares, D.T., Bitar, O., Childers, W.S., and Schrader, J.M. (2018). α-Proteobacterial RNA Degradosomes Assemble Liquid-Liquid Phase-Separated RNP Bodies. Mol. Cell *71*, 1027-1039.e14.

Alberti, S. (2017). Phase separation in biology. Curr. Biol. *27*, R1097–R1102.

Alpatov, R., Lesch, B.J., Nakamoto-Kinoshita, M., Blanco, A., Chen, S., Stützer, A., Armache, K.J., Simon, M.D., Xu, C., Ali, M., et al. (2014). A chromatin-dependent role of the fragile X mental retardation protein FMRP in the DNA damage response. Cell *157*, 869–881.

Anderson, P., and Kedersha, N. (2006). RNA granules. J. Cell Biol. *172*, 803–808.

Anderson, P., Kedersha, N., and Ivanov, P. (2015). Stress granules, P-bodies and cancer. Biochim. Biophys. Acta - Gene Regul. Mech. *1849*.

Antar, L.N., Afroz, R., Dictenberg, J.B., Carroll, R.C., and Bassell, G.J. (2004). Metabotropic Glutamate Receptor Activation Regulates Fragile X Mental Retardation Protein and Fmr1 mRNA Localization Differentially in Dendrites and at Synapses. J. Neurosci. *24*, 2648–2655.

Antar, L.N., Dictenberg, J.B., Plociniak, M., Afroz, R., and Bassell, G.J. (2005). Localization of FMRP-associated mRNA granules and requirement of microtubules for activity-dependent trafficking in hippocampal neurons. Genes, Brain Behav. *4*, 350–359.

Antar, L.N., Li, C., Zhang, H., Carroll, R.C., and Bassell, G.J. (2006). Local functions for FMRP in axon growth cone motility and activity-dependent regulation of filopodia and spine synapses. Mol. Cell. Neurosci. *32*, 37–48.

Arpag, G., Shastry, S., Hancock, W.O., and Tüzel, E. (2014). Transport by populations of fast and slow kinesins uncovers novel family-dependent motor characteristics important for in vivo function. Biophys. J. *107*, 1896–1904.

Ascano, M., Mukherjee, N., Bandaru, P., Miller, J.B., Nusbaum, J.D., Corcoran, D.L., Langlois, C., Munschauer, M., Dewell, S., Hafner, M., et al. (2012). FMRP targets distinct mRNA sequence elements to regulate protein expression. Nature *492*, 382–386.

Ashley, C.T., Wilkinson, K.D., Reines, D., and Warren, S.T. (1993). FMR1 protein: conserved RNP family domains and selective RNA binding. Science (80-.). *262*, 563–566.

Athar, Y.M., and Joseph, S. (2020). RNA-Binding Specificity of the Human Fragile X Mental Retardation Protein. J. Mol. Biol. *432*, 3851–3868.

Babinchak, W.M., Haider, R., Dumm, B.K., Sarkar, P., Surewicz, K., Choi, J.K., and Surewicz, W.K. (2019). The role of liquid-liquid phase separation in aggregation of the TDP-43 low-complexity domain. J. Biol. Chem. *294*, 6306–6317.

Banani, S.F., Rice, A.M., Peeples, W.B., Lin, Y., Jain, S., Parker, R., and Rosen, M.K. (2016). Compositional Control of Phase-Separated Cellular Bodies. Cell *166*, 651–663.

Banerjee, A., Ifrim, M.F., Valdez, A.N., Raj, N., and Bassell, G.J. (2018). Aberrant RNA translation in fragile X syndrome: From FMRP mechanisms to emerging therapeutic strategies. Brain Res. *1693*, 24–36.

Banjade, S., and Rosen, M.K. (2014). Phase transitions of multivalent proteins can promote clustering of membrane receptors. Elife *3*, e04123.

Barbee, S.A., Estes, P.S., Cziko, A.-M., Hillebrand, J., Luedeman, R.A., Coller, J.M., Johnson, N., Howlett, I.C., Geng, C., Ueda, R., et al. (2006). Staufen- and FMRP-containing neuronal RNPs are structurally and functionally related to somatic P bodies. Neuron *52*, 997–1009.

Bardoni, B., Castets, M., Huot, M.E., Schenk, A., Adinolfi, S., Corbin, F., Pastore, A., Khandjian, E.W., and Mandel, J.L. (2003). 82-FIP, a novel FMRP (Fragile X Mental Retardation Protein) interacting protein, shows a cell cycle-dependent intracellular localization. Hum. Mol. Genet. *12*, 1689–1698.

Bassell, G.J., and Warren, S.T. (2008). Fragile X syndrome: loss of local mRNA regulation alters synaptic development and function. Neuron *60*, 201–214.

Basu, H., Ding, L., Pekkurnaz, G., Cronin, M., and Schwarz, T.L. (2020).

Kymolyzer, a Semi-Autonomous Kymography Tool to Analyze Intracellular Motility. Curr. Protoc. Cell Biol. *87*.

Bear, M.F., Huber, K.M., and Warren, S.T. (2004). The mGluR theory of fragile X mental retardation. Trends Neurosci. *27*, 370–377.

Bechara, E.G., Didiot, M.C., Melko, M., Davidovic, L., Bensaid, M., Martin, P., Castets, M., Pognonec, P., Khandjian, E.W., Moine, H., et al. (2009). A novel function for fragile X mental retardation protein in translational activation. PLoS Biol. *7*, e1000016.

Berry, J., Brangwynne, C.P., and Haataja, M. (2018). Physical principles of intracellular organization via active and passive phase transitions. Reports Prog. Phys. *81*, 046601.

Bertrand, E., Chartrand, P., Schaefer, M., Shenoy, S.M., Singer, R.H., and Long, R.M. (1998). Localization of ASH1 mRNA particles in living yeast. Mol. Cell *2*, 437–445.

Boeynaems, S., Alberti, S., Fawzi, N.L., Mittag, T., Polymenidou, M., Rousseau, F., Schymkowitz, J., Shorter, J., Wolozin, B., Van Den Bosch, L., et al. (2018). Protein Phase Separation: A New Phase in Cell Biology. Trends Cell Biol. *28*, 420–435.

Bolognesi, B., Gotor, N.L., Dhar, R., Cirillo, D., Baldrighi, M., Tartaglia, G.G., and Lehner, B. (2016). A concentration-dependent liquid phase separation can cause toxicity upon increased protein expression. Cell Rep. *16*, 222–231.

Bolte, S., and Cordelières, F.P. (2006). A guided tour into subcellular colocalization analysis in light microscopy. J. Microsc. *224*, 213–232.

De Boulle, K., Verkerk, A.J.M.H., Reyniers, E., Vits, L., Hendrickx, J., Van Roy, B., Van Den Bos, F., de Graaff, E., Oostra, B.A., and Willems, P.J. (1993). A point mutation in the FMR-1 gene associated with fragile X mental retardation. Nat. Genet. *3*, 31–35.

Brand, A., and Perrimon, N. (1993). Targeted gene expression as a means of altering cell fates and generating dominant phenotypes. Development *118*, 401–415.

Brangwynne, C.P., Eckmann, C.R., Courson, D.S., Rybarska, A., Hoege, C., Gharakhani, J., Julicher, F., and Hyman, A.A. (2009). Germline P Granules Are Liquid Droplets That Localize by Controlled Dissolution/Condensation. Science (80-.). *324*,

1729–1732.

Brown, V., Jin, P., Ceman, S., Darnell, J.C., O'Donnell, W.T., Tenenbaum, S.A., Jin, X., Feng, Y., Wilkinson, K.D., Keene, J.D., et al. (2001). Microarray identification of FMRP-associated brain mRNAs and altered mRNA translational profiles in fragile X syndrome. Cell *107*, 477–487.

Buchan, J.R., and Parker, R. (2009). Eukaryotic Stress Granules: The Ins and Outs of Translation. Mol. Cell *36*, 932–941.

Bushey, D., Tononi, G., and Cirelli, C. (2009). The Drosophila Fragile X Mental Retardation Gene Regulates Sleep Need. J. Neurosci. *29*, 1948–1961.

Buxbaum, A.R., Wu, B., and Singer, R.H. (2014). Single β-actin mRNA detection in neurons reveals a mechanism for regulating its translatability. Science (80-.). *343*, 419–422.

Carson, J.H., Cui, H., and Barbarese, E. (2001). The balance of power in RNA trafficking. Curr. Opin. Neurobiol. *11*, 558–563.

Castrén, M., Castrén, C., Haapasalo, A., Oostra, B.A., and Castrén, E. (2001). Subcellular Localization of Fragile X Mental Retardation Protein with the I304N Mutation in the RNA-Binding Domain in Cultured Hippocampal Neurons.

Chakraborty, A., Jenjaroenpun, P., Li, J., El Hilali, S., McCulley, A., Haarer, B., Hoffman, E.A., Belak, A., Thorland, A., Hehnly, H., et al. (2020). Replication Stress Induces Global Chromosome Breakage in the Fragile X Genome. Cell Rep. *32*, 108179.

Cheever, A., and Ceman, S. (2009). Translation regulation of mRNAs by the fragile X family of proteins through the microRNA pathway. RNA Biol. *6*, 175–178.

Chen, E., Sharma, M.R., Shi, X., Agrawal, R.K., and Joseph, S. (2014). Fragile X Mental Retardation Protein Regulates Translation by Binding Directly to the Ribosome. Mol. Cell *54*, 407.

Cheney, P.P., Weisgerber, A.W., Feuerbach, A.M., and Knowles, M.K. (2017). Single lipid molecule dynamics on supported lipid bilayers with membrane curvature. Membranes (Basel). *7*.

Choi, J.M., Holehouse, A.S., and Pappu, R. V. (2020). Physical Principles Underlying the Complex Biology of Intracellular Phase Transitions. Annu. Rev. Biophys. *49*, 107–133.

Christie, S.B., Akins, M.R., Schwob, J.E., and Fallon, J.R. (2009). The FXG: A Presynaptic Fragile X Granule Expressed in a Subset of Developing Brain Circuits. J. Neurosci. *29*, 1514–1524.

Cioni, J.M., Lin, J.Q., Holtermann, A. V., Koppers, M., Jakobs, M.A.H., Azizi, A., Turner-Bridger, B., Shigeoka, T., Franze, K., Harris, W.A., et al. (2019). Late Endosomes Act as mRNA Translation Platforms and Sustain Mitochondria in Axons. Cell *176*, 56-72.e15.

Coffee, B., Ikeda, M., Budimirovic, D.B., Hjelm, L.N., Kaufmann, W.E., and Warren, S.T. (2008). Mosaic FMR1 deletion causes fragile X syndrome and can lead to molecular misdiagnosis: A case report and review of the literature. Am. J. Med. Genet. Part A *146A*, 1358–1367.

Coffee, B., Keith, K., Albizua, I., Malone, T., Mowrey, J., Sherman, S.L., and Warren, S.T. (2009). Incidence of Fragile X Syndrome by Newborn Screening for Methylated FMR1 DNA. Am. J. Hum. Genet. *85*, 503–514.

Coller, J., and Parker, R. (2005). General translational repression by activators of mRNA decapping. Cell *122*, 875–886.

Collins, S.C., Bray, S.M., Suhl, J.A., Cutler, D.J., Coffee, B., Zwick, M.E., and Warren, S.T. (2010). Identification of novel FMR1 variants by massively parallel sequencing in developmentally delayed males. Am. J. Med. Genet. Part A *152*, 2512–2520.

Cougot, N., Bhattacharyya, S.N., Tapia-Arancibia, L., Bordonné, R., Filipowicz, W., Bertrand, E., and Rage, F. (2008). Dendrites of mammalian neurons contain specialized P-body-like structures that respond to neuronal activation. J. Neurosci. *28*, 13793–13804.

Darnell, J.C., Jensen, K.B., Jin, P., Brown, V., Warren, S.T., and Darnell, R.B. (2001). Fragile X mental retardation protein targets G quartet mRNAs important for neuronal function. Cell *107*, 489–499.

Darnell, J.C., Fraser, C.E., Mostovetsky, O., Stefani, G., Jones, T.A., Eddy, S.R., and Darnell, R.B. (2005). Kissing complex RNAs mediate interaction between the Fragile-

X mental retardation protein KH2 domain and brain polyribosomes. Genes Dev. *19*, 903–918.

Darnell, J.C., Van Driesche, S.J., Zhang, C., Hung, K.Y.S., Mele, A., Fraser, C.E., Stone, E.F., Chen, C., Fak, J.J., Chi, S.W., et al. (2011). FMRP Stalls Ribosomal Translocation on mRNAs Linked to Synaptic Function and Autism. Cell *146*, 247–261.

Davidovic, L., Jaglin, X.H., Lepagnol-Bestel, A.-M., Tremblay, S., Simonneau, M., Bardoni, B., and Khandjian, E.W. (2007). The fragile X mental retardation protein is a molecular adaptor between the neurospecific KIF3C kinesin and dendritic RNA granules. Hum. Mol. Genet. *16*, 3047–3058.

Dictenberg, J.B., Swanger, S.A., Antar, L.N., Singer, R.H., and Bassell, G.J. (2008). A Direct Role for FMRP in Activity-Dependent Dendritic mRNA Transport Links Filopodial-Spine Morphogenesis to Fragile X Syndrome. Dev. Cell *14*, 926–939.

Didiot, M.C., Subramanian, M., Flatter, E., Mandel, J.L., and Moine, H. (2009). Cells lacking the fragile X mental retardation protein (FMRP) have normal RISC activity but exhibit altered stress granule assembly. Mol. Biol. Cell *20*, 428–437.

Dölen, G., Osterweil, E., Rao, B.S.S., Smith, G.B., Auerbach, B.D., Chattarji, S., and Bear, M.F. (2007). Correction of Fragile X Syndrome in Mice. Neuron *56*, 955–962.

Drozd, M., Bardoni, B., and Capovilla, M. (2018). Modeling fragile X syndrome in drosophila. Front. Mol. Neurosci. *11*, 124.

Eberhart, D.E., Malter, H.E., Feng, Y., and Warren, S.T. (1996). The fragile X mental retardation protein is a ribonucleoprotein containing both nuclear localization and nuclear export signals. Hum. Mol. Genet. *5*, 1083–1091.

Estes, P.S., O'Shea, M., Clasen, S., and Zarnescu, D.C. (2008). Fragile X protein controls the efficacy of mRNA transport in Drosophila neurons. Mol. Cell. Neurosci.

Eulalio, A., Rehwinkel, J., Stricker, M., Huntzinger, E., Yang, S.F., Doerks, T., Dorner, S., Bork, P., Boutros, M., and Izaurralde, E. (2007). Target-specific requirements for enhancers of decapping in miRNA-mediated gene silencing. Genes Dev. *21*, 2558–2570.

Falahati, H., and Wieschaus, E. (2017). Independent active and thermodynamic

processes govern the nucleolus assembly in vivo. PNAS *114*, 1335–1340.

El Fatimy, R., Davidovic, L., Tremblay, S., Jaglin, X., Dury, A., Robert, C., De Koninck, P., and Khandjian, E.W. (2016). Tracking the Fragile X Mental Retardation Protein in a Highly Ordered Neuronal RiboNucleoParticles Population: A Link between Stalled Polyribosomes and RNA Granules. PLOS Genet. *12*, e1006192.

Feng, Y., Absher, D., Eberhart, D.E., Brown, V., Malter, H.E., and Warren, S.T. (1997). FMRP associates with polyribosomes as an mRNP, and the I304N mutation of severe fragile X syndrome abolishes this association. Mol. Cell *1*, 109–118.

Fink, D.A., Nelson, L.M., Pyeritz, R., Johnson, J., Sherman, S.L., Cohen, Y., and Elizur, S.E. (2018). Fragile X Associated Primary Ovarian Insufficiency (FXPOI): Case Report and Literature Review. Front. Genet. *9*.

Fu, X., Yan, A., Xu, Y., Liao, J., Guo, X., Zhang, D., Yang, W., Zheng, D., and Lan, F. (2020). Splicing of exon 9a in FMR1 transcripts results in a truncated FMRP with altered subcellular distribution. Gene *731*, 144359.

Fu, Y.H., Kuhl, D.P.A., Pizzuti, A., Pieretti, M., Sutcliffe, J.S., Richards, S., Verkert, A.J.M.H., Holden, J.J.A., Fenwick, R.G., Warren, S.T., et al. (1991). Variation of the CGG repeat at the fragile X site results in genetic instability: Resolution of the Sherman paradox. Cell *67*, 1047–1058.

Garber, K.B., Visootsak, J., and Warren, S.T. (2008). Fragile X syndrome. Eur. J. Hum. Genet. *16*, 666–672.

Gareau, C., Houssin, E., Martel, D., Coudert, L., Mellaoui, S., Huot, M.-E., Laprise, P., and Mazroui, R. (2013a). Characterization of Fragile X Mental Retardation Protein Recruitment and Dynamics in Drosophila Stress Granules. PLoS One *8*, e55342.

Gareau, C., Martel, D., Coudert, L., Mellaoui, S., and Mazroui, R. (2013b). Characterization of fragile X mental retardation protein granules formation and dynamics in Drosophila. Biol. Open *2*, 68–81.

Goering, R., Hudish, L.I., Guzman, B.B., Raj, N., Bassell, G.J., Russ, H.A., Dominguez, D., and Taliaferro, J.M. (2020). FMRP promotes RNA localization to neuronal projections through interactions between its RGG domain and g-quadruplex RNA sequences. Elife *9*, e52621.

Harigaya, Y., and Parker, R. (2014). Fragile X Mental Retardation Protein and the Ribosome. Mol. Cell *54*, 330–332.

Hartwig, C.L., Worrell, J., Levine, R.B., Ramaswami, M., and Sanyal, S. (2008). Normal dendrite growth in Drosophila motor neurons requires the AP-1 transcription factor. Dev. Neurobiol. *68*, 1225–1242.

Hinnebusch, A.G. (2014). The Scanning Mechanism of Eukaryotic Translation Initiation. Annu. Rev. Biochem. *83*, 779–812.

Hollingworth, D., Candel, A.M., Nicastro, G., Martin, S.R., Briata, P., Gherzi, R., and Ramos, A. (2012). KH domains with impaired nucleic acid binding as a tool for functional analysis. Nucleic Acids Res. *40*, 6873–6886.

Hou, L., Antion, M.D., Hu, D., Spencer, C.M., Paylor, R., and Klann, E. (2006). Dynamic Translational and Proteasomal Regulation of Fragile X Mental Retardation Protein Controls mGluR-Dependent Long-Term Depression. Neuron *51*, 441–454.

Hsu, P.J., Shi, H., Zhu, A.C., Lu, Z., Miller, N., Edens, B.M., Ma, Y.C., and He, C. (2019). The RNA-binding protein FMRP facilitates the nuclear export of N6-methyladenosine-containing mRNAs. J. Biol. Chem. *294*, 19889–19895.

Hu, Y., Chen, Z., Fu, Y., He, Q., Jiang, L., Zheng, J., Gao, Y., Mei, P., Chen, Z., and Ren, X. (2015). The amino-terminal structure of human fragile X mental retardation protein obtained using precipitant-immobilized imprinted polymers. Nat. Commun. *6*, 6634.

Ingelfinger, D., Arndt-Jovin, D.J., Lührmann, R., and Achsel, T. (2002). The human LSm1-7 proteins colocalize with the mRNA-degrading enzymes Dcp1/2 and Xrn1 in distinct cytoplasmic foci. RNA *8*, 1489–1501.

Itoh, Y., Iida, S., Tamura, S., Nagashima, R., Shiraki, K., Goto, T., Hibino, K., Ide, S., and Maeshima, K. (2021). 1,6-hexanediol rapidly immobilizes and condenses chromatin in living human cells. Life Sci. Alliance *4*, e202001005.

Jain, S., Wheeler, J.R., Walters, R.W., Agrawal, A., Barsic, A., and Parker, R. (2016). ATPase-Modulated Stress Granules Contain a Diverse Proteome and Substructure. Cell *164*.

Jin, P., Zarnescu, D.C., Ceman, S., Nakamoto, M., Mowrey, J., Jongens, T.A., Nelson, D.L., Moses, K., and Warren, S.T. (2004). Biochemical and genetic interaction between the fragile X mental retardation protein and the microRNA pathway. Nat. Neurosci. *7*, 113–117.

Kanai, Y., Dohmae, N., and Hirokawa, N. (2004). Kinesin transports RNA: Isolation and characterization of an RNA-transporting granule. Neuron *43*, 513–525.

Kao, D.-I., Aldridge, G.M., Weiler, I.J., and Greenough, W.T. (2010). Altered mRNA transport, docking, and protein translation in neurons lacking fragile X mental retardation protein. Proc. Natl. Acad. Sci. *107*, 15601–15606.

Kapeli, K., and Yeo, G.W. (2012). Genome-wide approaches to dissect the roles of RNA binding proteins in translational control: implications for neurological diseases. Front. Neurosci. *6*.

Kenny, P., and Ceman, S. (2016). RNA secondary structure modulates FMRP's bi-functional role in the microRNA pathway. Int. J. Mol. Sci. *17*, 985.

Kiebler, M.A., and Bassell, G.J. (2006). Neuronal RNA Granules: Movers and Makers. Neuron.

Kikin, O., D'Antonio, L., and Bagga, P.S. (2006). QGRS Mapper: A web-based server for predicting G-quadruplexes in nucleotide sequences. Nucleic Acids Res. *34*.

Kim, T.H., Tsang, B., Vernon, R.M., Sonenberg, N., Kay, L.E., and Forman-Kay, J.D. (2019). Phospho-dependent phase separation of FMRP and CAPRIN1 recapitulates regulation of translation and deadenylation. Science *365*, 825–829.

Krichevsky, A.M., and Kosik, K.S. (2001). Neuronal RNA granules: A link between RNA localization and stimulation-dependent translation. Neuron *32*, 683–696.

Kroschwald, S., Maharana, S., Mateju, D., Malinovska, L., Nüske, E., Poser, I., Richter, D., and Alberti, S. (2015). Promiscuous interactions and protein disaggregases determine the material state of stress-inducible RNP granules. Elife *4*, 1–32.

Kroschwald, S., Maharana, S., and Simon, A. (2017). Hexanediol: a chemical probe to investigate the material properties of membrane-less compartments. Matters *3*, e201702000010.

Laggerbauer, B., Ostareck, D., Keidel, E.-M., Ostareck-Lederer, A., and Fischer, U. (2001). Evidence that fragile X mental retardation protein is a negative regulator of translation. Hum. Mol. Genet. *10*, 329–338.

Lahey, T., Gorczyca, M., Jia, X.X., and Budnik, V. (1994). The drosophila tumor suppressor gene dlg is required for normal synaptic bouton structure. Neuron *13*, 823–835.

Lai, A., Valdez-Sinon, A.N., and Bassell, G.J. (2020). Regulation of RNA granules by FMRP and implications for neurological diseases. Traffic.

Lee, E.K., Kim, H.H., Kuwano, Y., Abdelmohsen, K., Srikantan, S., Subaran, S.S., Gleichmann, M., Mughal, M.R., Martindale, J.L., Yang, X., et al. (2010). HnRNP C promotes APP translation by competing with FMRP for APP mRNA recruitment to P bodies. Nat. Struct. Mol. Biol. *17*, 732–739.

Li, C., Bassell, G., and Sasaki, Y. (2009). Fragile X mental retardation protein is involved in protein synthesis-dependent collapse of growth cones induced by Semaphorin-3A . Front. Neural Circuits *3*, 11.

Li, M., Shin, J., Risgaard, R.D., Parries, M.J., Wang, J., Chasman, D., Liu, S., Roy, S., Bhattacharyya, A., and Zhao, X. (2020). Identification of FMR1-regulated molecular networks in human neurodevelopment. Genome Res. *30*, 361–374.

Li, P., Banjade, S., Cheng, H.C., Kim, S., Chen, B., Guo, L., Llaguno, M., Hollingsworth, J. V., King, D.S., Banani, S.F., et al. (2012). Phase transitions in the assembly of multivalent signalling proteins. Nature *483*, 336–340.

Li, Y., Lin, L., and Jin, P. (2008). The microRNA pathway and fragile X mental retardation protein. Biochim. Biophys. Acta - Gene Regul. Mech. *1779*, 702–705.

Lim, J., and Yue, Z. (2015). Neuronal Aggregates: Formation, Clearance, and Spreading. Dev. Cell *32*, 491–501.

Lin, Y., Protter, D.S.W., Rosen, M.K., and Parker, R. (2015). Formation and Maturation of Phase-Separated Liquid Droplets by RNA-Binding Proteins. Mol. Cell *60*.

Liu, X., Shen, J., Xie, L., Wei, Z., Wong, C., Li, Y., Zheng, X., Li, P., and Song, Y. (2020). Mitotic Implantation of the Transcription Factor Prospero via Phase Separation Drives Terminal Neuronal Differentiation. Dev. Cell *52*, 277-293.e8.

Luo, Y., Na, Z., and Slavoff, S.A. (2018). P-Bodies: Composition, Properties, and Functions. Biochemistry *57*, 2424–2431.

Magee, J.C., and Grienberger, C. (2020). Synaptic Plasticity Forms and Functions. Annu. Rev. Neurosci. *43*, 95–117.

Majumder, M., Johnson, R.H., and Palanisamy, V. (2020). Fragile X-related protein family: a double-edged sword in neurodevelopmental disorders and cancer. Crit. Rev. Biochem. Mol. Biol. *55*, 409–424.

Martin, E.W., and Holehouse, A.S. (2020). Intrinsically disordered protein regions and phase separation: sequence determinants of assembly or lack thereof. Emerg. Top. Life Sci. *4*.

Mathieu, C., Pappu, R. V., and Paul Taylor, J. (2020). Beyond aggregation: Pathological phase transitions in neurodegenerative disease. Science (80-.). *370*, 56–60.

Matsuki, H., Takahashi, M., Higuchi, M., Makokha, G.N., Oie, M., and Fujii, M. (2013). Both G3BP1 and G3BP2 contribute to stress granule formation. Genes to Cells *18*, 135–146.

Maurin, T., Lebrigand, K., Castagnola, S., Paquet, A., Jarjat, M., Popa, A., Grossi, M., Rage, F., and Bardoni, B. (2018). HITS-CLIP in various brain areas reveals new targets and new modalities of RNA binding by fragile X mental retardation protein. Nucleic Acids Res. *46*, 6344–6355.

Mazroui, R., Hout, M.E., Tremblay, S., Fillion, C., Labelle, Y., and Khandjian, E.W. (2002). Trapping of messenger RNA by Fragile X Mental Retardation protein into cytoplasmic granules induces translation repression. Hum. Mol. Genet. *11*, 3007–3017.

McBride, S.M.J., Choi, C.H., Wang, Y., Liebelt, D., Braunstein, E., Ferreiro, D., Sehgal, A., Siwicki, K.K., Dockendorff, T.C., Nguyen, H.T., et al. (2005). Pharmacological rescue of synaptic plasticity, courtship behavior, and mushroom body defects in a Drosophila model of Fragile X syndrome. Neuron *45*, 753–764.

McBride, S.M.J., Holloway, S.L., and Jongens, T.A. (2013). Using Drosophila as a tool to identify pharmacological therapies for fragile X syndrome. Drug Discov. Today Technol. *10*, e129–e136.

Menon, K.P., Carrillo, R.A., and Zinn, K. (2013). Development and plasticity of the *Drosophila* larval neuromuscular junction. Wiley Interdiscip. Rev. Dev. Biol. *2*, 647–670.

Merrill, M.A., Chen, Y., Strack, S., and Hell, J.W. (2005). Activity-driven postsynaptic translocation of CaMKII. Trends Pharmacol. Sci. *26*, 645–653.

Mészáros, B., Erdös, G., and Dosztányi, Z. (2018). IUPred2A: Context-dependent prediction of protein disorder as a function of redox state and protein binding. Nucleic Acids Res. *46*, W329–W337.

Miyashiro, K.Y., Beckel-Mitchener, A., Purk, T.P., Becker, K.G., Barret, T., Liu, L., Carbonetto, S., Weiler, I.J., Greenough, W.T., and Eberwine, J. (2003). RNA cargoes associating with FMRP reveal deficits in cellular functioning in Fmr1 null mice. Neuron *37*, 417–431.

Molliex, A., Temirov, J., Lee, J., Coughlin, M., Kanagaraj, A.P., Kim, H.J., Mittag, T., and Taylor, J.P. (2015). Phase Separation by Low Complexity Domains Promotes Stress Granule Assembly and Drives Pathological Fibrillization. Cell *163*, 123–133.

Muddashetty, R.S., Nalavadi, V.C., Gross, C., Yao, X., Xing, L., Laur, O., Warren, S.T., and Bassell, G.J. (2011). Reversible inhibition of PSD-95 mRNA translation by miR-125a, FMRP phosphorylation, and mGluR signaling. Mol. Cell *42*, 673–688.

Mueller, F., Senecal, A., Tantale, K., Marie-Nelly, H., Ly, N., Collin, O., Basyuk, E., Bertrand, E., Darzacq, X., and Zimmer, C. (2013). FISH-quant: automatic counting of transcripts in 3D FISH images. Nat. Methods *10*, 277–278.

Murthy, A.C., Dignon, G.L., Kan, Y., Zerze, G.H., Parekh, S.H., Mittal, J., and Fawzi, N.L. (2019). Molecular interactions underlying liquid−liquid phase separation of the FUS low-complexity domain. Nat. Struct. Mol. Biol. *26*, 637–648.

Myrick, L.K., Nakamoto-Kinoshita, M., Lindor, N.M., Kirmani, S., Cheng, X., and Warren, S.T. (2014). Fragile X syndrome due to a missense mutation. Eur. J. Hum. Genet. *22*, 1185–1189.

Myrick, L.K., Hashimoto, H., Cheng, X., and Warren, S.T. (2015a). Human FMRP contains an integral tandem Agenet (Tudor) and KH motif in the amino terminal domain. Hum. Mol. Genet. *24*, 1733–1740.

Myrick, L.K., Deng, P.Y., Hashimoto, H., Oh, Y.M., Cho, Y., Poidevin, M.J., Suhl, J.A., Visootsak, J., Cavalli, V., Jin, P., et al. (2015b). Independent role for presynaptic FMRP revealed by an FMR1 missense mutation associated with intellectual disability and seizures. Proc. Natl. Acad. Sci. U. S. A. *112*, 949–956.

Nabavi, S., Fox, R., Proulx, C.D., Lin, J.Y., Tsien, R.Y., and Malinow, R. (2014). Engineering a memory with LTD and LTP. Nature *511*, 348–352.

Nakamoto, M., Nalavadi, V., Epstein, M.P., Narayanan, U., Bassell, G.J., and Warren, S.T. (2007). Fragile X mental retardation protein deficiency leads to excessive mGluR5-dependent internalization of AMPA receptors. Proc. Natl. Acad. Sci. *104*, 15537–15542.

Napoli, I., Mercaldo, V., Boyl, P.P., Eleuteri, B., Zalfa, F., De Rubeis, S., Di Marino, D., Mohr, E., Massimi, M., Falconi, M., et al. (2008). The Fragile X Syndrome Protein Represses Activity-Dependent Translation through CYFIP1, a New 4E-BP. Cell *134*, 1042–1054.

Neri, G. (2017). The clinical phenotype of the fragile X syndrome and related disorders. In Fragile X Syndrome: From Genetics to Targeted Treatment, (Elsevier), pp. 3–18.

Otero, Y.D.D., Severijnen, L.-A., Cappellen, G. van, Schrier, M., Oostra, B., and Willemsen, R. (2002). Transport of Fragile X Mental Retardation Protein via Granules in Neurites of PC12 Cells. Mol. Cell. Biol. *22*, 8332–8341.

Parker, R., and Sheth, U. (2007). P bodies and the control of mRNA translation and degradation. Mol. Cell *25*, 635–646.

Patel, A., Lee, H.O., Jawerth, L., Maharana, S., Jahnel, M., Hein, M.Y., Stoynov, S., Mahamid, J., Saha, S., Franzmann, T.M., et al. (2015). A Liquid-to-Solid Phase Transition of the ALS Protein FUS Accelerated by Disease Mutation. Cell *162*, 1066–1077.

Pechstein, A., Tomilin, N., Fredrich, K., Vorontsova, O., Sopova, E., Evergren, E., Haucke, V., Brodin, L., and Shupliakov, O. (2020). Vesicle Clustering in a Living Synapse Depends on a Synapsin Region that Mediates Phase Separation. Cell Rep. *30*, 2594-2602.e3.

Phan, A.T., Kuryavyi, V., Darnell, J.C., Serganov, A., Majumdar, A., Ilin, S., Raslin, T., Polonskaia, A., Chen, C., Clain, D., et al. (2011). Structure-function studies of

FMRP RGG peptide recognition of an RNA duplex-quadruplex junction. Nat. Struct. Mol. Biol. *18*, 796–804.

Pieretti, M., Zhang, F., Fu, Y.H., Warren, S.T., Oostra, B.A., Caskey, C.T., and Nelson, D.L. (1991). Absence of expression of the FMR-1 gene in fragile X syndrome. Cell *66*, 817–822.

Pilkington, G.R., and Parker, R. (2008). Pat1 Contains Distinct Functional Domains That Promote P-Body Assembly and Activation of Decapping. Mol. Cell. Biol. *28*, 1298–1312.

Pradhan, S.J., Nesler, K.R., Rosen, S.F., Kato, Y., Nakamura, A., Ramaswami, M., and Barbee, S.A. (2012). The conserved P body component HPat/Pat1 negatively regulates synaptic terminal growth at the larval Drosophila neuromuscular junction. J. Cell Sci. *125*, 6105–6116.

Protter, D.S.W., and Parker, R. (2016). Principles and Properties of Stress Granules. Trends Cell Biol. *26*, 668–679.

Protter, D.S.W., Rao, B.S., Treeck, B. Van, Lin, Y., Mizoue, L., Rosen, M.K., and Correspondence, R.P. (2018). Intrinsically Disordered Regions Can Contribute Promiscuous Interactions to RNP Granule Assembly. Cell Rep. *22*, 1401–1412.

Ray, D., Kazan, H., Cook, K.B., Weirauch, M.T., Najafabadi, H.S., Li, X., Gueroussov, S., Albu, M., Zheng, H., Yang, A., et al. (2013). A compendium of RNA-binding motifs for decoding gene regulation. Nature *499*, 172–177.

Reeve, S.P., Bassetto, L., Genova, G.K., Kleyner, Y., Leyssen, M., Jackson, F.R., and Hassan, B.A. (2005). The Drosophila Fragile X Mental Retardation Protein Controls Actin Dynamics by Directly Regulating Profilin in the Brain. Curr. Biol. *15*, 1156–1163.

Rehwinkel, J., Behm-Ansmant, I., Gatfield, D., and Izaurralde, E. (2005). A crucial role for GW182 and the DCP1:DCP2 decapping complex in miRNA-mediated gene silencing. RNA *11*, 1640–1647.

Richter, J.D., and Zhao, X. (2021). The molecular biology of FMRP: new insights into fragile X syndrome. Nat. Rev. Neurosci. 1–14.

De Rubeis, S., Pasciuto, E., Li, K.W., Fernández, E., DiMarino, D., Buzzi, A.,

Ostroff, L.E., Klann, E., Zwartkruis, F.J.T., Komiyama, N.H., et al. (2013). CYFIP1 coordinates mRNA translation and cytoskeleton remodeling to ensure proper dendritic spine formation. Neuron *79*, 1169–1182.

Rueden, C.T., Schindelin, J., Hiner, M.C., DeZonia, B.E., Walter, A.E., Arena, E.T., and Eliceiri, K.W. (2017). ImageJ2: ImageJ for the next generation of scientific image data. BMC Bioinformatics *18*.

Ryan, V.H., and Fawzi, N.L. (2019). Physiological, Pathological, and Targetable Membraneless Organelles in Neurons. Trends Neurosci. *42*, 693–708.

Santoro, M.R., Bray, S.M., and Warren, S.T. (2012). Molecular Mechanisms of Fragile X Syndrome: A Twenty-Year Perspective. Annu. Rev. Pathol. Mech. Dis. *7*, 219–245.

Sawicka, K., Hale, C.R., Park, C.Y., Fak, J.J., Gresack, J.E., Van Driesche, S.J., Kang, J.J., Darnell, J.C., and Darnell, R.B. (2019). FMRP has a cell-type-specific role in CA1 pyramidal neurons to regulate autism-related transcripts and circadian memory. Elife *8*, e46919.

Schaeffer, C., Bardoni, B., Mandel, J.L., Ehresmann, B., Ehresmann, C., and Moine, H. (2001). The fragile X mental retardation protein binds specifically to its mRNA via a purine quartet motif. EMBO J. *20*, 4803–4813.

Scharf, S.H., Jaeschke, G., Wettstein, J.G., and Lindemann, L. (2015). Metabotropic glutamate receptor 5 as drug target for Fragile X syndrome. Curr. Opin. Pharmacol. *20*, 124–134.

Schenck, A., Bardoni, B., Moro, A., Bagni, C., and Mandel, J.L. (2001). A highly conserved protein family interacting with the fragile X mental retardation protein (FMRP) and displaying selective interactions with FMRP-related proteins FXR1P and FXR2P. Proc. Natl. Acad. Sci. U. S. A. *98*, 8844–8849.

Schindelin, J., Arganda-Carreras, I., Frise, E., Kaynig, V., Longair, M., Pietzsch, T., Preibisch, S., Rueden, C., Saalfeld, S., Schmid, B., et al. (2012). Fiji: An open-source platform for biological-image analysis. Nat. Methods *9*, 676–682.

Schrier, M., Severijnen, L.A., Reis, S., Rife, M., Van't Padje, S., Van Cappellen, G., Oostra, B.A., and Willemsen, R. (2004). Transport kinetics of FMRP containing the I304N mutation of severe fragile X syndrome in neurites of living rat PC12 cells. Exp.

Neurol. *189*, 343–353.

Schwartz, J.C., Wang, X., Podell, E.R., and Cech, T.R. (2013). RNA Seeds Higher-Order Assembly of FUS Protein. Cell Rep. *5*, 918–925.

Scotto-Lomassese, S., Nissant, A., Mota, T., Néant-Féry, M., Oostra, B.A., Greer, C.A., Lledo, P.M., Trembleau, A., and Caillé, I. (2011). Fragile X mental retardation protein regulates new neuron differentiation in the adult olfactory bulb. J. Neurosci. *31*, 2205–2215.

Shah, S., Molinaro, G., Liu, B., Wang, R., Huber, K.M., and Richter, J.D. (2020). FMRP Control of Ribosome Translocation Promotes Chromatin Modifications and Alternative Splicing of Neuronal Genes Linked to Autism. Cell Rep. *30*, 4459-4472.e6.

Das Sharma, S., Metz, J.B., Li, H., Hobson, B.D., Hornstein, N., Sulzer, D., Tang, G., and Sims, P.A. (2019). Widespread Alterations in Translation Elongation in the Brain of Juvenile Fmr1 Knockout Mice. Cell Rep. *26*, 3313-3322.e5.

Shin, Y., and Brangwynne, C.P. (2017). Liquid phase condensation in cell physiology and disease. Science (80-.). *357*.

Shu, H., Donnard, E., Liu, B., Jung, S., Wang, R., and Richter, J.D. (2020). FMRP links optimal codons to mRNA stability in neurons. Proc. Natl. Acad. Sci. U. S. A. *117*, 30400–30411.

Sidorov, M.S., Auerbach, B.D., and Bear, M.F. (2013). Fragile X mental retardation protein and synaptic plasticity. Mol. Brain *6*.

Siomi, H., Choi, M., Siomi, M.C., Nussbaum, R.L., and Dreyfuss, G. (1994). Essential role for KH domains in RNA binding: Impaired RNA binding by a mutation in the KH domain of FMR1 that causes fragile X syndrome. Cell *77*, 33–39.

Siomi, M.C., Zhang, Y., Siomi, H., and Dreyfuss, G. (1996). Specific sequences in the fragile X syndrome protein FMR1 and the FXR proteins mediate their binding to 60S ribosomal subunits and the interactions among them. Mol. Cell. Biol. *16*, 3825–3832.

Sjekloća, L., Konarev, P. V., Eccleston, J., Taylor, I.A., Svergun, D.I., and Pastore, A. (2009). A study of the ultrastructure of fragile-X-related proteins. Biochem. J. *419*, 347–357.

Sjekloća, L., Pauwels, K., and Pastore, A. (2011). On the aggregation properties of FMRP - a link with the FXTAS syndrome? FEBS J. *278*, 1912–1921.

Soden, M.E., and Chen, L. (2010). Fragile X protein FMRP is required for homeostatic plasticity and regulation of synaptic strength by retinoic acid. J. Neurosci. *30*, 16910–16921.

Sossin, W.S., and DesGroseillers, L. (2006). Intracellular Trafficking of RNA in Neurons. Traffic *7*, 1581–1589.

Standart, N., and Weil, D. (2018). P-Bodies: Cytosolic Droplets for Coordinated mRNA Storage. Trends Genet. *34*, 612–626.

Stefani, G., Fraser, C.E., Darnell, J.C., and Darnell, R.B. (2004). Fragile X Mental Retardation Protein Is Associated with Translating Polyribosomes in Neuronal Cells. J. Neurosci. *24*, 7272–7276.

Stoppel, L.J., Osterweil, E.K., and Bear, M.F. (2017). The mGluR Theory of Fragile X: From Mice to Men (Elsevier Inc.).

Su, X., Ditlev, J.A., Hui, E., Xing, W., Banjade, S., Okrut, J., King, D.S., Taunton, J., Rosen, M.K., and Vale, R.D. (2016). Phase separation of signaling molecules promotes T cell receptor signal transduction. Science (80-.). *352*, 595–599.

Subramanian, M., Rage, F., Tabet, R., Flatter, E., Mandel, J., and Moine, H. (2011). G–quadruplex RNA structure as a signal for neurite mRNA targeting. EMBO Rep. *12*, 697–704.

Suhl, J.A., Chopra, P., Anderson, B.R., Bassell, G.J., and Warren, S.T. (2014). Analysis of FMRP mRNA target datasets reveals highly associated mRNAs mediated by G-quadruplex structures formed via clustered WGGA sequences. Hum. Mol. Genet. *23*, 5479–5491.

Taliaferro, J.M., Vidaki, M., Oliveira, R., Olson, S., Zhan, L., Saxena, T., Wang, E.T., Graveley, B.R., Gertler, F.B., Swanson, M.S., et al. (2016). Distal Alternative Last Exons Localize mRNAs to Neural Projections. Mol. Cell *61*, 821–833.

Teixeira, D., Sheth, U., Valencia-Sanchez, M.A., Brengues, M., and Parker, R. (2005). Processing bodies require RNA for assembly and contain nontranslating mRNAs.

RNA *11*, 371–382.

Thomson, S.R., Seo, S.S., Barnes, S.A., Louros, S.R., Muscas, M., Dando, O., Kirby, C., Wyllie, D.J.A., Hardingham, G.E., Kind, P.C., et al. (2017). Cell-Type-Specific Translation Profiling Reveals a Novel Strategy for Treating Fragile X Syndrome. Neuron *95*, 550-563.e5.

Tran, S.S., Jun, H.I., Bahn, J.H., Azghadi, A., Ramaswami, G., Van Nostrand, E.L., Nguyen, T.B., Hsiao, Y.H.E., Lee, C., Pratt, G.A., et al. (2019). Widespread RNA editing dysregulation in brains from autistic individuals. Nat. Neurosci. *22*, 25–36.

Van Treeck, B., and Parker, R. (2019). Principles of stress granules revealed by imaging approaches. Cold Spring Harb. Perspect. Biol. *11*, a033068.

Tsang, B., Arsenault, J., Vernon, R.M., Lin, H., Sonenberg, N., Wang, L.-Y., Bah, A., and Forman-Kay, J.D. (2019). Phosphoregulated FMRP phase separation models activity-dependent translation through bidirectional control of mRNA granule formation. PNAS *116*, 4218–4227.

Tucker, B., Richards, R.I., and Lardelli, M. (2006). Contribution of mGluR and Fmr1 functional pathways to neurite morphogenesis, craniofacial development and fragile X syndrome. Hum. Mol. Genet. *15*, 3446–3458.

Turrigiano, G.G. (2008). The Self-Tuning Neuron: Synaptic Scaling of Excitatory Synapses. Cell *135*, 422–435.

Tushev, G., Glock, C., Heumüller, M., Biever, A., Jovanovic, M., and Schuman, E.M. (2018). Alternative 3′ UTRs Modify the Localization, Regulatory Potential, Stability, and Plasticity of mRNAs in Neuronal Compartments. Neuron *98*, 495-511.e6.

Udagawa, T., Farny, N.G., Jakovcevski, M., Kaphzan, H., Alarcon, J.M., Anilkumar, S., Ivshina, M., Hurt, J.A., Nagaoka, K., Nalavadi, V.C., et al. (2013). Genetic and acute CPEB1 depletion ameliorate fragile X pathophysiology. Nat. Med. *19*, 1473–1477.

Valverde, R., Pozdnyakova, I., Kajander, T., Venkatraman, J., and Regan, L. (2007). Fragile X mental retardation syndrome: structure of the KH1-KH2 domains of fragile X mental retardation protein. Structure *15*, 1090–1098.

Vasilyev, N., Polonskaia, A., Darnell, J.C., Darnell, R.B., Patel, D.J., and Serganov, A. (2015). Crystal structure reveals specific recognition of a G-quadruplex RNA by a β-turn in the RGG motif of FMRP. Proc. Natl. Acad. Sci. U. S. A. *112*, E5391-400.

Wan, L., Dockendorff, T.C., Jongens, T.A., and Dreyfuss, G. (2000). Characterization of dFMR1, a Drosophila melanogaster Homolog of the Fragile X Mental Retardation Protein. Mol. Cell. Biol. *20*, 8536–8547.

Wheeler, J.R., Matheny, T., Jain, S., Abrisch, R., and Parker, R. (2016). Distinct stages in stress granule assembly and disassembly. Elife *5*.

Xu, K., Bogert, B.A., Li, W., Su, K., Lee, A., and Gao, F.B. (2004). The fragile X-related gene affects the crawling behavior of Drosophila larvae by regulating the mRNA level of the DEG/ENaC protein Pickpocket1. Curr. Biol. *14*, 1025–1034.

Yan, J., Porch, M.W., Court-Vazquez, B., Bennett, M.V.L., and Zukin, R.S. (2018). Activation of autophagy rescues synaptic and cognitive deficits in fragile X mice. Proc. Natl. Acad. Sci. *115*, E9707–E9716.

Yang, J., Gao, M., Xiong, J., Su, Z., and Huang, Y. (2019). Features of molecular recognition of intrinsically disordered proteins via coupled folding and binding. Protein Sci. *28*, 1952–1965.

Yang, P., Mathieu, C., Kolaitis, R.M., Zhang, P., Messing, J., Yurtsever, U., Yang, Z., Wu, J., Li, Y., Pan, Q., et al. (2020). G3BP1 Is a Tunable Switch that Triggers Phase Separation to Assemble Stress Granules. Cell *181*, 325-345.e28.

Yoshimura, A., Fujii, R., Watanabe, Y., Okabe, S., Fukui, K., and Takumi, T. (2006). Myosin-Va Facilitates the Accumulation of mRNA/Protein Complex in Dendritic Spines. Curr. Biol. *16*, 2345–2351.

Zalfa, F., Giorgi, M., Primerano, B., Moro, A., Penta, A. Di, Reis, S., Oostra, B., and Bagni, C. (2003). The Fragile X Syndrome Protein FMRP Associates with BC1 RNA and Regulates the Translation of Specific mRNAs at Synapses. Cell *112*, 317–327.

Zalfa, F., Achsel, T., and Bagni, C. (2006). mRNPs, polysomes or granules: FMRP in neuronal protein synthesis. Curr. Opin. Neurobiol.

Zang, J.B., Nosyreva, E.D., Spencer, C.M., Volk, L.J., Musunuru, K., Zhong, R.,

Stone, E.F., Yuva-Paylor, L.A., Huber, K.M., Paylor, R., et al. (2009). A Mouse Model of the Human Fragile X Syndrome I304N Mutation. PLoS Genet. *5*, e1000758.

Zhang, Y., Gaetano, C.M., Williams, K.R., Bassell, G.J., and Mihailescu, M.R. (2014). FMRP interacts with G-quadruplex structures in the 3'-UTR of its dendritic target Shank1 mRNA. RNA Biol. *11*, 1364–1374.

Zhang, Y.Q., Bailey, A.M., Matthies, H.J., Renden, R.B., Smith, M.A., Speese, S.D., Rubin, G.M., and Broadie, K. (2001). Drosophila fragile X-related gene regulates the MAP1B homolog Futsch to control synaptic structure and function. Cell *107*, 591–603.

APPENDIX 1: TABLE OF REAGENTS AND RESOURCES

	SOURCE	IDENTIFIER
Antibodies		
Primary antibodies		
Mouse anti-Fmr1 [6A15]	Abcam	ab10299
Rabbit anti-EGFP	Proteintech	50430-2-AP
Mouse anti-α tubulin	DSHB	12G10
Mouse anti-discs large	DSHB	4F3
Rabbit anti-Pat1	(Pradhan et al., 2012)	
Secondary antibodies		
Horse anti-mouse HRP	Cell Signaling	7074S
Goat anti-rabbit HRP	Cell Signaling	7076S
Goat anti-mouse Alexa 488	Invitrogen	A11029
Goat anti-rabbit Alexa 594	Invitrogen	A11037
Goat anti-HRP 647	Jackson ImmunoResearch Labs	AB_2338967
Chemicals		
1,6-hexanediol	Sigma-Aldrich	240117
Sodium meta-arsenite	Sigma-Aldrich	S7400
Critical Commercial Assay kits		
Q5 Site-Directed Mutagenesis kit	New England Biolabs	E0554S
One-Taq Polymerase	New England Biolabs	M0480
Dual Glo Luciferase Assay System	Promega	E2920
Effectene Transfection kit	Qiagen	301425
Experimental Models: Cell Lines		
D. melanogaster: Schneider's 2 cells (S2R+)	*Drosophila* Genomics Resource Center	NIH Grant 2P40OD010949

D. melanogaster: Schneider's 2 cells (S2)	*Drosophila* Genomics Resource Center	NIH Grant 2P40OD010949
Experimental Models: Organisms/Genotypes		
D. melanogaster: BL Canton S	Bloomington *Drosophila* Stock Center	BDSC:64349
D. melanogaster: C380-Gal4	Bloomington *Drosophila* Stock Center	BDSC:80580
D. melanogaster: w^{1118}*; UAS-FMR1*	Bloomington *Drosophila* Stock Center	BDSC:6931
D. melanogaster: w^{1118}*;; FMR1*$^{\Delta 50M}$*/TM6B,Tb*$^{+}$	Bloomington *Drosophila* Stock Center	BDSC:6928
D. melanogaster: w;; FMR1*$^{\Delta 113M}$*/TM6B,Tb*$^{+}$	Bloomington *Drosophila* Stock Center	BDSC:67403
D. melanogaster: C380-Gal4, cha-Gal80	(Hartwig et al., 2008)	
D. melanogaster: w^{1118}*;* $wg^{Sp\text{-}1}$*/CyO, P{*w^{+mC}*=2xTb*^{1}*-RFP}CyO; MKRS/TM6B,* Tb^{1}	Bloomington *Drosophila* Stock Center	*BDSC: 76359*
D. melanogaster: C380-Gal4;; Sb/ TM6B,Ser	This paper	
D. melanogaster: pUAST-attB-EGFP	This paper	
D. melanogaster: pUAST-attB-EGFP:FMRP	This paper	
*D. melanogaster: pUAST-attB-EGFP:FMRP:KH1**	This paper	
*D. melanogaster: pUAST-attB-EGFP:FMRP:KH2**	This paper	
*D. melanogaster: pUAST-attB-EGFP:FMRP:KH1*KH2**	This paper	
D. melanogaster: pUAST-attB-EGFP:ΔKH	This paper	
D. melanogaster: w^{+}*;* $FMR1^{\Delta 50M}$*, pUAST-attB-EGFP/TM6BTb*	This paper	
D. melanogaster: w^{+}*;* $FMR1^{\Delta 50M}$*, pUAST-attB-EGFP:FMRP/TM6BTb*	This paper	

D. melanogaster: w^+; $FMR1^{\Delta 50M}$, pUAST-attB-EGFP:FMRP:KH1/TM6BTb*	This paper	
D. melanogaster: w^+; $FMR1^{\Delta 50M}$, pUAST-attB-EGFP:FMRP:KH2/TM6BTb*	This paper	
*D. melanogaster: w^+; $FMR1^{\Delta 50M}$, pUAST-attB-EGFP:FMRP:KH1*KH2*/TM6BTb*	This paper	
D. melanogaster: w^+; $FMR1^{\Delta 50M}$, pUAST-attB-EGFP:ΔKH/TM6BTb	This paper	
D. melanogaster: C380,cha-Gal80;; TM6BTb/TM3BSb	This paper	
D. melanogaster: C380,cha-Gal80;; TM6BTb/$FMR1^{\Delta 113M}$	This paper	
D. melanogaster: C380-Gal4;; $FMR1^{\Delta 113M}$/TM6BTb	This paper	
Oligonucleotides		
FMR1 deletion (PCR forward primer): 5'-AAGGAAAAAAGCGGCCGCAAAGATATCGCGAAAATCCCCCCAG-3'	(Zhang et al., 2001)	
FMR1 deletion (PCR reverse primer): 5'-CGGGATCCGTTATGCTACGTGAATAAATC-3'	(Zhang et al., 2001)	
FMRP-pUAST (PCR amplification forward primer with 5'-KpnI site):	This paper	
FMRP-pUAST (PCR amplification forward primer with 3'-EcoRI site):	This paper	
KH1 SDM (Forward primer for mutagenesis of the KH1 domain in dmFMRP [Gly269Glu]): 5' CAAAATCAGCGAAGAGACCGAGG -3'	This paper	
KH1 SDM (Reverse primer for mutagenesis of the KH1 domain in dmFMRP [Gly269Glu]): 5'-AATGTGCAGGACTTCTCC-3'	This paper	
KH2 SDM (Forward primer for mutagenesis of the KH2 domain in dmFMRP [Ile307Asn]): 5'-GGGCGCATTAACCAGGAGATTG-3'	This paper	
KH2 SDM (Reverse primer for mutagenesis of the KH2 domain in dmFMRP [Ile307Asn]): 5'-ATTCTTGCCAATCACCTTGC-3'	This paper	

DP-90 (FMRP PCR amplification forward primer with 5'-HindIII site): 5'-ACAAGCCAAGCTTTATGGAAGAT-3'	This paper	
ES-51 (FMRP:ΔIDR amplification reverse primer with 3' EcoRI): 5'-TACGGAATTCTTACTTCTCCTGACGCAACTGTT-3'	This paper	
ES-135 (EGFP amplification forward primer): 5'-GGTACCAACATGGTGAGCAA-3'	This paper	
ES-136 (EGFP amplification reverse primer with 3'-XbaI site): 5'-GTTCATCTAGACTACTTGTACAGCTCGTCCATGC-3'	This paper	
ES-83 (KH1+2 amplification forward primer with 5' HindIII site): 5'-AAGCCAAGCTTTGGAAACTACGTTGAGGAGTT-3'	This paper	
ES-82 (KH1+2 amplification reverse primer with 3' AscI site): 5'-ATCTCGGCGCGCCGCGACAGATGATACTCCAAC-3'	This paper	
ES-60 (IDR amplification forward primer with 5' HindIII site): 5'-GTCAAAGCTTCGAGATTGATCAGCAGCTTC-3'	This paper	
ES-53 (IDR amplification reverse primer with 3' EcoRI site): 5'-TACGGAATTCTTAGGACGTGCCATTGACCA-3'	This paper	
DP-140 (FMRP KH0 deletion amplification reverse primer with BamHI 5' site): 5'-ATGACGGATCCCAGACGACCCAATTCACAGATT-3'	This paper	
DP-141 (FMRP KH0 deletion amplification forward primer with BamHI 3' site): 5'-ATGACGGATCCTACGTTGAGGAGTTCCGTGTG-3'	This paper	
DP-142 (FMRP KH1+2 deletion amplification reverse primer with BamHI site): 5'-ATGACGGATCCCTCAACGTAGTTTCCACGGC-3'	This paper	

DP-143 (FMRP KH1+2 deletion amplification forward primer with BamHI site): 5'-ATGACGGATCCCTGGCGCATGTACCCTTTGT-3'	This paper	
DP-93 (FMRP amplification primer with EcoRI 3' site): 5'-TCTGCAGAATTCTTAGGACGTG-3'	This paper	
DP-91 (FMRP RGG deletion amplification reverse primer with EcoRI site): 5'-TGACGGATCCATCGTTGTAGCCACGCTGCT-3'	This paper	
DP-92 (FMRP RGG deletion amplification primer with EcoRI site): 5'-TGACGGATCCCCGCCACGCAACGATCAGCA-3'	This paper	
ES-139 (FMRP LIC amplification forward primer): 5'-TACTTCCAATCCAATGCAGAAGATCTCCTCGTGGAAGTTCGGC-3'	This paper	
ES-140 (FMRP LIC amplification reverse primer): 5'-TTATCCACTTCCAATGTTATTAGGACGTGCCATTGACCAGGCC-3'	This paper	
DP-204 (mcherry amplification forward primer with 5' HindIII site): 5'-AGTACAAGCTTATGGTGAGCAAGGGCGAGGAG-3'	This paper	
DP-205 (mcherry amplification reverse primer with 3' BamHI site): 5'-AGTACGGATCCTTACTTGTACAGCTCGTCCATGCCG-3'	This paper	
DP-206 (Top oligonucleotide for cloning (Gly4Ser)3 linker upstream of mcherry, containing a 5' ApaI site, and 3' HindIII site to clone directionally into pAc5.1): 5'-CGGTGGAGGAGGCTCTGGTGGAGGCGGTAGCGGAGGCGGAGGGTCGA-3'	This paper	
DP-207 (Bottom oligonucleotide for cloning (Gly4Ser)3 linker upstream of mcherry, containing ApaI and HindIII sites): 5'-AGCTTCGACCCTCCGCCTCCGCTACCGCCTCCACCAGAGCCTCCTCCACCGGGCC-3'	This paper	

ES-170 (Rasputin RT-PCR primer with 5' KpnI site): 5'-TGACATGGTCATGGATGCGACCCA-3'	This paper	
ES-171 (Rasputin RT-PCR primer with in-frame stop codon and 3'-EcoRI site): 5'-ATACGAATTCGCGACGTCCGTAGTTGCCA-3'	This paper	
CaMKIIUTRFwdGA (CaMKII 3'UTR Gibson assembly primer for cloning into FLuc backbone vector cut with EcoRI and XhoI): 5'-CGGAAAGTCCAAATTGTAATGGGCATTAATCAATGGAATATAAAC-3'	This paper	
CaMKIIUTRRvsGA (CaMKII 3'UTR Gibson assembly primer for cloning into FLuc backbone vector cut with EcoRI and XhoI): 5'-CTTACCTTCGAATGGGTGACAAAATTGCATTATGCTTTGAATTC-3'	This paper	
FMR1Fwd (Forward restriction primer for cloning FMR1's 3'UTR containing the 5' EcoRI site): 5'-TACTGAATTCAGGAGCAACAGCTCACAG-3'	This paper	
FMR1Rvs (Reverse restriction primer for cloning FMR1's 3'UTR containing the 3' XhoI site): 5'-ATACCTCGAGGCTTGATGGTTTGTGTTTTG-3'	This paper	
Recombinant DNA		
Plasmid: *pUAST-attB*	DGRC	NIH Grant 2P40OD010949
Plasmid: *pUAST-attB-EGFP*	This paper	
Plasmid: *pUAST-attB-EGFP:FMRP*	This paper	
Plasmid: *pUAST-attB-EGFP:FMRP:KH1**	This paper	
Plasmid: *pUAST-attB-EGFP:FMRP:KH2**	This paper	
Plasmid: *pUAST-attB-EGFP:FMRP:KH1*KH2**	This paper	
Plasmid: *pAc5.1B-EGFP*	Addgene	21181
Plasmid: *pAc5.1-EGFP:FMRP*	This paper	
Plasmid: *pAc5.1-EGFP:FMRP:KH1**	This paper	
Plasmid: *pAc5.1-EGFP:FMRP:KH2**	This paper	
Plasmid: *pAc5.1-EGFP:FMRP:KH1*KH2**	This paper	
Plasmid: *pAc5.1-EGFP:FMRP:ΔKH*	This paper	

Plasmid: *pAc5.1-EGFP:FMRP:ΔIDR*	This paper	
Plasmid: *pAc5.1-EGFP:FMRP:IDR*	This paper	
Plasmid: *pAc5.1-EGFP:FMRP:KH+IDR*	This paper	
Plasmid: *pAc5.1-Rasputin-(Gly$_4$Ser)$_3$-mCherry*	This paper	
Plasmid: *pAc5.1B-λN:HA*	Addgene	21302
Plasmid: *pAc5.1-λN:HA:FMRP*	This paper	
Plasmid: *pAc5.1-λN:HA:FMRP:KH1**	This paper	
Plasmid: *pAc5.1-λN:HA:FMRP:KH2**	This paper	
Plasmid: *pAc5.1-λN:HA:FMRP:KH1*KH2**	This paper	
Plasmid*: pAc5.1B*	Invitrogen	V411020
Plasmid: *pAc5.1-FMRP*	This paper	
Plasmid: *pAc5.1-FMRP:KH1**	This paper	
Plasmid: *pAc5.1-FMRP:KH2**	This paper	
Plasmid: *pAc5.1-FMRP:KH1*KH2**	This paper	

APPENDIX 2: smFISH PROBE OLIGONUCLEOTIDES

Sequence Name	Sequence	Three Modification
camkii-1_1	GAAAAACGCGTACAGGCTGC	Quasar 670
camkii-1_2	CCAACTCTTCTTTGATGTCG	Quasar 670
camkii-1_3	GCAGCAAATTCAAAGCCAGT	Quasar 670
camkii-1_4	CACTATGTTGGGATGGTGTA	Quasar 670
camkii-1_5	CTCCTGTATACTGTCATGTA	Quasar 670
camkii-1_6	AATGTGATGCATCAGCTTCT	Quasar 670
camkii-1_7	CATTTTGGTGGCAGTGATTG	Quasar 670
camkii-1_8	ATTCTCTGGTTTCAGATCTC	Quasar 670
camkii-1_9	AGACCAAAGTCAGCGAGTTT	Quasar 670
camkii-1_10	CTGATGATCGCCTTGAACTT	Quasar 670
camkii-1_11	CTCCTTTTTCAATACCTCAG	Quasar 670
camkii-1_12	AAGAATAACTCCACATGCCC	Quasar 670
camkii-1_13	TGCTGATCTTCATCCCAAAA	Quasar 670
camkii-1_14	ACGGATAATCATAAGCTCCC	Quasar 670
camkii-1_15	TTTAGCTTCTGGAGTAACCG	Quasar 670
camkii-1_16	GATGTTTTAAAGCCTCAGCT	Quasar 670
camkii-1_17	CACACGTTCGCGTTGACAAA	Quasar 670
camkii-1_18	CTTGAGACAGTCTACGGTTT	Quasar 670
camkii-1_19	CGCCAACATTGTCGTAAGTA	Quasar 670
camkii-1_20	GTTATCATACTTCTGCTCGA	Quasar 670
camkii-1_21	GTTGATTCTTTGACCTGTGA	Quasar 670
camkii-1_22	CGTCTTCAAGAGTAGTGCTA	Quasar 670
camkii-1_23	GCCACTGTTAATTGCTTCAA	Quasar 670
camkii-1_24	CAAAGGCAGTTAGATGCGGA	Quasar 670
camkii-1_25	ATTCCTTCTACAAGGTTACC	Quasar 670
camkii-1_26	GCTTTGCAGTTTTTACCAAG	Quasar 670
camkii-1_27	CTTCACCAAGTAAGTGCACA	Quasar 670
camkii-1_28	GTCTCACATAGGCAATGCAA	Quasar 670

camkii-1_29	CATTCTGCCATTTGTTATCG	Quasar 670
camkii-1_30	CTTATTTTGGCAGATGCACT	Quasar 670